2011

DYNAMIC RESPONSE OF STRUCTURAL MATERIALS TO SHOCK LOADING

Puneet Kumar
University of Rhode Island

DYNAMIC RESPONSE OF STRUCTURAL MATERIALS TO SHOCK LOADING

BY

PUNEET KUMAR

A DISSERTATION SUBMITTED IN PARTIAL FULFILLMENT OF THE REQUIREMENTS FOR THE DEGREE OF

DOCTOR OF PHILOSOPHY

IN

MECHANICAL, INDUSTRIAL & SYSTEMS ENGINEERING

UNIVERSITY OF RHODE ISLAND

2011

DOCTOR OF PHILOSOPHY DISSERTATION

OF

PUNEET KUMAR

APPROVED:

Dissertation Committee:

Major Professor Arun Sharma

M.H. Stadd

Carl Rousseau

Arijit Sarkar

DEAN OF THE GRADUATE SCHOOL

UNIVERSITY OF RHODE ISLAND
2011

ABSTRACT

An analytical and experimental study has been conducted to investigate the blast resistance and mitigation behaviors of structural materials. Understanding the failure mechanisms in these materials will lead to an optimal design of light weight structures capable of withstanding blast loadings. This improved blast mitigation property is extremely important in protecting many commercial, naval, aerospace and defense structures.

A controlled study has been performed to understand fracture and damage in glass panels subjected to air blast. A shock tube apparatus has been utilized to obtain the controlled blast loading. Five different panels, namely plain glass, sandwiched glass, wired glass, tempered glass and sandwiched glass with film on both the faces are used in the experiments. Fully clamped boundary conditions are applied to replicate the actual loading conditions in windows. Real-time measurements of the pressure pulses affecting the panels are recorded. A post-mortem study of the specimens was also performed to evaluate the effectiveness of the materials to withstand these shock loads. The real time full-field in-plane strain and out-of-plane deformation data on the back face of the glass panel is obtained using 3D Digital Image Correlation (DIC) technique. The experimental results show that the sandwich glass with two layers of glass joined with a Polyvinyl butyral (PVB) interlayer and protective film on both the front and back face maintains structural integrity and out performs the other four types of glass tested.

Experimental and numerical studies were conducted to understand the effect of plate curvature on blast response of aluminum panels. A shock tube apparatus was

utilized to impart controlled shock loading to aluminum 2024-T3 panels having three different radii of curvatures: infinity (panel A), 304.8 mm (panel B), and 111.76 mm (panel C). Panels with dimensions of 203.2 mm x 203.2 mm x 2 mm were held with mixed boundary conditions before applying the shock loading. A 3D Digital Image Correlation (DIC) technique coupled with high speed photography was used to obtain out-of-plane deflection and velocity, as well as in-plane strain on the back face of the panels. Macroscopic postmortem analysis was performed to compare the yielding and plastic deformation in the three panels. The results showed that panel C had the least plastic deformation and yielding as compared to the other panels. A dynamic computational simulation that incorporates the fluid-structure interaction was also conducted to evaluate the panel response. The computational study utilized the Dynamic System Mechanics Analysis Simulation (DYSMAS) software. The model consisted of the shock tube wall, the aluminum plate, and the air (both internal and external) to the tube walls. The numerical results were compared to the experimental data. The comparison between the experimental results and the numerical simulation showed a high level of correlation using the Russell error measure.

Experimental studies were conducted to understand the effect of plate curvature on the blast response of 32 layered carbon fiber epoxy panels. A shock tube apparatus was utilized to impart controlled shock loading on carbon fiber panels having three different radii of curvatures; infinite (panel A), 305 mm (panel B), and 112 mm (panel C). These panels with dimensions of 203 mm x 203 mm x 2 mm were held under clamped boundary conditions during the shock loading. A 3D Digital Image Correlation (DIC) technique coupled with high speed photography was used to obtain

out-of-plane deflection and velocity, as well as in-plane strain on the back face of the panels. There were two types of failure mechanism observed in all the three panels: fiber breakage and inter-layer delamination. The fiber breakage was induced from on the face exposed to the shock loading (front face) and continued to the interior. Delamination occurred on the side of the specimen as well as on the front face. Macroscopic postmortem analysis and DIC results showed that panel C can mitigate higher intensity (pressure) shock waves without initiation of catastrophic damage in the panel. Panel B could sustain the least shock wave intensity and exhibited catastrophic failure. Panel A exhibited intermediate blast mitigation capacity.

Experimental studies were conducted to understand the effect of varying plate thickness on the blast response of doubly curved E-glass/vinyl Ester panels. A shock tube apparatus was utilized to impart controlled shock loading on glass fiber panels having three different thickness: 1.37 mm (panel A), 2.54 mm (panel B), and 4.40 mm (panel C). These panels with an 18.28 mm radius of curvature were held under clamped boundary conditions during the shock loading. A 3D Digital Image Correlation (DIC) technique coupled with high speed photography was used to obtain out-of-plane deflection and velocity, as well as in-plane strain on the back face of the panels. There were two types of failure mechanism observed in all the three panels: fiber breakage and inter-layer delamination. Macroscopic postmortem analysis and DIC results showed that panel C can mitigate higher intensity (pressure) shock waves without initiation of catastrophic damage in the panel. Panel A could sustain the least shock wave intensity and exhibited catastrophic failure.

ACKNOWLEDGMENTS

First and foremost I would like to thank Dr. Arun Shukla for his continuous guidance and support through this research. It has been an honor for me to be one of his Ph.D. student. His patience, adamant work ethic and inspiring nature have been a great source of motivation throughout my doctoral research. I cannot thank him enough for all of the positive things he has instilled into me to help me grow and prosper in the future. He is not only an outstanding professor and mentor but a truly inspirational human being. I am also thankful for his help in improving my communication skills.

I would also like to sincerely thank Dr. Sadd, Dr. Bose, Dr. Rousseau, Dr. Datseris and Dr. Brown for consenting to serve as my committee members. A special thanks to Dr. Sadd for his critical discussion in the group discussion. I would also like to thank Dr. David S. Stargel at Air Force Research Lab for providing the specimens which led to the studies in chapter 2 and 3.

The help and encouragement from my friends and colleagues are greatly appreciated. I would like to thank all of my lab mates in Dynamic Photomechanics Laboratory: Addis Kidane, Mathew Jackson, James LeBlanc, Nathaniel Gardner, Erheng Wang, Vijayalakshimi Manneth, Nicholas Heeder, Ryan Sekac, Jefferson Wright, Sandeep Abotula, Sachin Gupta, Daniel Gracia, and Alexander Escher. The time spent with everyone has made it an incredible experience as well as provided me with many great friendships. I would like to thank James LeBlanc for his additional support and help during the research which led to the publication of chapters 2 and 4. In addition, I would also like to thank Joe Gomez, Jim Byrnes, Rob D'Ambrosca, Jen

Cerullo, Nancy Dubee and the rest of the mechanical engineering department faculty and staff.

The financial support of the Department of Homeland Security (DHS) under Cooperative Agreement No. 2008-ST-061-ED0002 is greatly acknowledged.

Last but not list, I would like to thank my beloved family; my father, my mother, my wife, and my sisters, for their understanding nature, love and moral and material support.

PREFACE

An analytical and experimental study has been conducted to investigate the blast resistance and mitigation behaviors of structural materials. Understanding the failure mechanisms will lead to optimally designed light weight structures when subjected to blast loadings. This is a very important parameter for structural as well as naval, aerospace and defense applications. This dissertation addresses the dynamic behaviors and the failure mechanisms of structural materials under air shock wave loading. This thesis is prepared using the manuscript format.

Chapter 1 details a controlled study performed to understand fracture and damage in glass panels subjected to air blast. A shock tube apparatus has been utilized to obtain the controlled blast loading. Five different panels, namely plain glass, sandwiched glass, wired glass, tempered glass and sandwiched glass with film on both the faces are used in the experiments. Fully clamped boundary conditions are applied to replicate the actual loading conditions in windows. Real-time measurements of the pressure pulses affecting the panels are recorded. A post-mortem study of the specimens was also performed to evaluate the effectiveness of the materials to withstand these shock loads.

Chapter 2 details the experimental and numerical studies conducted to understand the effect of plate curvature on blast response of aluminum panels. A shock tube apparatus was utilized to impart controlled shock loading to aluminum 2024-T3 panels having three different radii of curvatures: infinity (panel A), 304.8 mm (panel B), and 111.76 mm (panel C). Panels with dimensions of 203.2 mm x 203.2 mm x 2 mm were held with mixed boundary conditions before applying the shock loading. A 3D Digital

Image Correlation (DIC) technique coupled with high speed photography was used to obtain out-of-plane deflection and velocity, as well as in-plane strain on the back face of the panels. Macroscopic postmortem analysis was performed to compare the yielding and plastic deformation in the three panels. A dynamic computational simulation that incorporates the fluid-structure interaction was also conducted to evaluate the panel response. The computational study utilized the Dynamic System Mechanics Analysis Simulation (DYSMAS) software. The model consisted of the shock tube wall, the aluminum plate, and the air (both internal and external) to the tube walls. The numerical results were compared to the experimental data.

Chapter 3 concentrates on the experimental studies conducted to understand the effect of plate curvature on the blast response of 32 layered carbon fiber epoxy panels. A shock tube apparatus was utilized to impart controlled shock loading on carbon fiber panels having three different radii of curvatures; infinite (panel A), 305 mm (panel B), and 112 mm (panel C). These panels with dimensions of 203 mm x 203 mm x 2 mm were held under clamped boundary conditions during the shock loading. A 3D Digital Image Correlation (DIC) technique coupled with high speed photography was used to obtain out-of-plane deflection and velocity, as well as in-plane strain on the back face of the panels.

Chapter 4 details the experimental studies were conducted to understand the effect of varying plate thickness on the blast response of doubly curved E-glass/vinyl Ester panels. A shock tube apparatus was utilized to impart controlled shock loading on glass fiber panels having three different thickness: 1.37 mm (panel A), 2.54 mm (panel B), and 4.40 mm (panel C). These panels with an 18.28 mm radius of curvature

were held under clamped boundary conditions during the shock loading. A 3D Digital Image Correlation (DIC) technique coupled with high speed photography was used to obtain out-of-plane deflection and velocity, as well as in-plane strain on the back face of the panels.

TABLE OF CONTENTS

LIST OF TABLES

TABLE PAGE

LIST OF FIGURES

FIGURE PAGE

CHAPTER 1

FIGURE PAGE

CHAPTER 2

FIGURE PAGE

CHAPTER 3

FIGURE PAGE

FIGURE PAGE

CHAPTER 4

FIGURE PAGE

CHAPTER 1

DYNAMIC RESPOSE OF GLASS PANELS SUBJECTED TO SHOCK LOADING

by

Puneet Kumar and Arun Shukla

has been published in Journal of Non-Crystalline Solids, Volume 357, Issue 24, December 2011, Pages 3917-3923

Corresponding Author: Arun Shukla

Dynamic Photo Mechanics Laboratory

Department of Mechanical, Industrial and Systems Engineering

University of Rhode Island

206 Wales Hall, 92 Upper College Rd

Kingston, RI, 02881, USA

Phone: +1-401-874-2283

Email Address: shuklaa@egr.uri.edu

1. Abstract

A controlled study has been performed to understand fracture and damage in glass panels subjected to air blast. A shock tube apparatus has been utilized to obtain the controlled blast loading. Five different panels, namely plain glass, sandwiched glass, wired glass, tempered glass and sandwiched glass with film on both the faces are used in the experiments. Fully clamped boundary conditions are applied to replicate the actual loading conditions in windows. Real-time measurements of the pressure pulses affecting the panels are recorded. A post-mortem study of the specimens was also performed to evaluate the effectiveness of the materials to withstand these shock loads. The real time full-field in-plane strain and out-of-plane deformation data on the back face of the glass panel is obtained using 3D Digital Image Correlation (DIC) technique. The experimental results show that the sandwich glass with two layers of glass joined with a Polyvinyl butyral (PVB) interlayer and protective film on both the front and back face maintains structural integrity and out performs the other four types of glass tested.

Keywords

Glass panel, 3D-digital image correlation, Shock tube, Air blast loading, Blast mitigation.

2. Introduction

Accidental explosions or bomb blasts cause extreme loading on glass structures. This results in the shattering of glass panels into small pieces which have sharp edges and move at very high velocities. These high velocity glass fragments are the major cause of injuries to people. Apart from this, the blast pressure entering the

building through the shattered window panels can also cause additional injuries to the occupants. Five different types of glass panels are subjected to blast loading using a shock tube to study their dynamic response. Post-mortem analysis has been conducted on the blast loaded panels to evaluate the effectiveness of the material to mitigate blast loading. Previously, the main focus of research in this area has been on the numerical/theoretical analysis of glass panels subjected to an explosion. Recently, experimental studies have been done on glass panels to analyze their blast mitigation properties. However, these experiments used either an indenter or an impactor to simulate the blast condition. The aim of this study is to analyze the damaged area, midpoint transient deflection, and other characteristics of the dynamic response of glass panels subjected to a controlled blast loading.

Saito *et. al* [1] modeled the blast process on glass using the indenting method. They discussed the mechanism of formation of residual stress in the indenting process, both analytically and experimentally, in order to optimize the processing conditions to produce the desired residual stress in a blast loading. Gogotsi *et al.* [2] used different shapes of indenters to analyze the fracture in rectangular shaped optical and technical glasses and showed that the fracture resistance of float glass was higher than that of fused silica and other optical glasses Bouzid et al. [3] studied glass material under impact conditions where stress waves and their interactions are dominant. They proposed a damage model characterized by the damage volume to evaluate the damage development and fragmentation. It was found that damage volume is a function of impact duration and critical stress.

Wei *et al.* [4] formulated a failure criterion based on the energy balance approach for a laminated glass panel subjected to a blast loading. They developed a damage factor to assess the failure of the laminated glass panel. According to them, the negative phase of the blast load will cause the breakage of the laminated glass if the positive phase of the blast load is not violent enough to cause failure. They also predicted the size of the glass shards using the surface energy based failure model. Wei *at al.* [5] developed a 3-D nonlinear dynamic finite element model to characterize the stress distribution in a laminated architectural glazing subjected to blast loading. They considered the viscoelastic parameter of the PVB interlayer on the dynamic response of the glass panel. The parametric study showed that the panel exhibited a non-linear response to the blast overpressure. At the same time they found that the through thickness stress and displacement distribution are nearly linear.

Karuthammer *et al.* [6] analyzed the effect of the negative phase of blast waves on glass panels. They developed an approximate numerical model for the dynamic response simulation of glass panels subjected to blast loading. This also included the stochastic considerations of the glass flaw characteristics. They also conducted a parametric study showing that the glass panels exhibit different responses at different scaled ranges, and for different charge sizes. In one of the other publications, Wei *et al.* [7] studied the response of a rectangular laminated glass panel based on the classical small deflection and large deflection theory. Their main conclusion was that the mid-span deflection and tensile stress due to the negative pressure is almost double of that in the case of positive pressure. They also showed that the tensile stress develops on the back face of the laminate panel where as the compressive stress

develops on the front face or the face which experiences the blast loading. Glasses have higher compressive strength, which is about ten times that of their tensile strength [8]. Hooper *et al.* [9] studied the post-fracture behavior of laminated glass under full scale blast loading. They used 3D digital image correlation for full-field deflection measurement. They studied the delamination between the interlayer to glass interface using high-speed photoelasticity and concluded that panels having interlayer thickness less than 1.52 mm fail prematurely and should not be used in blast resistant glass panels. Carson and Papanu [10] developed an aqueous-based solution which provides substantial increases in strength to the cut edges of planer glass. The application and then subsequent curing of this aqueous solution to the damaged glass surface showed a significant increase in fracture strength.

The present paper focuses on the response of five different types of glass panels subjected to a controlled blast loading applied by a shock tube. Real-time measurements of the pressure pulses affecting the panels are recorded. Post-mortem study is used to evaluate the effectiveness of the panels to withstand these shock loads. The real time deformation mapping is done using the Digital Image Correlation (DIC) technique [11]. In the following sections, the methods used to carry out these experiments are presented, and the experimental results are discussed in detail.

3. Experimental Procedure

3.1 Material Details

The five different panels used during these experiments include a clear glass panel, tempered glass panel, wired glass panel, sandwiched glass panel and laminated sandwiched glass panel with a protective film on both of its faces (three specimens are shown in fig. 1). Each experiment is repeated three times. The specimens are 305 mm long x 305 mm wide x 6.5 mm thick. Laminated sandwiched glass panel has a thickness of 7.5 mm because of the protective film on both front and back face of the sandwiched panel.

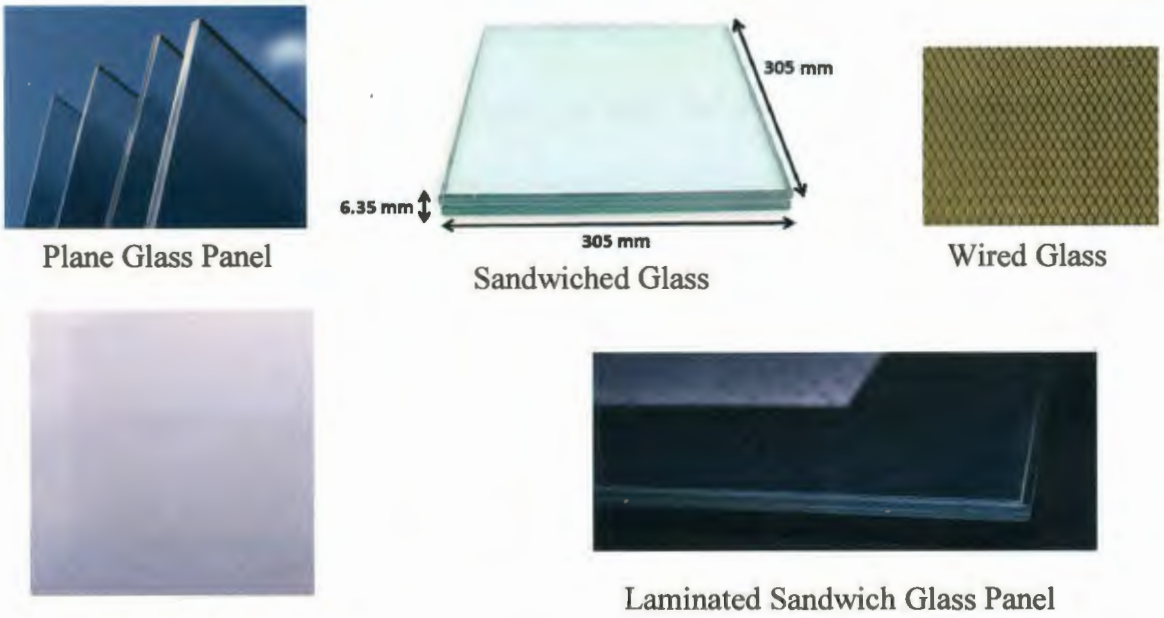

Figure 1: Specimens

The panels are made out of soda-lime-silica glass which has a tensile strength in the range of 20-100 MPa and a compressive strength of approximately 10 times of that. The clear glass panel is the regular glass panel on which no additional treatment is performed. The tempered glass panel is made from the clear glass panel. Specimens

of a specific size are cut out from the clear glass panel which is then heat treated to release the pre-stress and induce beneficial residual stresses. The wired glass panel is manufactured by building the whole panel on a wire frame such that the wire frame is imbedded within it. The sandwiched glass panel consists of two clear glass panels which are bonded by a polyvinyl butyral (PVB) interlayer. This bonding process takes place utilizing heat and pressure treatment. The PVB layer has good bonding strength, is optically clear and does not diminish the optical properties of the glass panel. The laminated sandwiched glass panel is made by adhering a protective film from XO ARMOR® on both of the outer faces of the sandwiched glass panel. The XO® protective film is 0.5 mm thick and a special adhesive XO® bond was used to adhere the protective film onto both of the face of the sandwiched glass panel. According to the manufacturers, XO® bond penetrates the glass surface and forms a chemical bond between the glass and XO® film at the nano level. The protective film was used as a measure of retrofitting existing windows for possible improvement in blast mitigation properties.

3.2 Shock loading apparatus

The shock tube apparatus used in this study to obtain the controlled dynamic loading is shown in fig. 2. A complete description of the shock tube and its calibration can be found in [12]. The shock tube consists of a long rigid cylinder, divided into a high-pressure driver section and a low pressure driven section, which are separated by a diaphragm. By pressurizing the high-pressure section a pressure difference across the diaphragm is created. When this pressure differential reaches a critical value, the

diaphragm ruptures. The subsequent rapid release of gas creates a shock wave, which travels down the tube to impart a shock loading on the specimen.

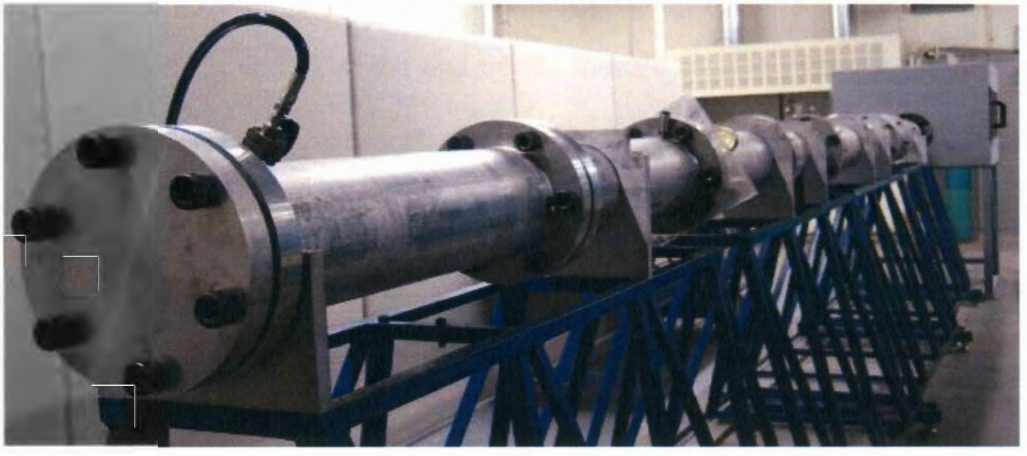

Figure 2: The URI shock tube facility

When the shock wave impacts the test panel located at the end of the muzzle, the gas becomes superheated and the wave is reflected at a higher pressure than that of the incident shock pressure. The theoretical detail on the equations for shock tubes has been previously established in the literature and is briefly discussed in the following section [13]. There are four basic theoretical assumptions which are used to describe the gas flow in a shock tube:

1. The gas flow is one-dimensional.

2. The gas is ideal and has constant specific heats.

3. Heat transfer and viscosity effects are neglected.

4. Diaphragm rupture is instantaneous and does not disturb the subsequent gas flow.

The shock tube utilized in the present study has an overall length of 8 m, consisting of a driver, driven, converging and muzzle sections. The diameter of the driver and driven section is 0.15 m. The final muzzle diameter is 0.07 m. Two pressure transducers (fig. 3), mounted at the end of the muzzle section measure the incident shock pressure and the reflected shock pressure during the experiment. All of the glass specimens are subjected to the same level of incident pressure in this experiment. A typical pressure profile obtained at the transducer location closer to the specimen is shown in fig. 4. The reflected velocity for the plane glass panel is 450 m/s, for tempered glass is 330 m/s, for the wired glass panel is 400 m/s, for sandwich glass panel is 310 m/s and for laminated sandwich glass panel is 300 m/s.

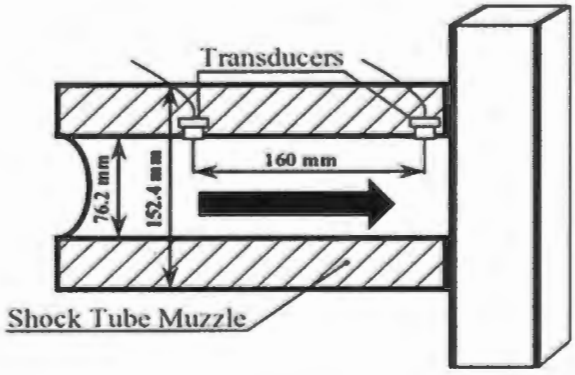

Figure 3: Schematics of the muzzle of the shock tube and fixture

3.3 Loading conditions

The square flat plate specimens utilized in this experimental study are held under fully clamped boundary conditions prior to blast loading. The size of the specimens is 305 mm × 305 mm x 6.5/7.5 mm. The dynamic loading is applied over a central circular area of 76.2 mm in diameter.

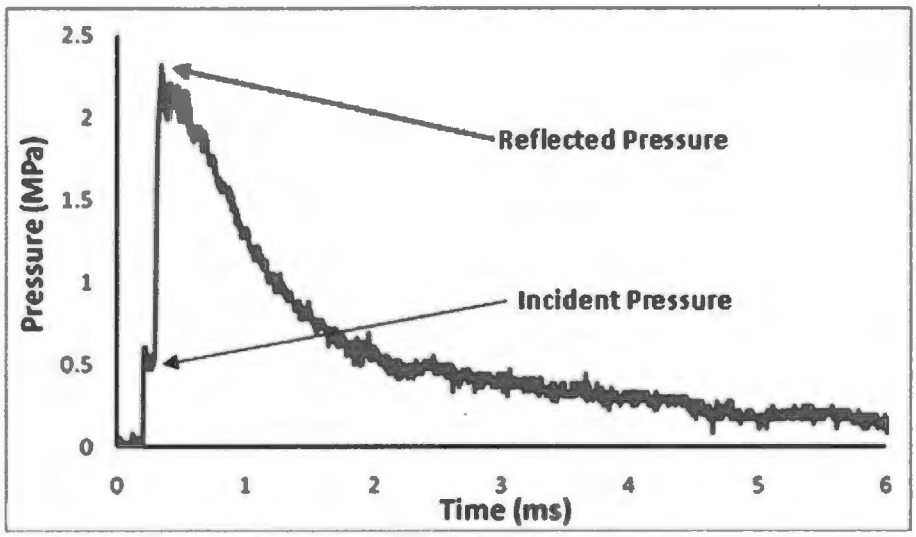

Figure 4: A typical pressure profile

3.4 Digital Image Correlation (DIC) technique

The digital image correlation technique is one of the most recent non-contact techniques for analyzing full-field shape and deformation. The main process involves the capture and storage of high speed images in digital form and subsequent post-processing of these images using the commercially available software to get the full-field shape and deformation measurements. The full-field shape and deformation measurement is obtained by the mapping of predefined points on the specimen. Two cameras are required for capturing the three dimensional response of the plates. These cameras must also be calibrated and have synchronized image recording throughout the event. The calibration of the cameras is performed by placing a predefined grid of dots in the test space where the glass specimens is located during the test. This grid is then translated and rotated both in and out of plane while recording the images. As this grid pattern has predetermined distances between the dots, the coordinates of the center of each dot is extracted from each image. The coordinate locations of each dot

extracted uniquely for each camera allows for a correspondence of the coordinate system for each camera. The DIC is then performed on the image pairs that are recorded during the shock event. Prior to testing the back face of the sample is painted white and then coated with a randomized speckle pattern (Figure 5). The post processing is performed with the VIC-3D software package which matches common pixel subsets of the random speckle pattern between the deformed and un-deformed images. The correlation of pixel subsets is used to calculate the three dimensional location of distinct points on the face of the panel throughout the duration of the experiment.

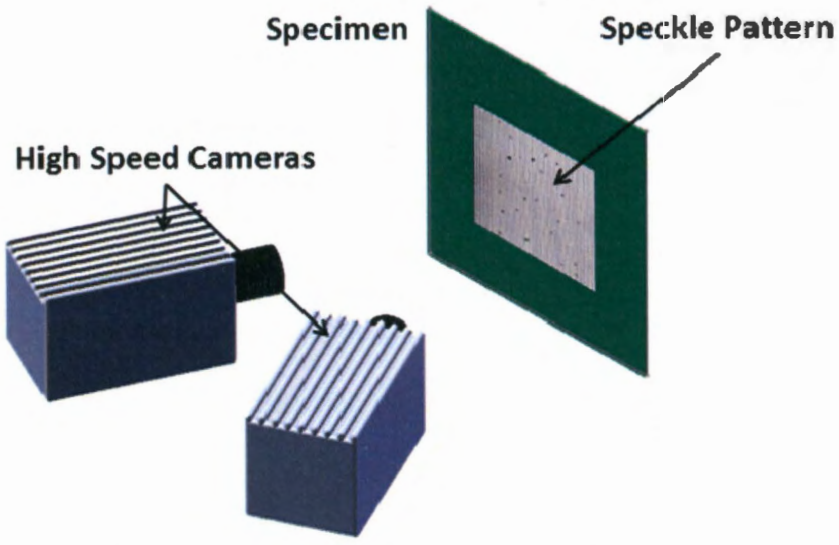

Figure 5: Schematic of DIC system

A speckle pattern is placed on the back face of the glass panel (as seen in fig. 5). Two high speed digital cameras, Photron SA1s, are positioned behind the shock tube apparatus to capture the real time deformation and displacement of the glass panel, along with the speckle pattern. The high speed cameras are set to capture images at 20,000 frames per second (inter frame time of 50 μs). During the blast

loading event, as the panel responds, the cameras track the individual speckles on the back face sheet. Once the event is over, the high speed images are analyzed using DIC software to correlate the images from the two cameras and generate real time in-plane strain and out-of-plane deflection histories. A schematic of the set-up is shown in fig. 5.

There are two key assumptions which are used in converting images to experimental measurements of objects shape, deflection and strain. Firstly, it is assumed that there is a direct correspondence between the motion of the points in the image and that in the object. This will ensure that the displacement of points on the image have a correlation with the displacement of points on the object. Secondly, it is assumed that each sub-region has adequate contrast so that accurate matching can be preformed to define local image motion.

4. Experimental results

The DIC technique (as discussed in section 2.4) is used to obtain the out-of-plane deflection and the in-plane strain on the back surface for all the five panels. The speckle pattern is applied onto the back face of the panels (fig. 5) which are subjected to shock loading. The high speed images captured using two Photron SA1 cameras are analyzed to get the back face deflections from the DIC as shown in fig. 6. Experiments have already been done to compare the back face deflection from the real time transient image and DIC to verify the accuracy of the DIC results. The error between the maximum deflection from DIC and real-time transient images is about 4% [14]. The DIC results are within the acceptable error limits and so the DIC results can be used to better understand the failure and damage mechanism in the panel.

The real-time full-field deflection of the different panels for the first 600 μs is shown in fig. 6. For a better understanding of blast mitigation properties, the center-point of this full-field analysis was chosen and out of plane deflection and in-plane strain data were extracted at this point. The center point deflections of all five panels are shown in fig. 7. The sandwich glass panel has a maximum deflection of 18 mm prior to complete fracture, whereas at the same time, the laminated sandwich glass panel shows a deflection of 9mm and no through hole formation. The tempered glass panel has a maximum deflection of 8 mm prior to fracture, the wired glass panel has a deflection of 6 mm and the plane glass panel shows a deflection of only 2 mm before shattering. The laminated sandwich glass panel did not fail catastrophically and had further deflection. The deflection history over an extended time for the laminated sandwich glass panel is shown in fig. 8. Also, the in-plane strains on the back face of the five different glass panels tested are shown in fig. 9. The sandwich glass panel has a strain of 5% before fracture initiates and at the same time the laminated sandwich glass panel only has a 1.7% strain (there was no through hole formation at this time), whereas in the case of the tempered glass panel it is 2%, 1% for the wired glass panel and 0.01% for the plane glass panel before fracture. The laminated sandwich glass panel did not fail catastrophically and deflected further which resulted in higher in-plane strain. The in-plane strain history for the laminated sandwich glass panel over an extended time is shown in fig. 10.

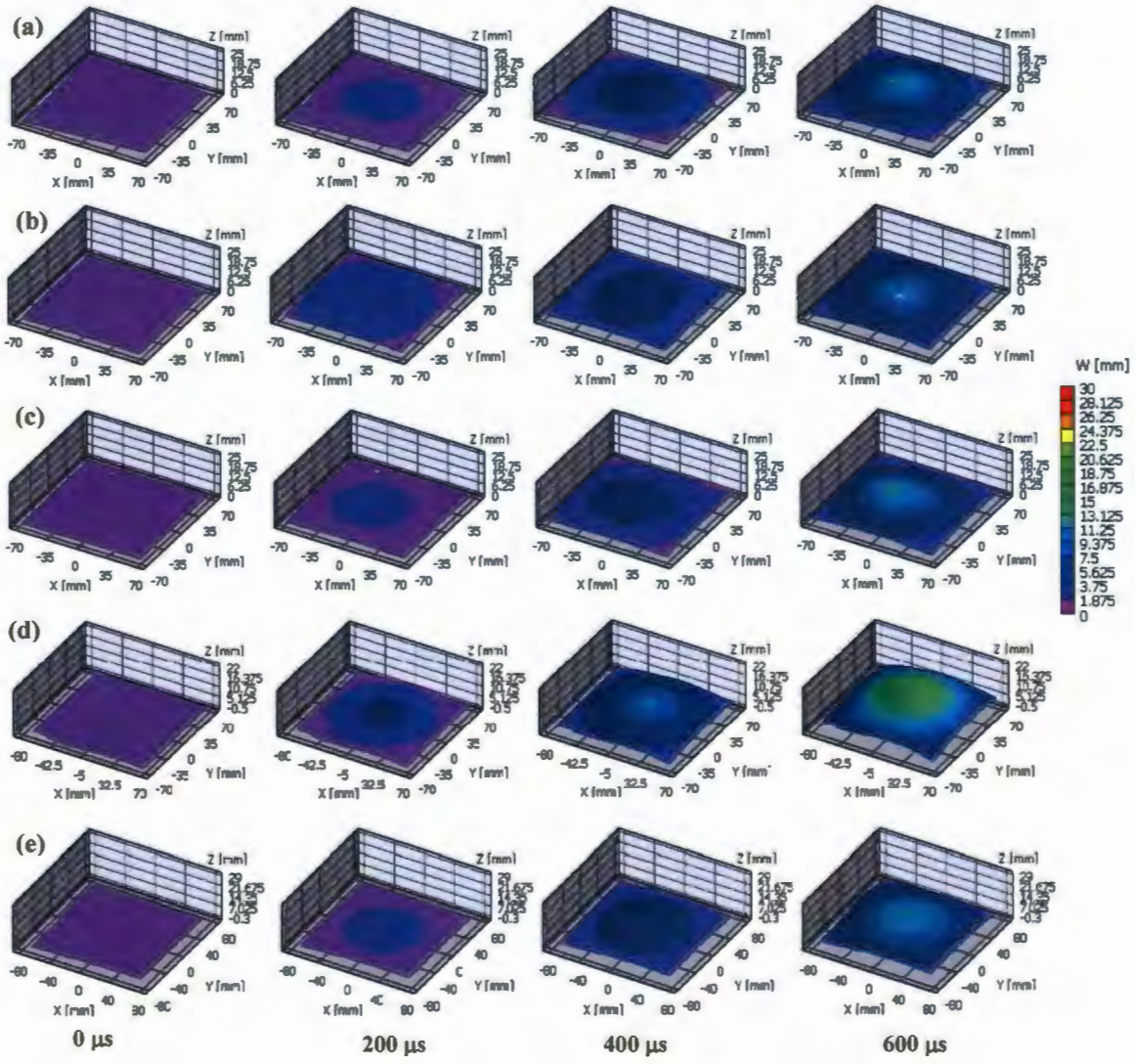

Figure 6: Time-deflection history of the back face for: (a) Plane Glass, (b) Tempered Glass, (c) Wired Glass, (d) Sandwiched Glass, & (e) Laminated Sandwiched Glass Panels

5. Discussion

5.1 DIC Analysis

The lamination of the sandwiched glass panel improved the blast mitigation properties of the laminate and also resulted in delayed deflection and damage

propagation (fig. 6). Also the laminated sandwich glass panel did not fail catastrophically. The deflection history over an extended time for the laminated sandwich glass panel (fig. 8) shows that the laminated sandwich panel has a maximum deflection of 28 mm and recovers back to a final deflection of 16 mm. The other important point is that it experiences fragmentation and cracking in the glass panel, but the protective film is able to contain the shattered glass pieces from flying off. Also, the extended in-plane strain history for the laminated sandwich glass panel (fig. 10) shows that the laminated sandwich panel has a maximum in-plane strain of 6% after which it recovers to 3%. Both, the time-deflection and in-plane strain history shows that the laminated sandwiched glass panel behaves in a more ductile manner as compared to the other glass panels. In reality, glass is a brittle material, but adhering the protective film on both the front and back face of the panel makes it more ductile as a structure and it helps in containing the shattered glass pieces. This avoids the catastrophic failure of laminated sandwich glass panel. The protective film also helps in dampening the incident shock wave as well as slowing the out of plane deflection of the glass which results in a lower strain rate.

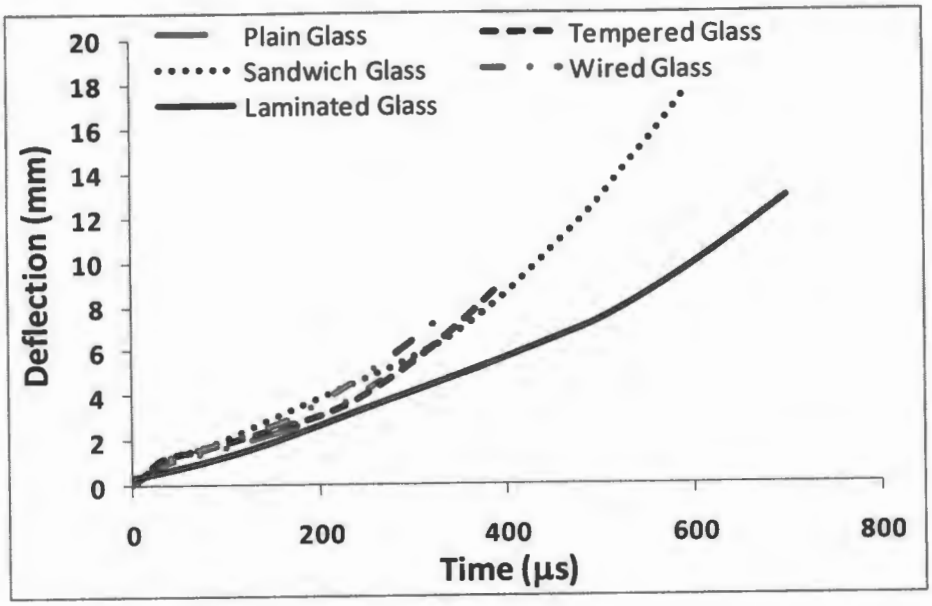

Figure 7: Time-deflection history of the back face for five glass panels

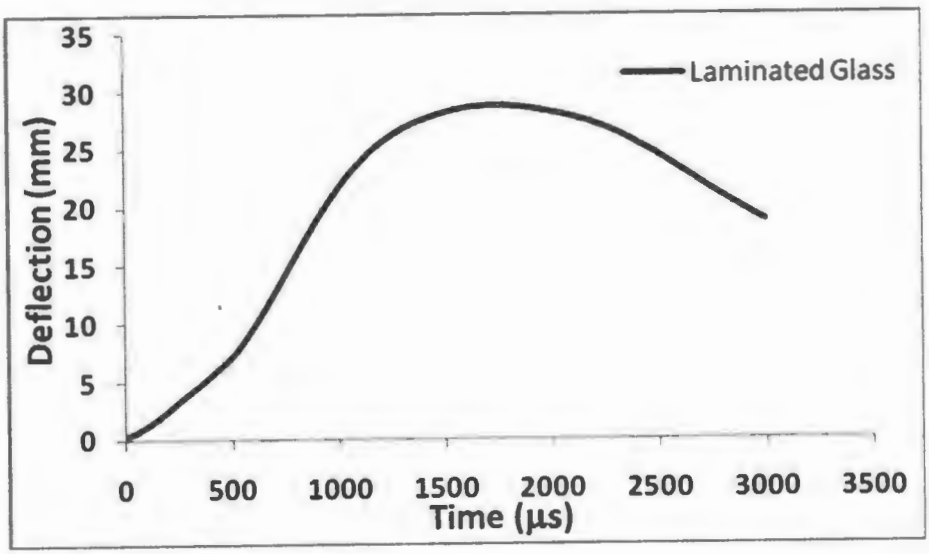

Figure 8: Time-deflection history of the back face for laminated sandwich glass panel

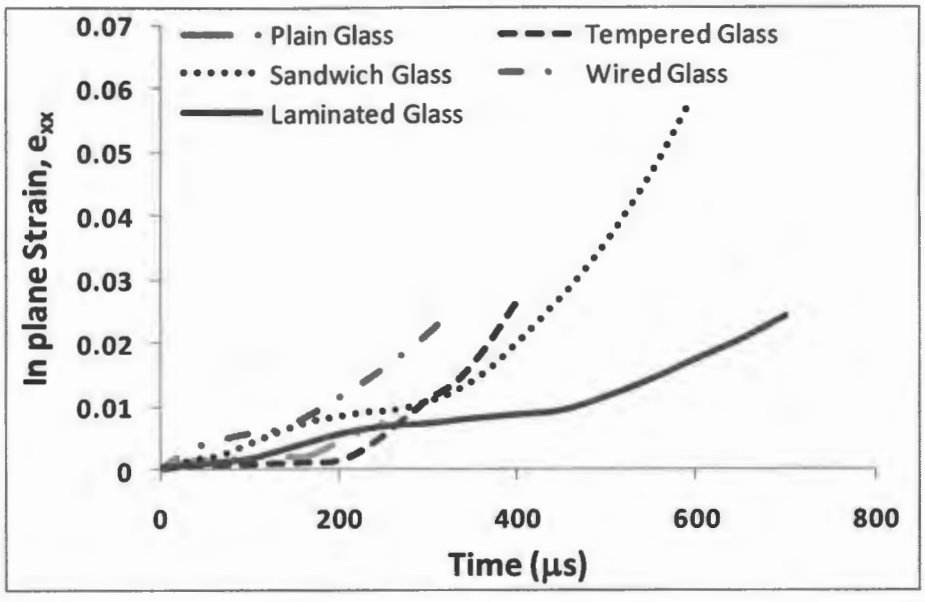

Figure 9: Time-in-plane strain history of the back face for five glass panels

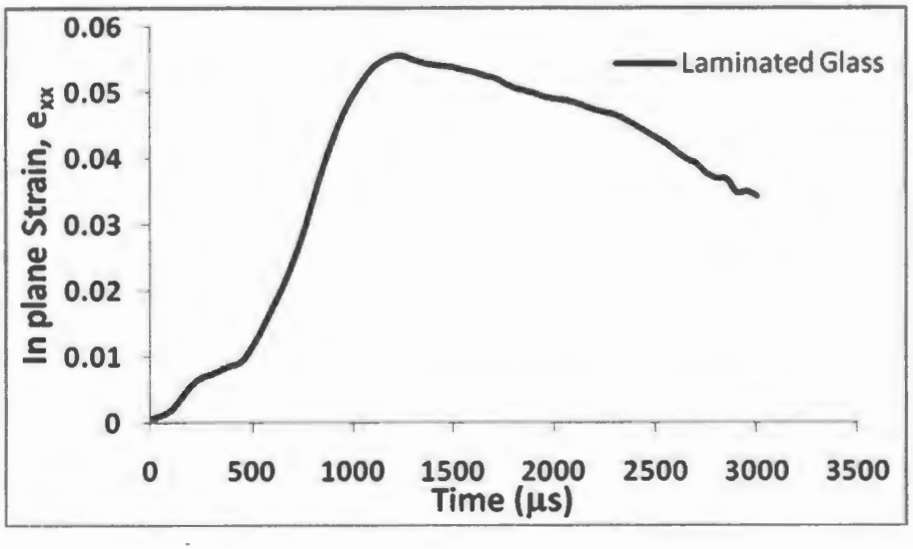

Figure 10: Time-in-plane strain history of the back face for laminated sandwich glass panel

5.2 Macroscopic post-mortem analysis

The result of post-mortem evaluation of the shock loaded glass panels is shown in Fig. 11-13. The post-mortem analysis of the clear glass and tempered glass panels have not been shown as they completely lost their structural integrity and shattered into pieces. The post-mortem analysis of a wired glass panel is shown in fig. 11. The panel shows a large amount of fragmentation but in comparison to the clear and tempered glass panel, which shattered completely, it retained structural integrity. The post-mortem image of the sandwiched glass panel is shown in fig. 12. There is heavy fragmentation on both the front and back face as seen in figs. 12(a)-12(b). The PVB interlayer is able to withhold a substantial amount of these fragments. The post-mortem images of the laminated sandwich glass panel are shown in Fig. 13. It is evident from the post-mortem images that there is substantial fragmentation in the case of the laminated sandwich glass panel. However, the protective film is able to contain these pieces and prevent them from flying off. Also, there is no cracking in either of the layers (both on the front and back face of the glass panel) of the protective film. The laminated sandwich glass panel is around 15% thicker than the other panels because of the protective film that had been adhered to both the front and back face of the panel. The higher thickness also contributes to the improved performance of the laminated sandwich glass panel. The laminated sandwich glass panel was also tested at a higher incident pressure (1 MPa, which is twice that of the incident pressure at which the other panels were tested) and it was found that the panel survived the shock loading and that there was no catastrophic failure.

(a) (b)

Figure 11: Post-mortem evaluation of Wired Glass Panel (a) Front view; (b) Back view

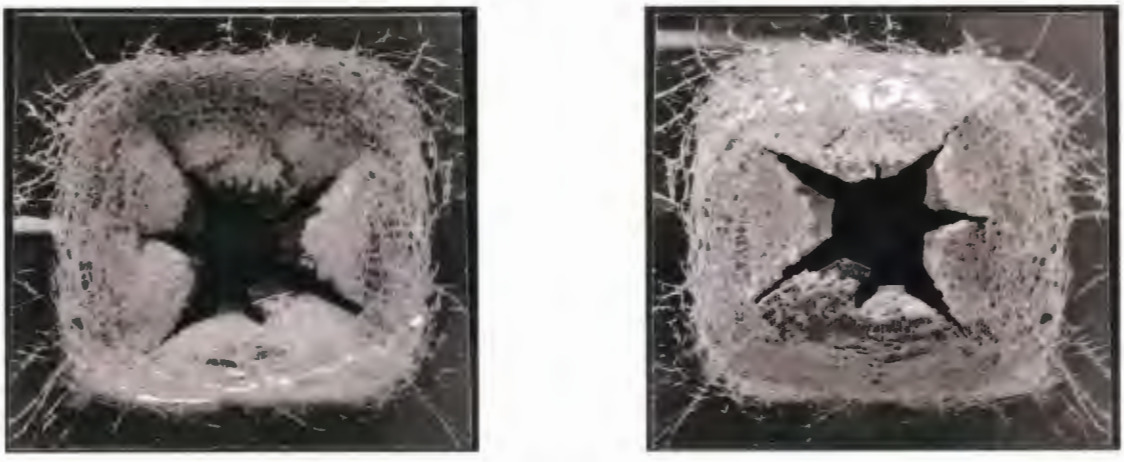

(a) (b)

Figure 12: Post-mortem evaluation of Sandwich Glass Panel (a) Front view; (b) Back view

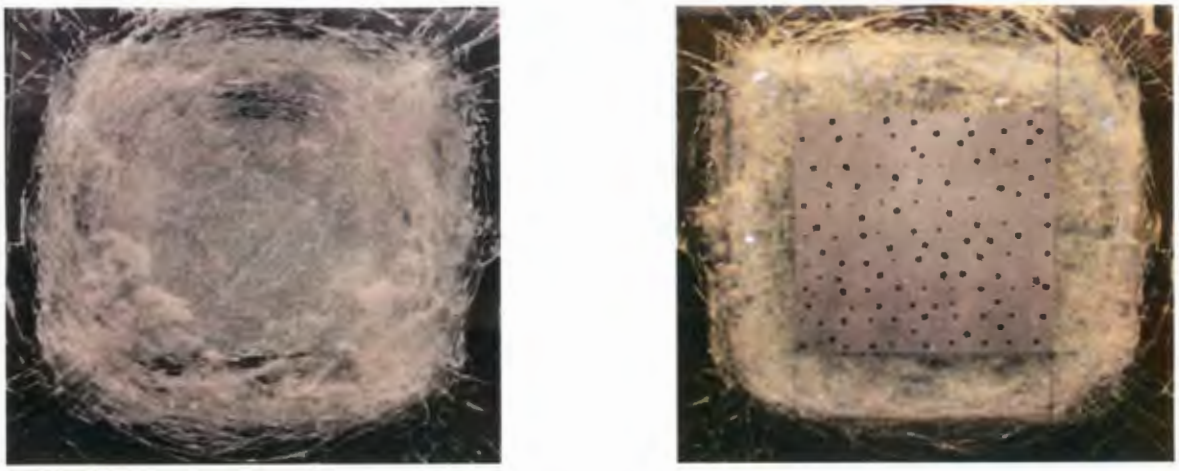

(a) (b)

Figure 13: Post-mortem evaluation of Laminated Sandwich Glass Panel (a) Front view; (b) Back view

Overall, it can be concluded that the laminated sandwich glass panel has better blast mitigation properties than the other four panels. The clear glass panel and tempered glass panel have the worst blast mitigation properties and are shattered into pieces when subjected to the shock loading. The sandwiched glass performs better than the wired glass panel, but it still has fragmentation and shattered glass pieces flying around. The fragmentation in the case of the sandwich glass panel is lower as compared to that in the wired glass panel. Also, the diameter of the through hole formed in the wired glass panel is larger as compared to that in the sandwich glass panel. This improvement in the blast response of the sandwich glass panel can be attributed to the PVB interlayer which helps in withholding some of the shattered glass pieces.

6. Conclusions

Five different panels are subjected to a controlled air blast loading using a shock tube. The high speed photography and DIC analysis is applied to obtain the out-of-plane deflection and in-plane strain on the back face of all the five panels.

1. The macroscopic post-mortem analysis and DIC deflection analysis shows that the sandwich glass panel has less damage due to blast loading as compared to the wired, tempered and clear glass panels. The PVB interlayer increases the flexural rigidity of the panels, and results in less damage when subjected to the shock loading.

2. The area of the through hole formed in the case of the sandwich glass panel was smaller as compared to that in the case of the other three glass panels. This will minimize the blast overpressure entering in the buildings and thus lower the damage inflicted as compared to the wired, tempered and plain glass panels.

3. The application of the protective film (XO-ARMOR®) on the front and back face of the sandwich panel further improves the blast mitigation property of the sandwich glass panel.

4. The laminated sandwich glass panel has fragmentation and cracking in the glass panel but the protective film is able to withhold the shattered glass pieces from flying off. Also, there is no through hole formation in the case of the laminated sandwich glass panel. This prevents the blast overpressure from entering the building and thus restricting the damage because of the overpressure.

Overall, the laminated sandwiched glass panels with PVB interlayer and protective film on both the faces has a better blast mitigation properties as compared to the other four panels.

7. Acknowledgement

The authors acknowledge the financial support provided by the Department of Homeland Security (DHS) under Cooperative Agreement No. 2008-ST-061-ED0002. We also thank XO-Armor for providing the XO- Film® for the preparation of laminated sandwich glass panel.

8. References

[1] H. Saito, and M. Masuda, Modeling of blast process using indenting method, Precis. Eng., pp. 369-377, 2004.

[2] G. A. Gogotsi, and S. P. Mudrik, Glasses: New approach to fracture behavior analysis, J. Non-Cryst. Solids, pp. 1021-1026, 2010.

[3] S. Bouzid, A. Nyoungue, Z. Azari, N. Bouaouadja, and G. Pluvinage, Fracture criterion for glass under impact loading, Int. J. Impact Eng., pp. 831-845, 2001.

[4] J. Wei, and L. R. Dharani, Fracture mechanics of laminated glass subjected to blast loading, Theor. Appl. Fract. Mech., pp. 157-167, 2005.

[5] J. Wei, M. S. Shetty, and L. R. Dharani, Stress characteristics of a laminated architectural glazing subjected to blast loading, Comput. Struct., pp. 699-707, 2006.

[6] T. Krauthammer, and A. Altenberg, Negative phase blast effects on glass panels, Int. J. Impact Eng., pp. 1-17, 2000.

[7] J. Wei, and L. R. Dharani, Response of laminated architectural glazing subjected to blast loading, Int. J. Impact Eng., pp. 2032-2047, 2006.

[8] J. Mencik, Strength and fracture of glass and ceramics, New York, Elsevier, 1992.

[9] P. Hooper, H. Arora, and J. P. Dear, Blast and impact resistance of laminated glass structures, Proceedings of the IMPLAST 2010 conference, October 12-14 2010, Providence, RI, USA.

[10] S. W. Carson, and V. D. Papanu, Improved mechanical performance of flat glass components through application of strength-increasing coatings, J. Non-Cryst. Solids, pp. 169-173, 1997.

[11] M. A. Sutton, Jean-Jose Orteu, and H. W. Schreier, Image Correlation for Shape, Motion and Deformation Measurements: Basic Concepts, Theory and Applications., Springer, 2009.

[12] J. LeBlanc, A. Shukla, C. Rousseau, and A. Bogdanovich, Shock loading of three-dimensional woven composite materials, Compos. Struct., pp. 344–355, 2007.

[13] J. Wright, Shock Tubes, John Wiley and Sons Inc., New York, 1961.

[14] N. Gardner, E. Wang, P. Kumar, and A. Shukla, Blast Mitigation in a Sandwich Composite Using Graded Core and Polyurea Interlayer, Exp. Mech., DOI 10.1007/s11340-011-9517-9

CHAPTER 2

EFFECT OF PLATE CURVATURE ON BLAST RESPONSE OF ALUMINUM PANELS

by

Puneet Kumar, James LeBlanc, David S. Stargel and Arun Shukla.

has been submitted in International Journal of Impact Engineering.

Corresponding Author: Arun Shukla

Dynamic Photo Mechanics Laboratory

Department of Mechanical, Industrial and Systems Engineering

University of Rhode Island

206 Wales Hall, 92 Upper College Rd

Kingston, RI, 02881, USA

Phone: +1-401-874-2283

Email Address: shuklaa@egr.uri.edu

1. Abstract

Experimental and numerical studies were conducted to understand the effect of plate curvature on blast response of aluminum panels. A shock tube apparatus was utilized to impart controlled shock loading to aluminum 2024-T3 panels having three different radii of curvatures: infinity (panel A), 304.8 mm (panel B), and 111.76 mm (panel C). Panels with dimensions of 203.2 mm x 203.2 mm x 2 mm were held with mixed boundary conditions before applying the shock loading. A 3D Digital Image Correlation (DIC) technique coupled with high speed photography was used to obtain out-of-plane deflection and velocity, as well as in-plane strain on the back face of the panels. Macroscopic postmortem analysis was performed to compare the yielding and plastic deformation in the three panels. The results showed that panel C had the least plastic deformation and yielding as compared to the other panels. A dynamic computational simulation that incorporates the fluid-structure interaction was also conducted to evaluate the panel response. The computational study utilized the Dynamic System Mechanics Analysis Simulation (DYSMAS) software. The model consisted of the shock tube wall, the aluminum plate, and the air (both internal and external) to the tube walls. The numerical results were compared to the experimental data. The comparison between the experimental results and the numerical simulation showed a high level of correlation using the Russell error measure.

Keywords

Plate Curvature, Aluminum Panels, Blast Loading, Digital Image Correlation, Numerical Simulation

2. Introduction

Accidental explosions or bomb blasts cause extreme loading on structures, which have both flat and curved geometries. Therefore it's important to understand the effect of curvature on the blast response. Aluminum panels having three different radii of curvature were subjected to shock loading using a shock tube in order to study their dynamic response. The choice of these panels was motivated by the study on the ballistic response of these panels by Stargel [1]. Real-time and post-mortem analysis was conducted on the panels to evaluate the effects of plate curvature on blast mitigation. In particular, the midpoint transient deflection, velocity, and final shape of the panel have been used to characterize the response of curved panels when subjected to a controlled blast loading. A computational model has been developed using DYSMAS which simulates the fluid-structure interaction during the blast loading process. The mid-point transient deflection and out-of-plane velocity obtained from the 3D-DIC analysis and numerical simulation have been compared. The Russell error measure has been used to quantify the level of correlation between the experimental results and numerical simulations.

In practice, there are two experimental methodologies used to impart shock loading to a structure: one is by using explosives and the other is by using shock tubes. Using real explosives in experiments is dangerous and has other disadvantages also. Spherical wave fronts and pressure signatures which are often spatially complex and difficult to measure are a few to mention. On the contrary, shock tubes offer the advantage of plane wave fronts and wave parameters that can be easily controlled.

Above all, these parameters are easy to replicate when using a shock tube and as such shock tube was the preferred choice of applying blast loading in our experiments.

There is a large volume of literature dealing with the blast loading of structures [2-5]. For brevity of space, only a few studies are mentioned here. Jacinto *et al.* [6] and Stoffle *et al.* [7] have studied the dynamic response of thin metallic plates subjected to varying levels of shock loading. Jacinto *et al.* [6] attached accelerometers to the non-impact face of the plates in order to measure the dynamic response, whereas Stoffle *et al.* [7] used a capacitance scheme to measure the center deflection during loading. Experimental studies performed by Nurick *et al.* [8], [9] and Wierzbicki *et al.* [10] examined the large deformations and failure modes of thin plates subjected to a blast loading. The plates were loaded with a pressure pulse of short duration generated by explosive charges. Langdon and Schleyer [11, 12] presented the results of experimental, analytical and numerical studies on the response of ¼ scale stainless steel blast wall panels and connection systems. ABAQUS was used to numerically simulate the process. Redekop [13] developed the linear elastic Mushtari-Vlasov-Donnel shell theory to study the problem of the moderately curved pipe subjected to local impulsive loading. Arora *et al.* [14] have recently presented a detailed experimental evaluation of glass-fiber reinforced polymer sandwich panels subjected to air-blast loading. They used high-speed photography coupled with digital image correlation (DIC) and post-mortem analysis to discuss various failure mechanisms. They also performed an in-depth numerical study using ABAQUS.

A comparative study of the effect of plate curvature on blast response of aluminum panels is lacking and thus the need for present study. The results from this

study show that the plate curvature has profound effect on blast mitigation. As the radius of curvature decreases (becomes more sharply curved), the area of plastic deformation decreases. The numerical simulations compared well with the experimental results.

3. Experimental Procedure

3.1 Material Details

Panels with three different radii of curvature were utilized in the experiments: infinite radius of curvature (Panel A), 304.8 mm radius of curvature (Panel B) and 111.76 mm radius of curvature (Panel C). The specimens are shown in fig. 1. Each experiment was repeated three times to assure consistent results. The specimens were 203.2 mm long x 203.2 mm wide x 2 mm thick, made out of 2024 T3 Aluminum. For the case of curved panels, the arc length of the curved edges is the same as (203.2 mm) the flat edges in these panels. Tensile testing of the material was performed in accordance with the ASTM E8 standard to characterize its material properties for use in the simulation. The tensile stress-strain curve is shown in fig. 2

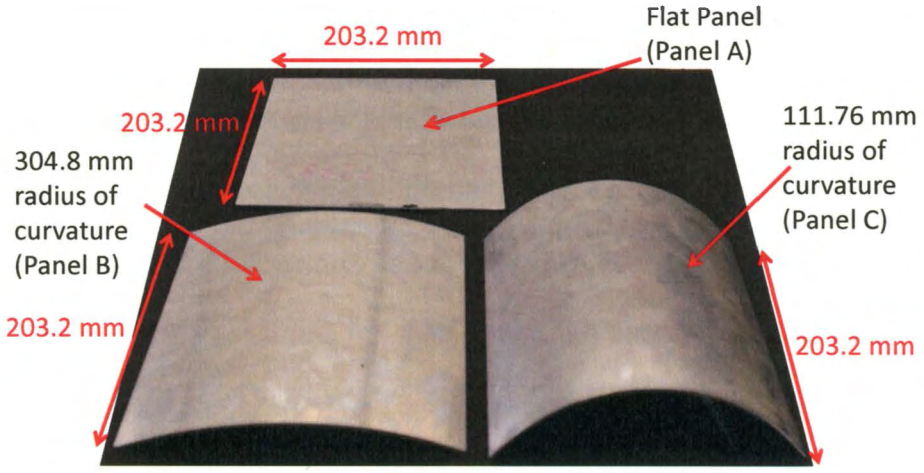

Figure 1: Specimens

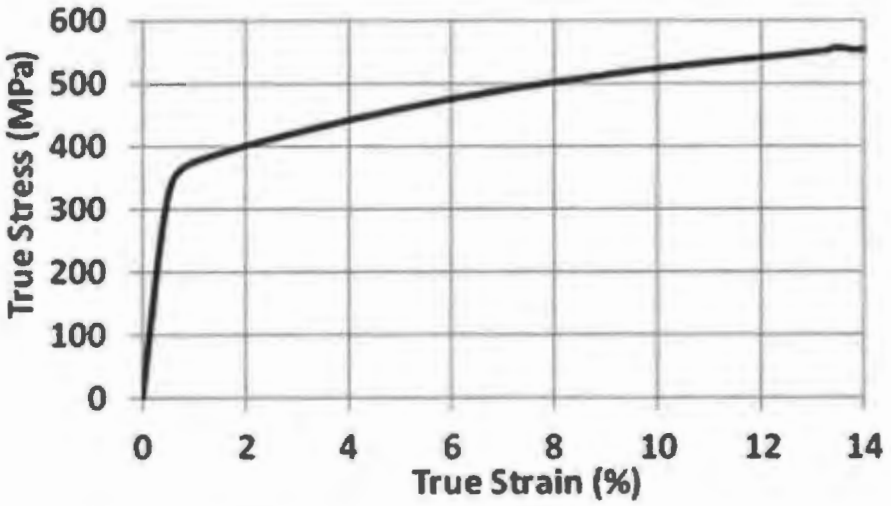

Figure 2: Aluminum 2024-T3 tensile Stress –Strain curve

3.2 Shock loading apparatus

The shock tube apparatus used in this study to obtain the controlled dynamic loading is shown in fig. 3. A complete description of the shock tube and its calibration can be found in [15]. In principle, the shock tube consists of a long rigid cylinder, divided into a high-pressure driver section and a low pressure driven section, which are separated by a diaphragm. By pressurizing the high-pressure section a pressure difference across the diaphragm is created. When this pressure differential reaches a critical value, the diaphragm ruptures. The subsequent rapid release of gas creates a shock wave, which travels down the tube to impart shock loading on the specimen.

When the shock wave impacts the specimen located at the end of the muzzle, the wave is reflected at a higher pressure than that of the incident shock pressure. The theoretical detail on the equations for shock tubes has been previously established in the literature and is briefly discussed in the following section [16]. There are four basic theoretical assumptions which are used to describe the gas flow in shock tube:

1. The gas flow is one-dimensional.

2. The gas is ideal and has constant specific heats.

3. Heat transfer and viscosity effects are neglected.

4. Diaphragm rupture is instantaneous and does not disturb the subsequent gas flow.

Using conservation of energy, mass, and momentum as described by Wright [16], the following relationships for pressure, temperature and density across a shock front can be derived:

$$\frac{P_2}{P_1} = \frac{2\gamma M_1^2 - (\gamma - 1)}{\gamma + 1}$$

$$\frac{T_2}{T_1} = \frac{\{2\gamma M_1^2 - (\gamma - 1)\}\{(\gamma - 1)M_1^2 + 2\}}{(\gamma + 1)^2 M_1^2}$$

$$\frac{\rho_2}{\rho_1} = \frac{M_1^2(\gamma + 1)}{(\gamma - 1)M_1^2 + 2}$$

where P_1, T_1, ρ_1 are pressure, temperature and density ahead of the shock front and P_2, T_2, ρ_2 are the pressure, temperature and density behind the shock front, γ is the adiabatic gas constant, and M_1 is the mach number of the shock wave relative to the driven gas.

Figure 3: The URI shock tube facility.

The shock tube utilized in the present study has an overall length of 8 m, consisting of driver, driven, converging and muzzle sections. The diameter of the driver and driven section is 0.15 m. The final muzzle diameter is 0.07 m. Two pressure transducers (fig. 4), mounted at the end of the muzzle section measure the incident shock pressure and the reflected shock pressure during the experiment. The incident shock wave pressure was kept constant for all of the experiments. A typical pressure profile obtained at the transducer location closer to the specimen is shown in fig. 5.

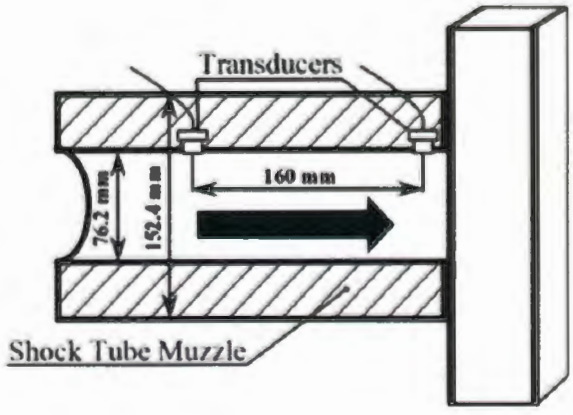

Figure 4: Schematics of the muzzle of the shock tube and fixture

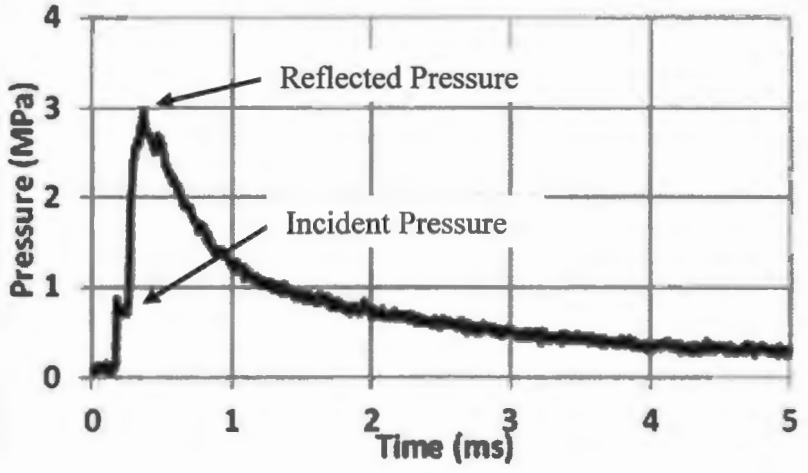

Figure 5: A typical pressure profile

3.3 Loading conditions

The specimens were held with clamped boundary conditions on the top and bottom edges and simply supported on the vertical edges. Appropriate fixtures for holding the three plate geometries are shown in fig. 6. The outer dimensions of the three fixtures are 305 mm x 305 mm (fig. 6(a)). For the two curved panels, appropriate curvature recess was welded on to the base plate (fig. 6(b) & 6(c)). The panels (fig. 1) were then placed in the recess in appropriate base fixtures. After this, two spacers were put over the panels on the top and bottom edges before putting the top plate over it and bolting it to the base fixture. The spacer on the top and bottom edges help in creating a clamped boundary condition. This whole arrangement is then mounted on a sturdy frame with base fixture resting on the frame and convex surface facing the shock tube. This frame prevents any rigid body motion of the whole arrangement.

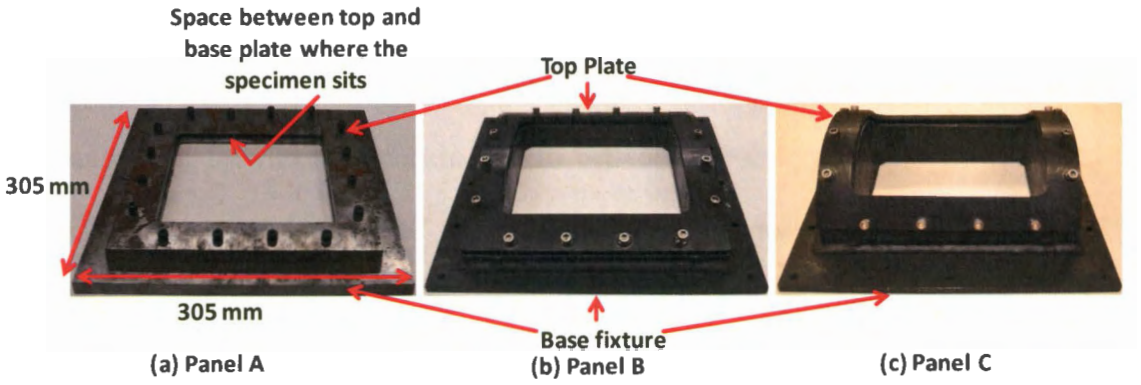

Figure 6: Loading Fixtures (test plates not included)

3.4 Digital Image Correlation (DIC) Technique

The digital image correlation technique is one of the most recent non-contact techniques for analyzing full-field shape and deformation [17]. The main process involves the capture and storage of high speed images in digital form and subsequent post-processing of these images using the commercially available software to get the full-field shape and deformation measurements. The full-field shape and deformation measurement is obtained by mapping of predefined points on the specimen. Two cameras are required for capturing the three dimensional response of the panels and they must be calibrated and have synchronized image recording throughout the event. The calibration of the cameras is performed by placing a predefined grid of pattern in the test space where the aluminum specimens is located during the experiment. This grid is then translated and rotated both in and out of plane while recording the images. As this grid pattern has predetermined distances between the speckles, the coordinates of the center of each dot is extracted from each image. The coordinate locations of each dot extracted uniquely for each camera allows for a correspondence of the coordinate system of each camera. The DIC is then performed on the image pairs that are recorded during the shock event. Prior to testing, the back face of the sample is

painted white and then coated with a randomized speckle pattern (Fig. 7). The post processing is performed with the VIC-3D software package which matches common pixel subsets of the random speckle pattern between the deformed and un-deformed images. The matching of pixel subsets is used to calculate the three dimensional location of distinct points on the face of the panel throughout time. Dynamic experiments have been done in the past [18] to compare the back face deflection from the real time transient image and DIC to verify the accuracy of the DIC results. The error between the maximum deflection from DIC and real-time transient images is 4%.

Two high speed digital cameras, Photron SA1s, were positioned behind the shock tube apparatus to capture the real time deformation and displacement of the panel. The high speed cameras were set to capture images at 20,000 frames per second (inter frame time of 50 μs). During the blast loading event, as the panel responds, the cameras record the speckles on the back face sheet. Once the event was over, the high speed images were analyzed using DIC software to correlate the images from the two cameras and generate real time in-plane strain and out-of-plane deflection/velocity histories. A schematic of the set-up is shown in fig. 7.

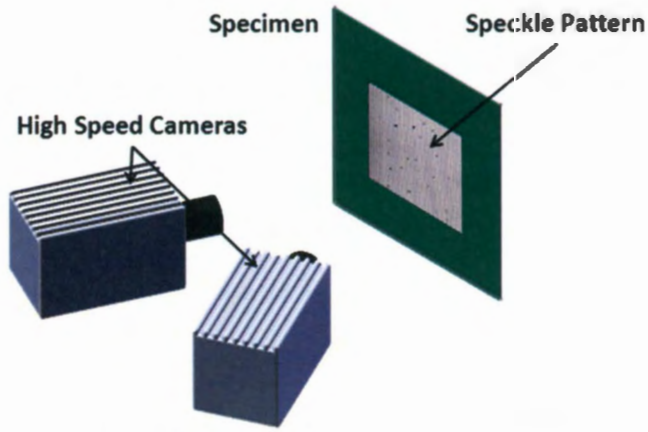

Figure 7: Schematics of DIC system

There are two key assumptions used in converting images to experimental measurements of objects shape, deflection and strain. First, it is assumed that there is a direct correspondence between the motion of the points in the image and that in the object. This will ensure that the displacement of points on the image have a correlation with the displacement of points on the object. Second, it is assumed that each sub-region has adequate contrast so that accurate matching can be performed to define local image motion.

4. Computational Modeling

Computational simulations of the shock loading events have been performed with the DYSMAS software. This software is developed and maintained by the Naval Surface Warfare Center, Indian Head. It consists of a Eulerian fluid solver, GEMINI, a Langrangian structural solver, DYNA_N, and an interface module which couples the two. Gemini is a high order Eulerian hydrocode solver for compressible, invicid fluids. DYNA_N is a Lagrangian non-linear, explicit finite element code for structural applications. The interface module is a standard coupler interface which allows the fluid and structural codes to share the required variables for the fluid structure interaction problem.

The computational models are built so as to capture the fluid structure interaction between the pressure front developed in the shock tube and the aluminum panels. The models consist of the shock tube wall, the aluminum plate, and the air within and external to the tube walls. The model results are compared to the experiment data and the correlations are discussed later in the paper.

4.1 Structural Model

The structural model consists of the shock tube wall and the aluminum panel. The model is a one-quarter (1/4) symmetry model with the plate lying in the x-y plane and the axis of the shock tube along the z axis. Both the panel and the tube wall are modeled with shell elements, which have 5 integration points through the thickness. The mid-surface of the panel has been modeled, while the inner surface of the tube wall is meshed. The Hughes-Liu element formulation is used for all elements, which for the shock tube wall allows for a shell thickness offset to be applied so that the inner surface may be modeled. The aluminum 2024-T3 panel is modeled with a tabular isotropic elastic–plastic (Type 24) material model with material properties taken from tensile test (fig. 2). The panel is modeled with quadrilateral elements with 1 mm edge lengths and a shell thickness of 2.032 mm. The elements comprising the shock tube wall have an edge length of 2 mm and a thickness of 25.4 mm.

4.2 Boundary Conditions

The boundary conditions applied to the model are representative of those applied in the experiments. During the experiments it was observed that the clamping force along the top edge is not sufficient to prevent the panel from slipping in the fixture. The clamping force however is able to prevent rotations along this edge. Therefore fully clamped conditions along this edge cannot be realistically applied in the simulation without over constraining the model. In lieu of fully clamped conditions a combination of three rigid walls and rotational constraints are applied. Two rigid walls are located on each side of the panel with a minimal clearance (>0.001 mm) to represent the front and back fixture plates. Additionally there is a rigid wall which is

perpendicular to the panel edge as seen in figure 8. This wall represents the top edge of the fixture recess that the plate would bottom out against if pushed up into the fixture as occurs in the curved plate simulations. In the test fixture there is a small gap (~1mm) between the plate and the fixture recess. The gap between the perpendicular rigid wall and the edge of the panel is taken to be that same as that of the actual clearance in the fixture. This method allows for the panel to pull or push away from the recess edge and to bottom out after an appropriate amount of motion. Only the nodes along the top edge of the panel are in contact with the rigid walls and the radius of curvature is neglected due to the small arc length being considered. Along this edge the three rotational degrees of freedom are fixed. The vertical edge is simply supported with the Z-translation set to zero. Along the X and Y planes appropriate symmetry conditions are applied, which along the X plane equates to X translation and Y/Z rotations being zero, and along the Y plane Y translation and X/Z rotations being zero. All degrees of freedom are fixed for the shock tube wall as this is assumed rigid during the test. Fig. 9 shows the orientation of three panels with respect to the shock tube muzzle. In this figure it is shown that each panel is oriented so that the convex face is towards the incoming shock front, and that the centerline of the curved plates is tangent with the face of the shock tube muzzle.

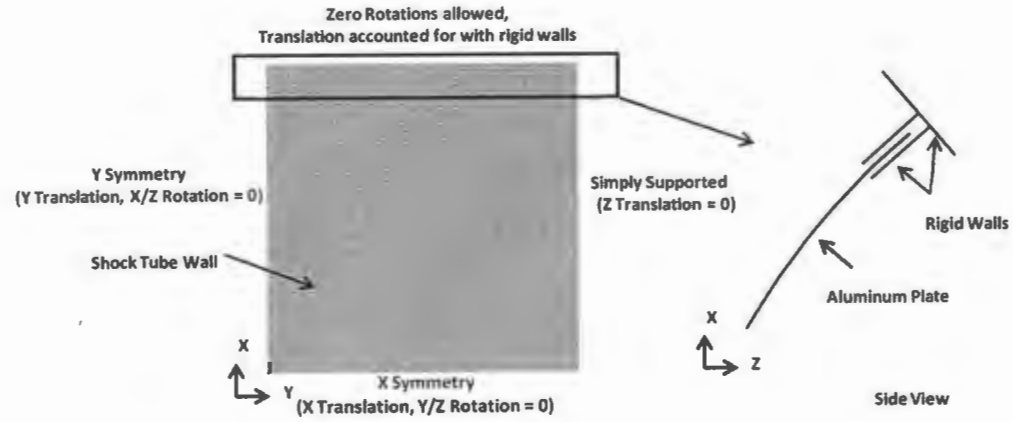

Figure 8: Structural Model (Boundary Conditions)

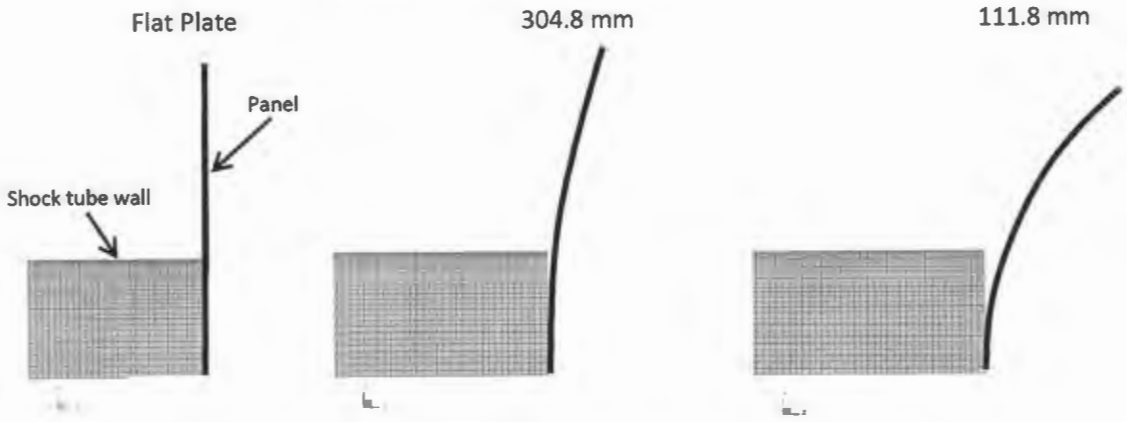

Figure 9: Orientation of Panels with respect to shock tube

4.3 Fluid Model

The fluid model consists of the air internal and external to the shock tube as well as the air surrounding the plate. The fluid domain is rectangular with a domain size of 400 mm in the X and Y directions and 2000 mm in the tube axis. There is 100 mm of air behind the plate to ensure that it remains in the fluid domain during the deformation event. Internal to the shock tube walls there are 12 fluid cells in the radial directions for a cell size of 3.175 mm. These cells are then tapered starting at the shock tube wall from 3.175 mm to 43 mm at the domain boundary. Along the tube axis the cells have an initial size of 5 mm at the end opposite of the plate and are

refined to 2.5 mm over 1000 mm in tube length. The cells have a size of 2.5 mm for the remainder of the tube length towards the plate. All cells in the fluid domain are initially air at 0.1 MPa which is modeled with an adiabatic, isentropic equation of state. The symmetry planes are modeled as wall boundary conditions and the outer extents of the domain have free (non-reflecting) conditions. The pressure field within the shock tube is developed by mapping in the pressure field resulting from a 2-D simulation. There are a total of 1.1 million fluid cells in the fluid domain.

4.4 Loading Conditions

The shock loading conditions at the plate are established using a two-step modeling approach. In the first stage an axisymmetric 2-D Euler domain is developed with a much more refined mesh than the full 3-D grid. This model contains the X-Z plane as shown in fig. 10. In this 2-D model a much more refined grid is used to ensure that the shock front develops correctly at the muzzle end of the tube and minimizes shock front distortion due to larger cell sizes. This model contains a region of high pressure air, ambient pressure air, and a region of blocked cells representing the shock tube wall, which GEMINI treats as a rigid material. In the 2-D simulation, the aluminum panel is omitted from the calculation as the goal is to establish the correct loading conditions before the wave front reaches the panel. The goal of the 2-D model is to establish a pressure field in the model that is equivalent to the pressure field that is measured during an experiment which was conducted with no plate. Several iterations of this model were run in which the magnitude and length of the high pressure region in fig. 10 were varied. For each iteration the pressure profile measured at the end of the shock tube in the simulation was compared to a

measurement taken during the test. Once the pressure profile in both the test and simulation were equivalent, the model was considered representative of the experiment with no test plate and was suitable for mapping into the fully coupled model. During the 2-D simulation, restart files are written during the propagation of the wave down the tube. By choosing a restart file just before the arrival of the shock front at the plate it is possible to use this file as a starting point in the full 3-D fluid domain which includes the panels. The axisymmetric pressure field in the 2-D simulation just before the shock front arrives at the plate location is then mapped into the 3-D full field fluid grid (fig. 11).

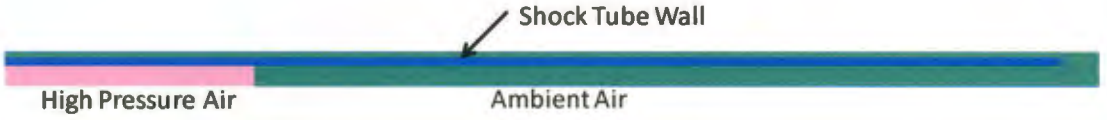

Figure 10: 2-D Axis-Symmetric Model – initial Conditions

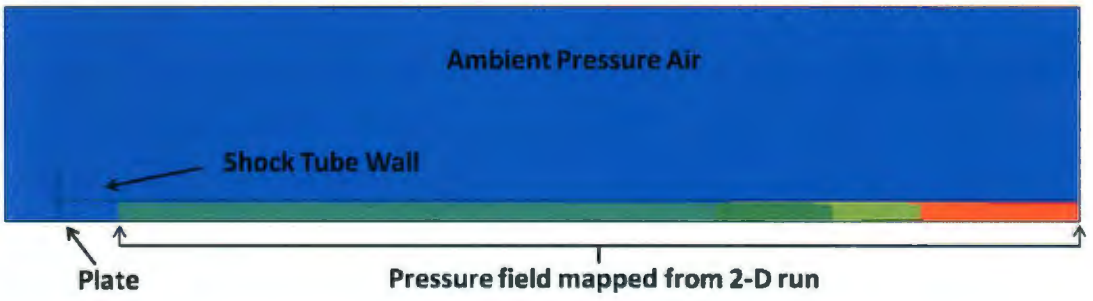

Figure 11: Full Model Pressure Field (Grid removed for clarity)

4.5 Complete DYSMAS Model

The complete computational model containing the structure and fluid is shown in fig. 12. In the model, the fluid and structure are coupled through the use of interface elements which define the "wetted surface" of the structure. In the model these surfaces are considered to be doubly wetted in which the fluid is considered to

act on both sides of the shell elements. For the case of the flat plate a mesh convergence study was conducted on both the structure and the fluid domain by beginning with a relatively coarse mesh and subsequently refining until a converged solution was obtained. The mesh presented in this paper represents the refinement level at which convergence occurred. This convergence study was performed for the flat plates, with the converged mesh sizing applied to the curved plates as well.

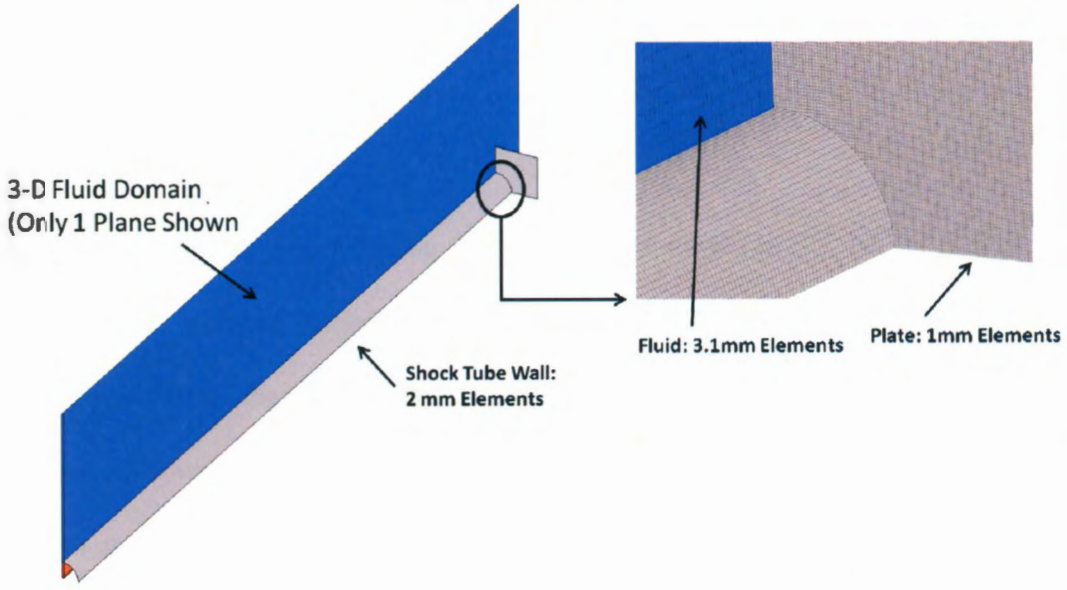

Figure 12: Full Computational Model (Only 1 GEMINI Plane Shown for Clarity)

5. Experimental results and Discussion

5.1 DIC Analysis

The DIC technique is used to obtain the out-of-plane deflections and velocities as well as the in-plane strains on the back surface for all the three geometries. The shock tube used in this study provides a uniform pressure pulse over a circular area of 4562.2 mm^2 (muzzle area). The DIC data in fig. 13 shows during initial time the deflection is approximately uniform (within 3mm $\pm$ 1 mm) over the central circular

region. The fig. also shows that the area of this circular deformation is the same as the area of the shock tube muzzle.

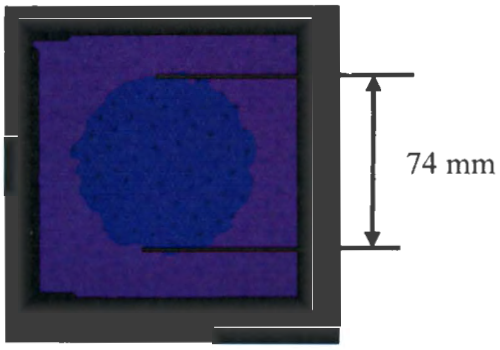

Figure 13: DIC analysis showing the deformed area during shock impingement at t = 50 μs

The full field deflection on the back face is shown in fig. 14. At 200 μs, there is a localized circular deflection contour in panel A which has roughly the same diameter as that of the muzzle. At this point the boundary conditions do not affect the deflection contours developing in the panel. Panels B and C had elliptical deflection contour at 200 μs. Since both these panels are curved, the shock wave impinges on the projected area and creates localized elliptical deflections as observed from the full-field deflection contours in fig. 14. These elliptical deflection contours are partially caused by the additional dissipation of the pressure pulse caused by the increased distance from the shock tube.

Around 400 μs, the circular deflection contour in panel A changes to square contour because of the boundary conditions. Simultaneously, the full field deflection overpasses the localized deflection in panel A. In case of panel B, the boundary conditions start affecting the deflection contours at around 600 μs when the elliptical contour changes to square shaped contour as seen in fig. 14.

The total deflection in these panels subjected to blast loading comprises of two distinct regions, namely, the indentation region followed by the flexural deflection. These different mechanisms are schematically shown in fig. 15. During indentation, localized deflection superpose onto the overall deflection. In case of flexure, the overall deflection starts to overpass the localized deflection. As seen in fig. 15, the indentation is localized around the loading area whereas a full field deflection over the area of the specimen being loaded is predominant in flexural mode.

As seen from the full-field out of deflection contours, panel A had an indentation mode of deformation till 400 μs at which time the deformation mechanism changes to flexural mode. In case of panel B, the indentation mode was dominant till 600 μs, when it changed to flexure mode. The deformation is primarily indentation in panel C as seen in fig. 14. Boundary conditions do not affect the deflection contour in panel C.

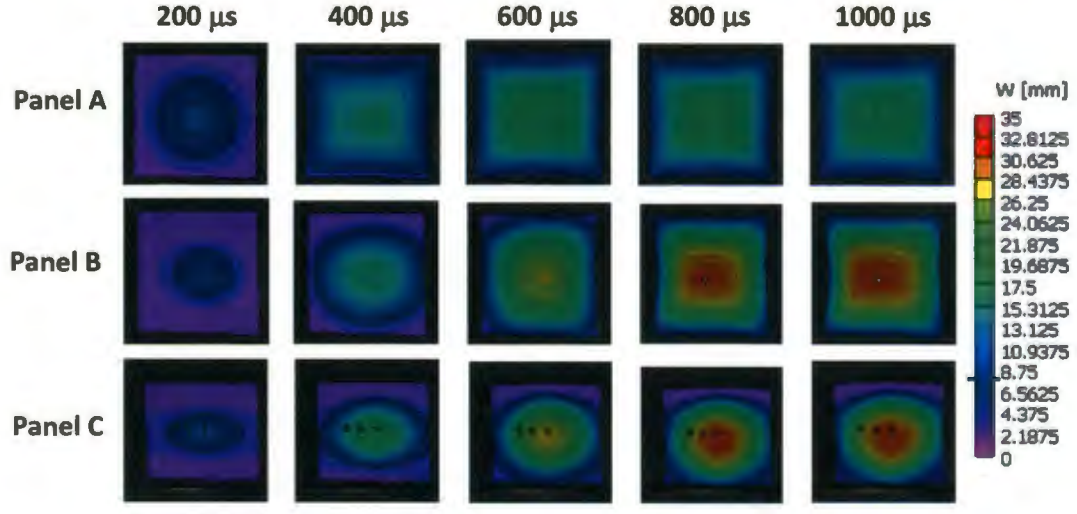

Figure 14: Full Field Deformation of panels from 3D-DIC analysis

Flexural mode of deflection Indentation mode of

Figure 15: Flexural and Indentation mode of deformation

From the full-field DIC analysis, the out-of-plane deflection and velocities and the in-plane strain data were extracted at the center point of the three panels using the commercially available VIC-3D software. A subset size of 27x27 pixel was chosen in the software. Lagrange finite tensor is used in in-plane strain determination. The Lagrangian finite strain tensor, also known as the Green-Lagrangian strain tensor, is a finite strain measure which includes higher order displacement terms; it defines gradients in terms of the original configuration.

From the time-deflection history (fig. 16) at the center point of the panels, it is seen that the deflection rate is almost same in all the three panels, but panels B & C attained a higher deflection as compared to panel A. This can be explained based on the fact that there is a longer duration of flexural deflection in the case of the panel A before it reaches the plateau region. In the case of the panel B, the initial deflection is because of indentation before it changes into flexural deformation, whereas in case of the panel C, it is because of indentation only.

Also, the in-plane strain, e_{yy}, (fig. 17) developed at a same rate in all of the three panels, but the peak strain is lower in case of panel A. This can be accounted for because of the different mechanism in deflection as explained above. In-plane strain rate was also calculated from the in-plane strain data obtained from full-field DIC analysis. Panel A had a strain rate of 43/sec, whereas the panel B had a strain rate of

36/sec, and the panel C had a strain rate of 41/sec. The in-plane strain rate was calculated from the in-plane strain data at the center point of the panel (fig. 17). It is calculated as the slope of the in-plane strain vs. time curve for the first 0.25 ms. Since the strain rates did not vary significantly, the curvature of the panel had no effect on the in-plane strain rate.

The kick-off velocity is almost same in all the three panels (fig. 18). The velocity in panel A decayed faster as compared to that in the other two panels, which accounts for the lower final deflection. The rate of velocity change (acceleration) was calculated from the out-of-plane velocity at the mid-point. It is 35.5 x 10^4 m/s^2 for the panel A, 30.5 x 10^4 m/s^2 for the panel B and 15.8 x 10^4 m/s^2 for the panel C. The acceleration in panel C is 0.44 times that of the infinite radius of curvature panel and 0.51 times the acceleration in panel B.

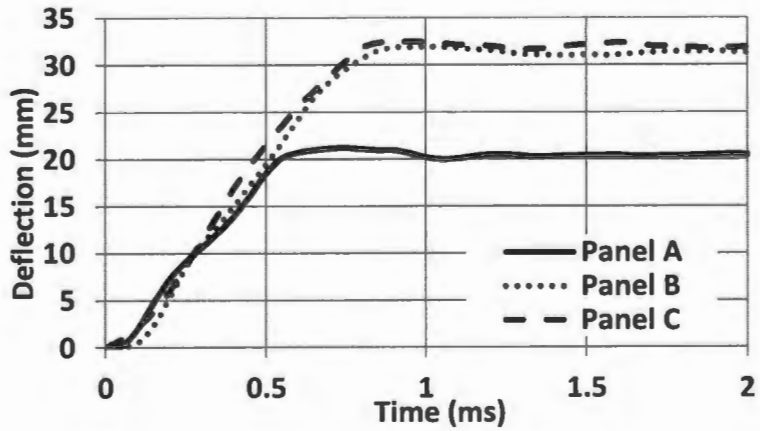

Figure 16: Time-deflection history of the back face for the three panels at the center point of the panels

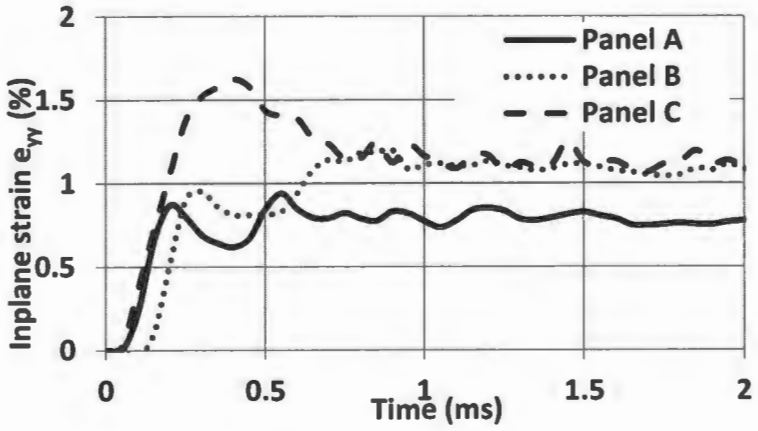

Figure 17: Time-in-plane strain history of the back face for the three panels at the center point of the panels

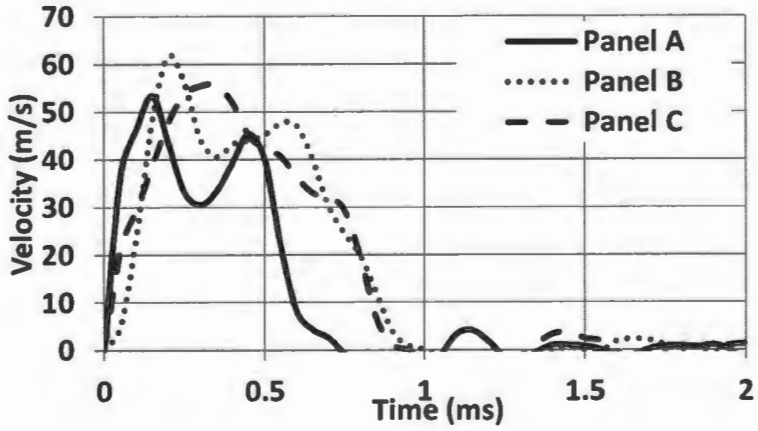

Figure 18: Time-Velocity history of the back face for the three panels at the center point of the panels

5.2 Macroscopic post-mortem analysis

The post-mortem images of the shock loaded aluminum panels are shown in fig. 19. Panels A and B had large inelastic deformations (Mode I deflection), whereas panel C exhibited localized indentation. The plastic deformation in panel A was much more pronounced when compared to the other two panels. It was the least in panel C. Panels A & B had plastic deformation over the whole non clamped surface, whereas panel C had plastic deformation over an arc length of 105 mm around the central

region. Panel A had perpendicular yield line formations (hinge formation) which extended from the panel corners towards the center of the panel as shown in fig. 19(a). A similar kind of hinge formation was observed in the panel B. These yield lines extended from the top corner to the bottom on both the edges as shown in fig. 19(b). Panel C had no yield line formation. It had an elliptically shaped plastically deformed region in the center (fig. 19(c)).

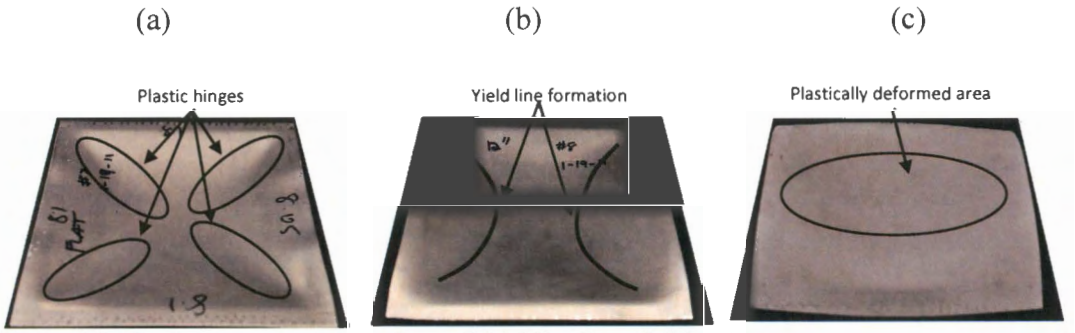

Figure 19: Post-mortem evaluation of (a) Flat Panel (b) 304.8 mm radius of curvature and (c) 111.76 mm radius of curvature

5.3 Finite Element Simulation Results

The DYSMAS simulation of the shock tube event allows for a visual observation of how the shock front interacts with and correspondingly loads the aluminum plate. In the actual experiment the pressure transducers only provide a point wise time history at the inner wall. The interaction from the simulation of the shock front and plate for the three plate geometries tested is shown in fig. 20. In this figure time zero is taken as the arrival of the shock front at the plate. From this figure it can be observed that although the inner radius of the tube is 38.1 mm the shock wave actually interacts with the plate over a larger area. This is due to the plate deformation and partial venting of the gas into the atmosphere. When the plate deforms, it allows an air gap to form between the plate and the face of the muzzle

which then allows the high pressure air comprising the shock front to act over a larger diameter area than the inner shock tube walls. It is also observed that although the incident shock front is narrow in width it quickly widens during the interaction with the plate due to the arrival of the still relatively high pressure air behind the shock front. This results in a reflected wave which is higher in magnitude than the incident wave (fig. 21). A comparison of the pressure history measured during the experiment and simulation for all the three different curvatures is shown in fig. 21. These pressure profiles are those which are measured by the transducer closest to the muzzle exit. Also, the pressure recorded by the transducer closer to the specimen is the pressure to which the specimen is subjected. This has been verified in an earlier publication and the details can be found in [19].

It is seen that the simulation is able to accurately model the incident and reflected pressure loading. Also the reflected peak pressures are different in all of the three panels. The peak reflected pressure for panel A and C is around 3 MPa and for panel B it is 2.5 MPa.

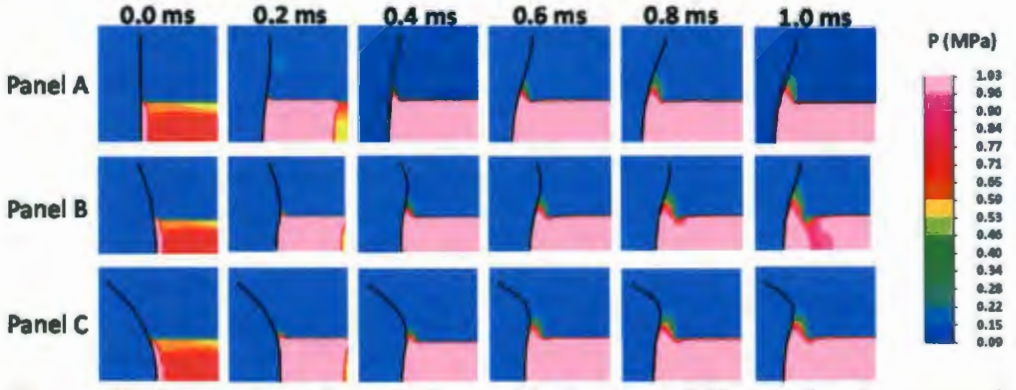

Figure 20: Interaction of shock front with the three different aluminum panels.

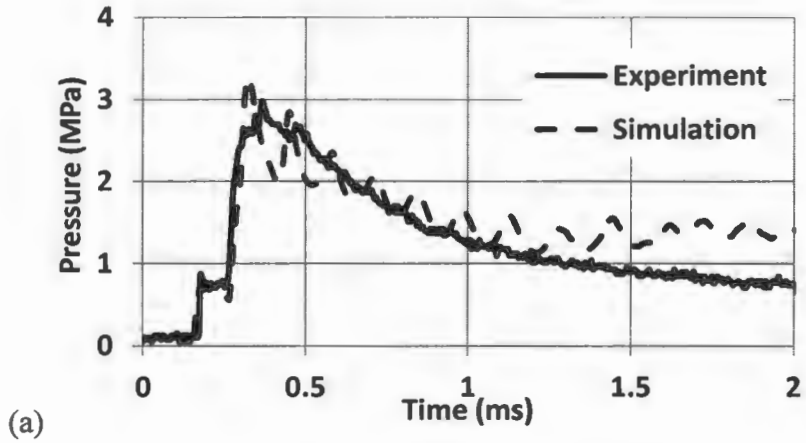

(a)

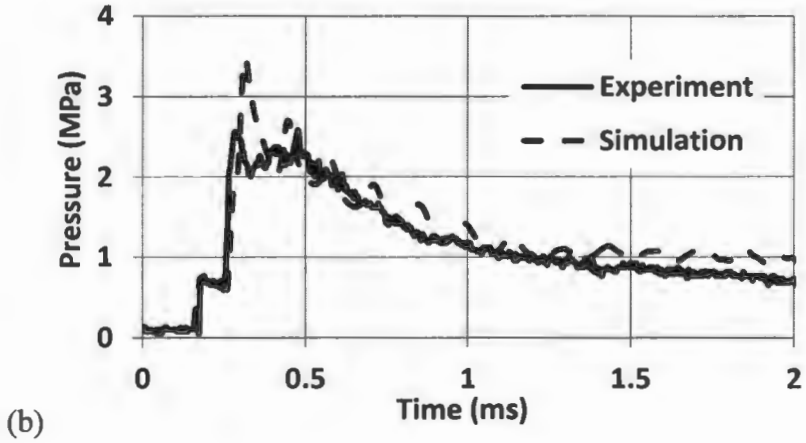

(b)

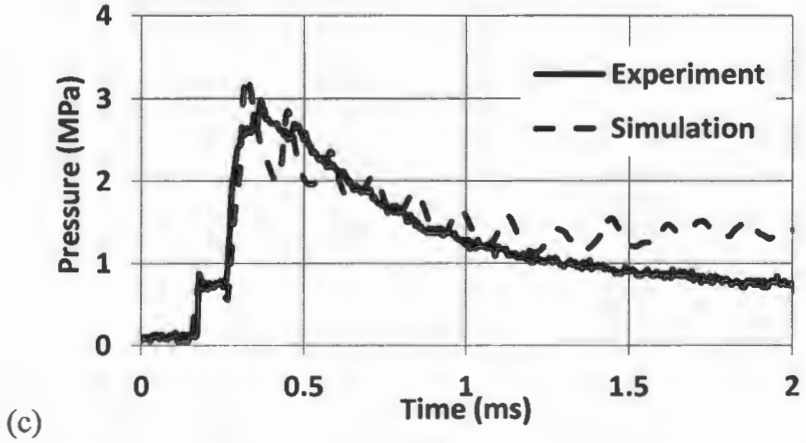

(c)

Figure 21: Experimental and Numerical Pressure profile for aluminum panels with (a) Infinite, (b) 304.8 mm and (c) 111.76 mm radii of curvatures.

6. Experiment and Simulation result correlation

6.1 RUSSELL ERROR MEASURE

The displacement and velocity data (fig. 22 & 23) that was captured during the experiments is used as a basis to correlate and validate the finite element model results. The quality of the correlation between the test data and numerical results in this study is quantified using the Russell Comprehensive Error measurement. The Russell error technique is one method which evaluates the differences in two transient data sets by quantifying the variation in magnitude and phase. The magnitude and phase error are then combined into a single error measure, the comprehensive error factor. The full derivation of the error measure is provided by Russell [20] with the phase, magnitude, and comprehensive error measures respectively given as:

$$RP = \frac{1}{\pi}\cos^{-1}\left(\left(\sum c_i \sum m_i\right) / \sqrt{\sum c_i^2 \sum m_i^2}\right)$$

$$RM = sign(m)\log_{10}\left(1+|m|\right)$$

where $$m = \left(\sum c_i^2 - \sum m_i^2\right) / \sqrt{\sum c_i^2 \sum m_i^2}$$

$$RC = \sqrt{\frac{\pi}{4}(RM^2 + RP^2)}$$

In the above equations c_i and m_i represent the simulated and experimentally measured responses respectively. Excellent, acceptable, and poor correlation using the Russell error measure is given as: Excellent - $RC \leq 0.15$, Acceptable – $0.15 < RC \leq 0.28$, and Poor $RC > 0.28$. These criteria levels are based on a study that was undertaken to determine the correlation opinions of a team in support of a ship shock trial. The details of the process used to determine the criteria are presented by Russell [21].

The DIC technique allows for the extraction of a large amount of data from the surface of the plates. The two variables that are used for correlation of the simulations to the experiments are the out of plane displacement and velocity. Time histories are extracted from the DIC data at the center point of the plates. The displacement comparisons are shown in fig. 22 and the velocity comparisons are provided in fig. 23. A summary of the Russell error for each of these comparisons is provided in table 1. From these comparison plots of the experimental and simulation data (fig. 22 & 23) it is seen that there is a high level of correlation between the experimental results and the computational simulations. It is noted here that the times of the simulation and experiments are arbitrary but are displayed using the simulation time. The two events are matched temporally by adjusting the experiment time until the first motions (deformation) of the center point align. This time offset is then held constant for all the velocity comparisons.

The displacement comparison for the panel A shows that the experiment and simulation results agree until 0.25 ms at which point the displacement in the experiment occurs slightly faster than the simulation for all the three panels. Also, the displacement takes place in a linear fashion until it reaches a plateau region. The peak deflection for the panel A is around 21 mm during the experiment and simulation before the motion arrests. For the case of panel B, the center point deflection correlates well between the experiment and simulation until 0.25 ms at which point the deflection in the experiment occur more rapidly than the simulation. The deflection reaches a maximum value of 31 mm and flattens out for the experiment, but during the simulation the deflection reaches a maximum value of 38 mm before flattening out at

a deflection of 34 mm. Panel C also shows a good correlation between the experimental and simulation deflection comparison until 0.25 ms, at which point the deflection in the experiments starts to occur at a slightly faster rate. Contrary to the behavior in panel B, the peak deflection is more pronounced during the experiment as compared to the simulation in panel C. The experimental peak deflection is around 34 mm, whereas it is 25 mm in the case of simulations.

In the velocity comparison, it is seen that there is an initial peak out□of□plane velocity of around 55 m/s for panel A and C. The kick-off velocity for the panel B is around 65 m/s. The velocities in all cases decay down to zero around 1 ms, corresponding to the time around which the deformation in the three panels reaches the plateau regime. It is seen that the simulation is not only able to capture the peak velocities seen in the experiments but also able to capture the secondary jumps in the velocity development over the time (fig. 23). Overall, it is shown that the Russell error values for the displacement comparisons show excellent correlation and the velocity comparisons have acceptable correlation for the center point. The velocity comparison at the center point for panel A and B falls just outside the excellent agreement criteria but well within the acceptable level (<0.28). Table 1 summarizes the Russell error values for magnitude, phase, and comprehensive for each comparison.

In addition to the point wise time histories, full field comparisons are made between the experiment and simulation. A comparison of the full field, out of plane displacement evolution is shown in figure 24. From this figure, it is seen that the experiment and simulation show good correlation both in times and in overall contour shape. The experiment shows some un-symmetric behavior in that the displacements

are slightly higher at the bottom edge of all the three panels, which can be accounted because of the variation in boundary condition and possible off-centered loading area. As expected, the simulation shows symmetric behavior because of the perfect boundary conditions and loading area. Overall, the displacements over the surface of the plate correlate well between the experiment and the simulation.

7. Conclusions

Three different panels have been subjected to a controlled shock loading using a shock tube. 3D DIC technique coupled with high speed photography is used to obtain the out-of-plane deformation/velocity and in-plane strain on the back face of all the three panels. Computational simulations using DYSMAS are performed.

1. The macroscopic post-mortem analysis and DIC deflection, velocity and in-plane strain analysis shows that the panel C (111.76 mm radius of curvature) has the least plastically deformed area out of the three panels. Also it has practically no yield line (hinge) formation as compared to the other two panels. This shows that panel C has a better blast mitigation property as compared to the other two panels.
2. As the radii of curvature becomes sharper the plastic deformation decreases. Also the flexural deformation decreases as the radius of curvature decreases. There is a limit to which the radius of curvature can be decreased. As the radius of curvature reduces to a limiting value, the shock wave will glide over the surface.

The displacement and velocity data from the DIC analysis from the experiments are correlated to the computational model by utilizing the Russell error. The Russell error

analysis showed that all the comparisons fall within the acceptable regime, including four in the excellent regime.

8. Acknowledgement

The authors acknowledge the financial support provided by the Department of Homeland Security (DHS) under Cooperative Agreement No. 2008-ST-061-ED0002. James LeBlanc acknowledges the financial support of the Naval Undersea Warfare Center, Division Newport through the NUWC Fellowship Program.

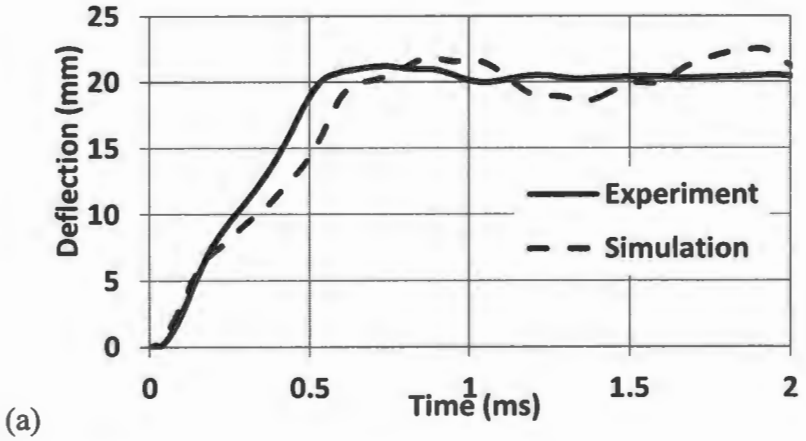

(a)

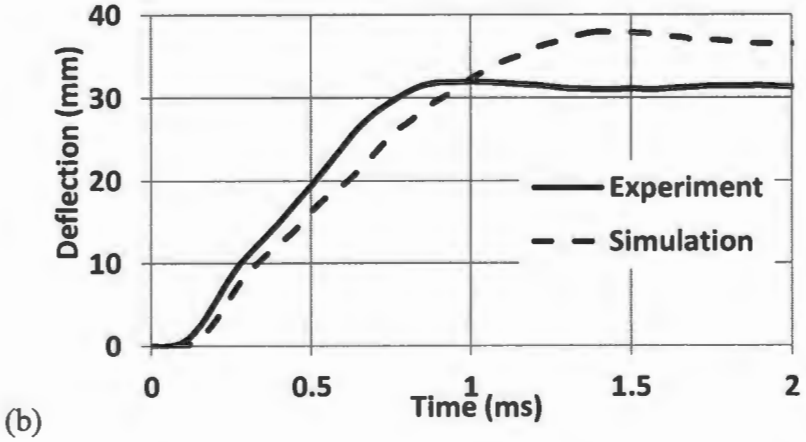

(b)

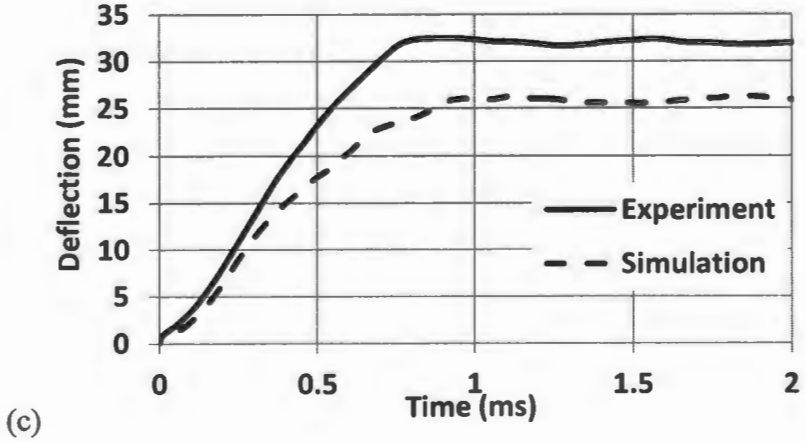

(c)

Figure 22: Experimental and Numerical comparison between center point deflection for aluminum panels with (a) Infinite, (b) 304.8 mm and (c) 111.76 mm radii of curvatures.

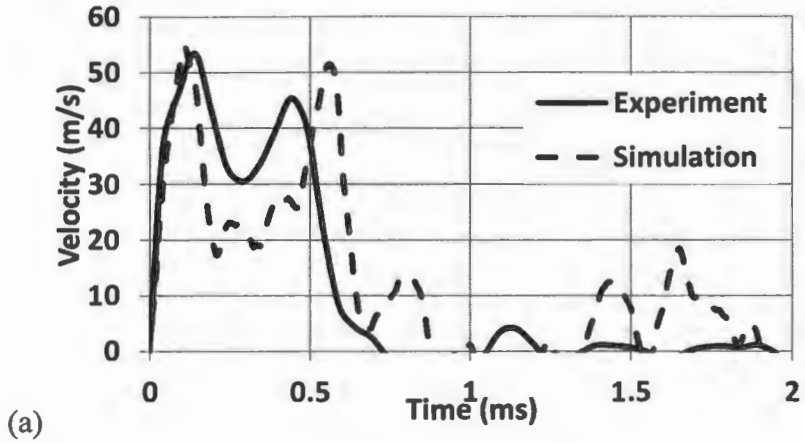

(a)

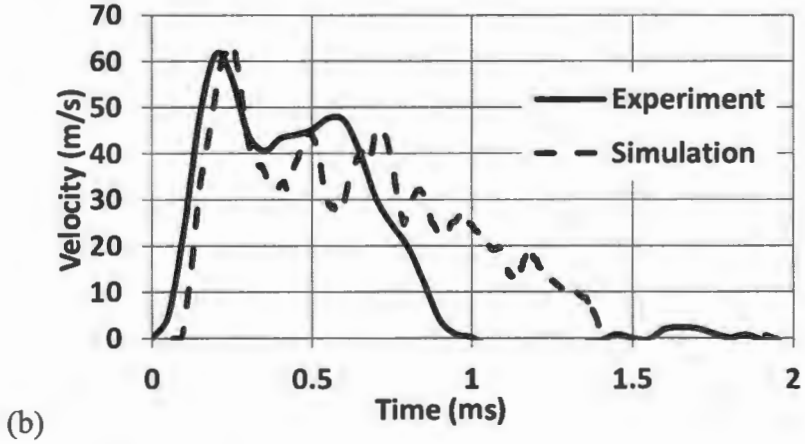

(b)

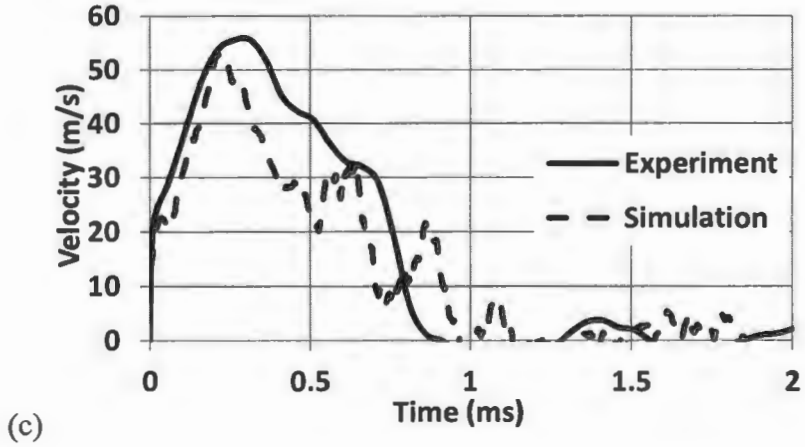

(c)

Figure 23: Experimental and Numerical comparison between center point velocity for aluminum panels with (a) Infinite, (b) 304.8 mm and (c) 111.76 mm radii of curvatures.

Table 1: Russell Error Summary.

	Magnitude Error	Phase Error	Comprehensive Error
Panel A			
Displacement	0.013	0.027	0.027
Velocity	0.023	0.189	0.169
Panel B			
Displacement	0.070	0.025	0.066
Velocity	0.004	0.156	0.138
Panel C			
Displacement	0.164	0.009	0.146
Velocity	0.170	0.090	0.170
Excellent (RC≤0.15)		**Acceptable (0.15<RC≤0.28)**	

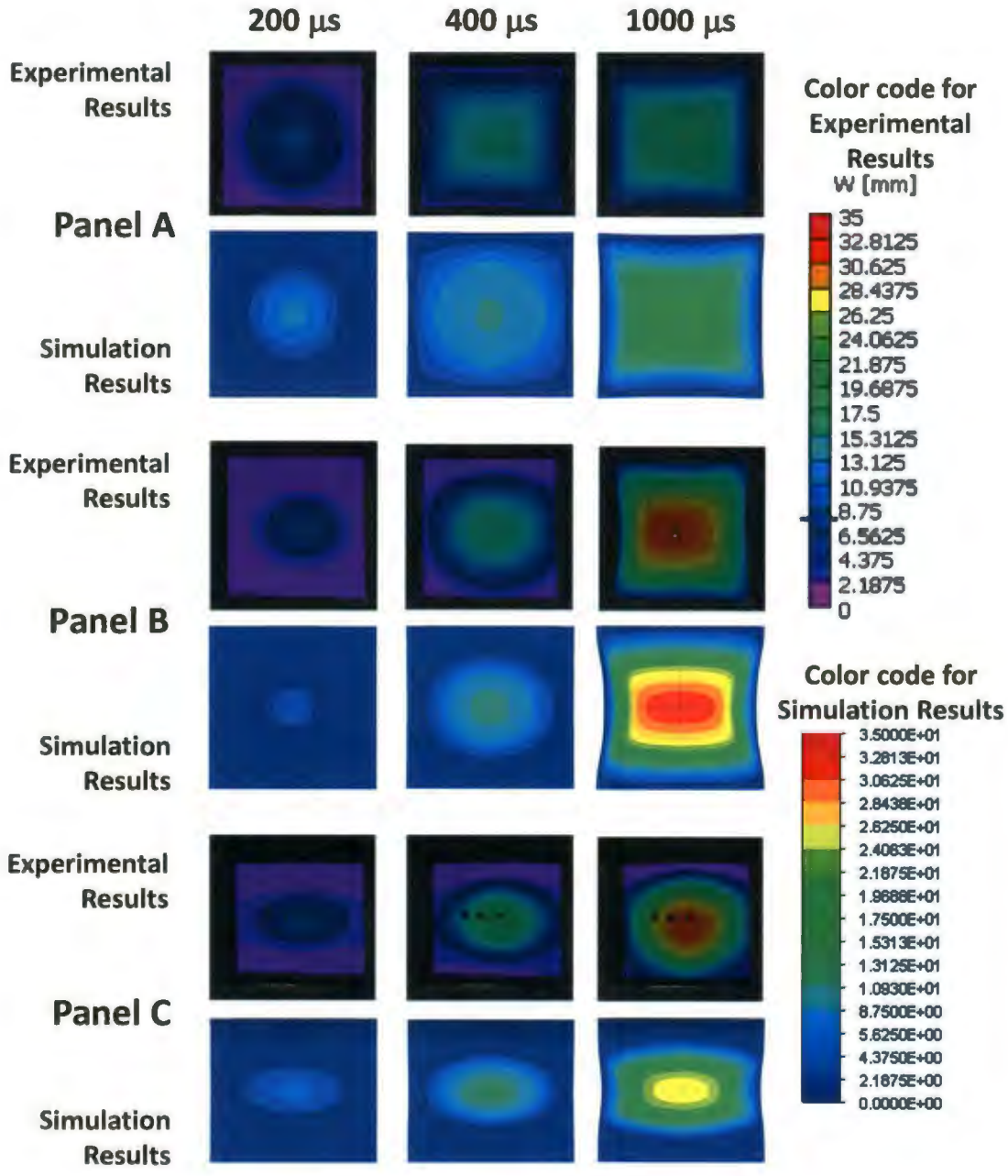

Figure 24: Full Field Deformation Comparison of Experiment and Simulation

9. References

[1] D.S. Stargel, Experimental and Numerical Investigation into the effects of Panel Curvature on the High Velocity Ballastic Impact Response of Aluminum and Composite Panels,. Doctor of Philosophy Dissertation, University of Maryland, College Park, 2005.

[2] L. Chun, and K.Y. Lam, Dynamic analysis of clamped laminated curved panels, Compos. Struct., 30 (1995) 389-398.

[3] R. Rajendran, and J.M. Lee, Blast loaded plates, Mar. struct., 22 (2009) 99-127.

[4] J.M. Biggs, Introduction to structural Dynamics, McGraw-Hill, New York, 1964.

[5] R.W. Clough, and J. Penzien, Dynamics of structures, McGraw-Hill, New York, 1975.

[6] A.C. Jacinto, R.D. Ambrosini, and R.F. Danesi, Experimental and computational analysis of plates under air blast loading, Int. J. Impact Eng., 25 (2001) 927-47.

[7] M. Stoffel, R. Schmidt, and D. Weichert, Shock wave loaded plates, Int. J. Solids Struct., 38 (2001) 7659-80, 2001.

[8] G. Nurick, M.D. Olson, J.R. Fagnan, and A. Levi, Deformation and tearing of blast loaded stiffened square plates, Int. J. Impact Eng., 16 (1995) 273-291.

[9] G. Nurick, and G.C. Shave, The deformation and tearing of thin square plates subjected to impulsive loads - an experimental study, Int. J. Impact Eng., 18 (1996) 99-116.

[10] T. Wierzbicki, and G. Nurick, Large deformation of thin plates under localized impulsive loading, Int. J. Impact Eng., 18 (1996) 899-918.

[11] G.S. Langdon, and G.K. Schleyer, Inelastic deformation and failure of profiled Stainless steel blast wall panels. Part I: experimental investigation, Int. J. Impact Eng., 31 (2005) 341-369.

[12] G.S. Langdon, and G.K. Schleyer, Inelastic deformation and failure of profiled Stainless steel blast wall panels. Part II: analytical modeling consideration, Int. J. Impact Eng., 31 (2005) 371-399.

[13] D. Redekop, Dynamic response of short curved pipes to impulsive loading, Int. J. Press. Vessels Pip., 61 (1995) 41-47.

[14] H. Arora, P.A. Hooper, and J.P. Dear, Dynamic response of full-scale sandwich composite Structures subject to air-blast loading, Composites Part A, 42 (2011), 1651-1662.

[15] J. LeBlanc, A. Shukla, C. Rousseau, and A. Bogdanovich, Shock loading of three-dimensional woven composite materials, Compos. Struct., 79 (2007) 344–355.

[16] J. Wright, Shock Tubes, John Wiley and Sons Inc., New York, 1961.

[17] V. Tiwari, M.A. Sutton, S.R. McNeill, S. Xu, X. Deng, W.L. Fourney, and D. Bretall, Application of 3D image correlation for full-field transient plate deformation measurements during blast loading, Int. J. Impact Eng., 36 (2009) 862-874.

[18] N. Gardner, E. Wang, P. Kumar, and A. Shukla, Blast Mitigation in a Sandwich Composite Using Graded Core and Polyurea Interlayer, Exp. Mech., DOI 10.1007/s11340-011-9517-9 (2011).

[19] E. Wang, and A. Shukla, Analytical and experimental evaluation of energies during shock wave loading, Int. J. Impact Eng., 37 (2010), 1188-1196.

[20] D.M. Russell, Error measure for comparing transient data, Part I: development of a comprehensive error measure, Part II: error measure case study, In Proceedings of the 68th shock & Vibration symposium, 3-6th November 1997.

[21] D.M. Russell, DDG53 Shock trial simulation acceptance criteria, In 69th shock and vibration symposium, 12-19th October 1998.

CHAPTER 3

EFFECT OF PLATE CURVATURE ON BLAST RESPONSE OF CARBON COMPOSITE PANELS: EXPERIMENTAL INVESTIGATION

by

Puneet Kumar, David S. Stargel and Arun Shukla.

Under preparation for submission in Journal.

Corresponding Author: Arun Shukla

Dynamic Photo Mechanics Laboratory

Department of Mechanical, Industrial and Systems Engineering

University of Rhode Island

206 Wales Hall, 92 Upper College Rd

Kingston, RI, 02881, USA

Phone: +1-401-874-2283

Email Address: shuklaa@egr.uri.edu

1. Abstract

Experimental studies were conducted to understand the effect of plate curvature on the blast response of 32 layered carbon fiber epoxy panels. A shock tube apparatus was utilized to impart controlled shock loading on carbon fiber panels having three different radii of curvatures; infinite (panel A), 305 mm (panel B), and 112 mm (panel C). These panels with dimensions of 203 mm x 203 mm x 2 mm were held under clamped boundary conditions during the shock loading. A 3D Digital Image Correlation (DIC) technique coupled with high speed photography was used to obtain out-of-plane deflection and velocity, as well as in-plane strain on the back face of the panels. There were two types of failure mechanism observed in all the three panels: fiber breakage and inter-layer delamination. The fiber breakage was induced from on the face exposed to the shock loading (front face) and continued to the interior. Delamination occurred on the side of the specimen as well as on the front face. Macroscopic postmortem analysis and DIC results showed that panel C can mitigate higher intensity (pressure) shock waves without initiation of catastrophic damage in the panel. Panel B could sustain the least shock wave intensity and exhibited catastrophic failure. Panel A exhibited intermediate blast mitigation capacity.

Keywords

Plate Curvature, Carbon Composite Panels, Blast Loading, Digital Image Correlation,

2. Introduction

A controlled experimental study has been conducted to understand the effect of plate curvature on the blast response of carbon composite panels. Accidental

explosions or bomb blasts cause extreme loading on structures, which have both flat and curved geometries (as in the USS Cole and Oklahoma State bombing). Therefore it is important to understand the effect of curvature on the blast response. Also, a better understanding of the effect of curvature will help in manufacturing new structures with better blast resistant property. Carbon composite panels having three different radii of curvature were subjected to shock loading using a shock tube in order to study their dynamic response. The choice of these panels was motivated by the study on the ballistic response of these panels by Stargel [1]. Real-time and post-mortem analysis was conducted on the panels to evaluate the effects of plate curvature on blast mitigation. In particular, the midpoint transient deflection, velocity, and macroscopic post-mortem analysis of the panels has been used to characterize the response of curved panels when subjected to a controlled blast loading.

Experimentally shock loading on structure can be imparted using two different methods: one is by using explosives and the other is by using shock tubes. The use of real explosives is dangerous and has spherical wave fronts and pressure signatures which are spatially complex and difficult to measure. On the contrary, shock tubes offer the advantage of planar wave fronts and wave parameters that can be easily controlled. Above all, these parameters are easy to replicate when using a shock tube and as such shock tube was the preferred choice of applying blast loading in our experiments.

There is a large volume of literature dealing with the blast loading of structures [2-11]. For brevity of space, only a few studies are mentioned here. Franz *et al.* [12] studied the response of glassfiber chopped-strand mat laminates to air pressure blast.

They found matrix cracking, delamination/debonding, and penetration as final damage in monolithic and layered laminates with varying areal density. Khalili *et al.* [13] concentrated on numerical analysis of composite laminates and shell structures subjected to low-velocity impacts using ABAQUS. They studied the effect of element type, solution method, impactor modeling method, meshing pattern and contact modeling on the accurate numerical modeling. Ochola *et al.* [14] concentrated on strain rate sensitivity of both carbon fiber reinforced polymer and glass fiber reinforced polymer by testing a single laminate configuration with strain rate varying from 10^{-3} and 450 s^{-1}. Results showed that the dynamic material strength for GFRP increases with increasing strain rate and the strain to failure for both CFRP and GFRP decreased with increasing strain rate. Hosur *et al.* [15] investigated the unidirectional and cross-ply carbon/epoxy laminates under high strain rate compression loading using modified split Hopkinson Pressure Bar. They found that the dynamic strength and stiffness increased considerably with the strain rates. LeBlanc and Shukla [16] studied the underwater shock loading response of E-glass/Vinyl ester curved composite panels. They used the 3D-DIC system for measuring the transient response during the experiments. They also compared the experimental results to simulation results obtained from the commercially available Ls-Dyna finite element code, which showed a high level of correlation using the Russell error measure. Pankow *et al.* [17] analyzed the effect of 3D weaving in composites to two different intensities of shock loading using the DIC technique. They found an optimal Z-fiber architecture (6%) out of the three different architectures, which was responsible for largest panel stiffness and least amount of damage. They also observed matrix micro-cracking at the center

of the panel which caused the failure initiation in the panels. Shen *et al.* [18] experimentally investigated the response of sandwich panels with aluminum face sheets and aluminum foam core. Panels with varying curvatures (two different curvatures), and different core/face sheet configurations were tested at three different blast intensities. They found that the initial curvature of the sandwich panel changes the deformation mode and improved the performance of the structure when compared to equivalent flat plate. Karagiozova *et al.* [19] studied the experimental and numerical response of sandwich panels to blast loading. They compared the response of panels with steel plates and polystyrene cores to panels with steel face sheets and aluminum honeycomb cores and found that the aluminum honeycomb cores performed better than those with the polystyrene core (in panels with comparable mass). Hause and Librescu [20] developed a closed-form solution for comparison with numerical based solutions based on the extended Galerkin method for designing doubly-curved sandwich panels operating under dynamic loading.

The literature review shows a data gap in the study of the effect of plate curvature on blast response of carbon composite panels. Thus the present study was performed to the fill up this gap. The results from this study show that the plate curvature affects the blast mitigation property. As the radius of curvature decreases (becomes more sharply curved), the response of panels to sustain shock loading changes.

3. Experimental Procedure

3.1 Material Details

Panels with three different radii of curvature were utilized in the experiments: infinite radius of curvature (Panel A), 304.8 mm radius of curvature (Panel B) and 111.8 mm radius of curvature (Panel C). The specimens are shown in fig. 1. The specimens were fabricated using ready-to-cure sheets of unidirectional AS4/3501-6 material manufactured by the Hercules corporation of Magna, Utah. These sheets were manufactured by pulling a row of uniformly spaced fibers through resin bath. The spacing between the fibers determines the ratio of fiber volume to total volume of the material. After stacking 32 plies of theses unidirectional material in the desired orientation, the panels were vacuum bagged and then placed in autoclave for curing. The curved panels were manufactured in the same way as described above with a difference that cylindrically curved pre-forms were used for laminate lay-up and curing.

The orientation of the individual unidirectional plies that comprised the composite laminate was selected to simulate quasi-isotropic properties ($[0/90/+45/-45]_{4s}$). Each experiment was repeated three times to assure consistent results. The specimens were 203 mm long x 203 mm wide x 2 mm thick, made out of 32 layers of carbon fibers. For the case of curved panels, the arc length of the curved edges corresponds to the plate length. The material properties of the laminates are listed below in table 1 [21].

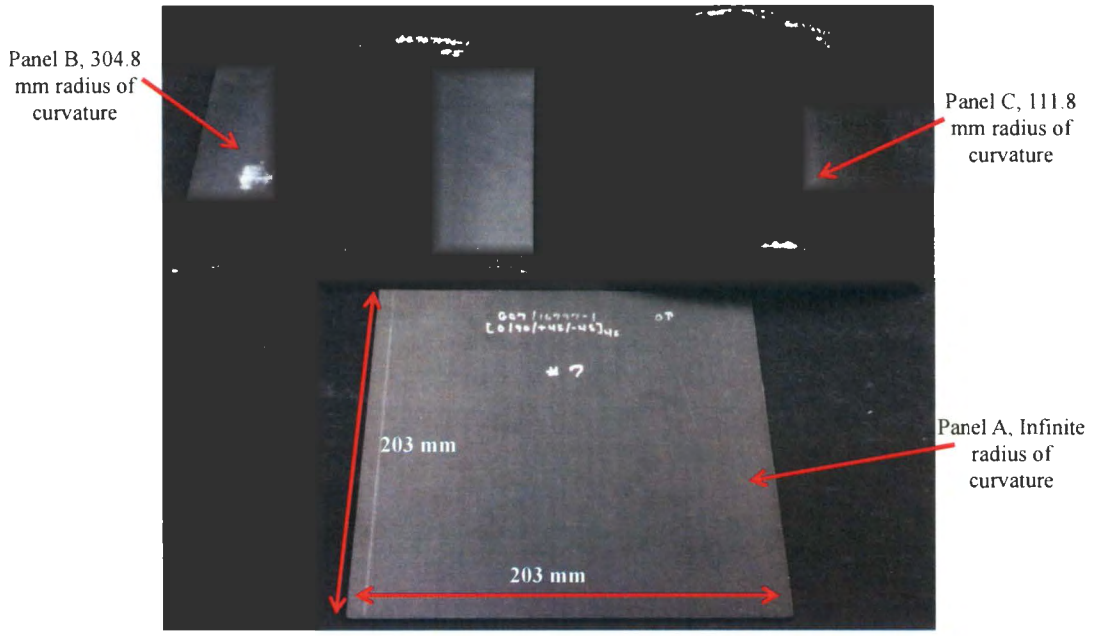

Figure 1: Geometries of specimens.

Table 1: Material Properties

Elastic Modulus	E_x = 147 GPa, E_y = 11 GPa, E_{xy} = 5 Gpa
Tensile strength in fiber direction	2004 MPa
Compressive strength in fiber direction	1197 MPa
Tensile strength in transverse direction	53 MPa
Compressive strength in transverse direction	200 MPa
Shear strength	137 MPa

3.2 Shock loading apparatus and loading conditions

The shock tube apparatus used in this study to obtain the controlled dynamic loading is shown in fig. 2. A complete description of the shock tube and its calibration can be found in [22]. The shock tube consists of a long rigid cylinder, divided into a high-pressure driver section and a low pressure driven section, which are separated by a diaphragm. By pressurizing the high-pressure section a pressure difference across the diaphragm is created. When this pressure differential reaches a critical value, the diaphragm ruptures. The subsequent rapid release of gas creates a shock wave, which travels down the shock tube to impart shock loading on the specimen at the muzzle end.

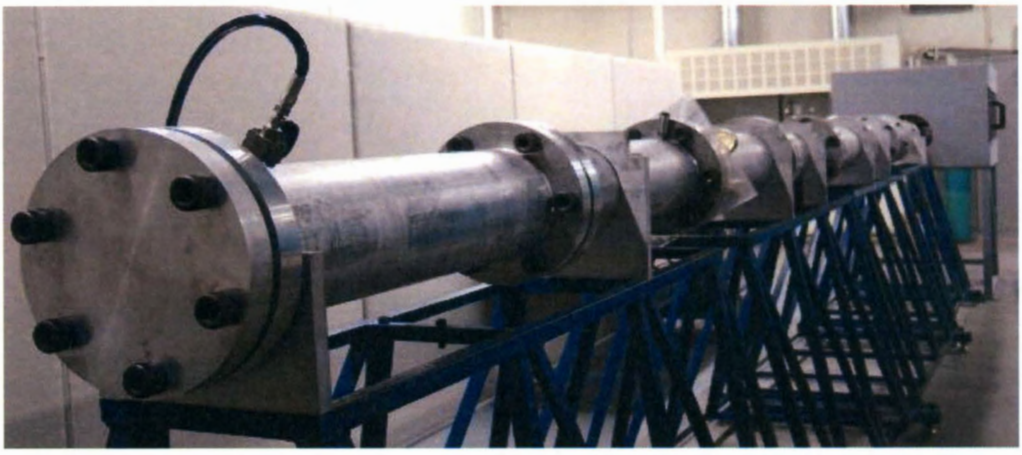

Figure 2: The URI shock tube facility.

When the shock wave impacts the specimen located at the end of the muzzle, the wave is reflected at a higher pressure than that of the incident shock pressure. The theoretical detail on the equations for shock tubes has been previously established in the literature and is briefly discussed in the following section [23]. There are four basic theoretical assumptions which are used to describe the gas flow in shock tube:

1. The gas flow is one-dimensional.

2. The gas is ideal and has constant specific heats.

3. Heat transfer and viscosity effects are neglected.

4. Diaphragm rupture is instantaneous and does not disturb the subsequent gas flow.

Using conservation of energy, mass, and momentum as described by Wright [23], the following relationships for pressure, temperature and density across a shock front can be derived:

$$\frac{P_2}{P_1} = \frac{2\gamma M_1^2 - (\gamma - 1)}{\gamma + 1} \tag{1}$$

$$\frac{T_2}{T_1} = \frac{\{2\gamma M_1^2 - (\gamma - 1)\}\{(\gamma - 1)M_1^2 + 2\}}{(\gamma + 1)^2 M_1^2} \tag{2}$$

$$\frac{\rho_2}{\rho_1} = \frac{M_1^2(\gamma + 1)}{(\gamma - 1)M_1^2 + 2} \tag{3}$$

where P_1, T_1, ρ_1 are pressure, temperature and density ahead of the shock front and P_2, T_2, ρ_2 are the pressure, temperature and density behind the shock front, γ is the adiabatic gas constant, and M_1 is the mach number of the shock wave relative to the driven gas. The pressure imparted on the specimen can be controlled by varying the above parameters in equations 1, 2, and 3. Different gases, such as nitrogen, and helium, were used in the shock tube and it was found that helium is the most suitable gas to replicate blast loading conditions and also offered the added advantage of repeatability.

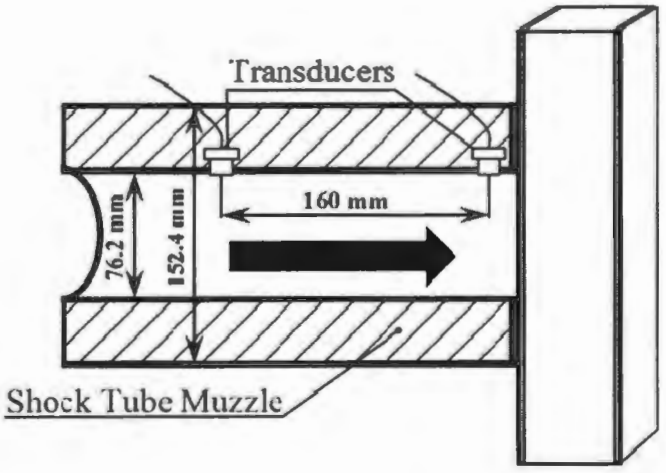

Figure 3: Schematic of the muzzle of the shock tube and fixture

The shock tube utilized in the present study has an overall length of 8 m, consisting of driver, driven, converging and muzzle sections. The diameter of the driver and driven section is 0.15 m. The final muzzle diameter is 0.07 m. Two pressure transducers (fig. 3), mounted at the end of the muzzle section measure the incident shock pressure and the reflected shock pressure during the experiment. The incident shock wave pressure was kept constant for all of the experiments. A typical pressure profile obtained at the transducer location closer to the specimen is shown in fig. 4. The specimens were shock loaded at three different pressures varying from 3 MPa to 8 MPa. At all of the three pressures, experiments were repeated at least three times to validate the consistency. The specimens were held with clamped boundary conditions on all the four edges. Appropriate fixtures for holding each of the plate geometries are shown in fig. 5.

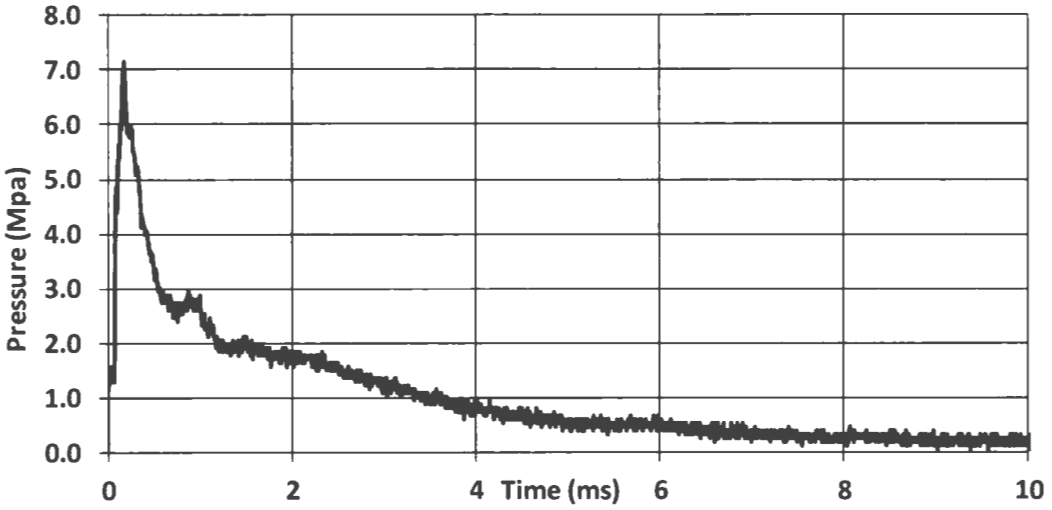

Figure 4: A typical pressure profile

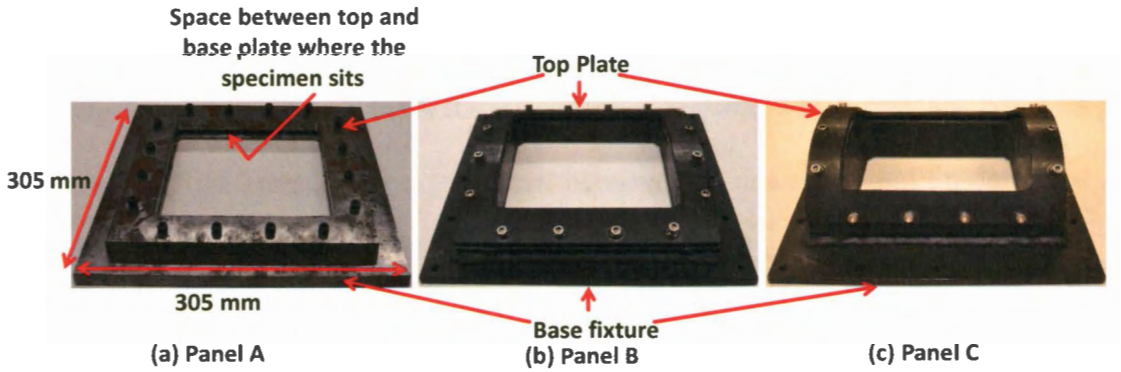

Figure 5: Loading fixtures

3.3 Digital Image Correlation (DIC) Technique

The digital image correlation technique is a recent non-contact optical method for analyzing full-field shape and deformation [24]. It involves the capture and storage of high speed images in digital form and subsequent post-processing of these images using the commercially available software to get the full-field shape and deformation measurements. The post-processing software obtains the full-field shape and deformation measurement by mapping the predefined points on the specimen. Capturing the three dimensional response of the panels requires two cameras which

must be calibrated and have synchronized image recording throughout the event. The calibration of the cameras is performed by placing a predefined grid of pattern in the test space where the aluminum specimens is located during the experiment. This grid is then translated and rotated both in and out of plane while recording the images. As this grid pattern has predetermined distances between the speckles, the coordinates of the center of each dot is extracted from each image. The coordinate locations of each dot extracted uniquely for each camera allows for a correspondence of the coordinate system of each camera. The DIC is then performed on the image pairs that are recorded during the shock event. Prior to testing, the back face of the sample is painted white and then coated with a randomized speckle pattern (fig. 6). The post processing is performed with the VIC-3D software package which matches common pixel subsets of the random speckle pattern between the deformed and un-deformed images. The matching of pixel subsets is used to calculate the three dimensional location of distinct points on the face of the panel throughout time. Dynamic experiments have been done in the past [25] to compare the back face deflection from the real time transient image and DIC to verify the accuracy of the DIC results. The error between the maximum deflection from DIC and real-time transient images is 4%.

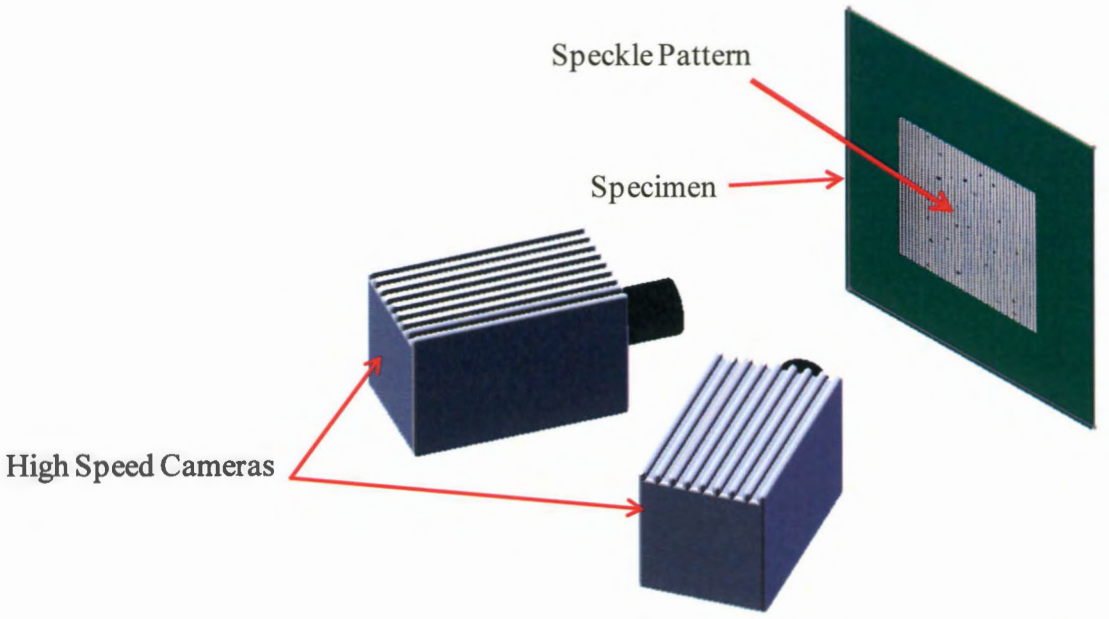

Figure 6: Schematic of DIC system

Two high speed digital cameras, Photron SA1s, were positioned behind the shock tube apparatus to capture the real time deformation and displacement of the panel. The high speed cameras were set to capture synchronized images at 20,000 frames per second (inter frame time of 50 μs). During the blast loading event, as the panel responds, the cameras record the speckles on the back face sheet. Once the event was over, the high speed images were analyzed using DIC software to correlate the images from the two cameras and generate real time in-plane strain and out-of-plane deflection/velocity histories. A schematic of the set-up is shown in fig. 6.

There are two key assumptions used in converting images to experimental measurements of objects shape, deflection and strain. First, it is assumed that there is a direct correspondence between the motion of the points in the image and that in the object. This will ensure that the displacement of points on the image have a correlation

with the displacement of points on the object. Second, it is assumed that each sub-region has adequate contrast so that accurate matching can be performed to define local image motion.

4. Experimental results and Discussion

4.1 Shock Loading

The URI shock tube apparatus (fig. 2) was used to obtain the controlled shock loading on the panels. Two pressure transducers were used to record the pressure profile of the shock wave. The pressure profile recorded by the sensor closest to the specimen (fig. 3) represents the loading profile which the specimen experiences. The pressure profile for the three panels (A to C) is shown in fig. 7. The first jump in the pressure pulse for all the three panels represents the intensity of the incoming shock wave. The second jump represents the intensity of the actual shock loading experienced by the specimen and depends on the blast mitigation property of the panel.

The pressure profile for panels A & B (fig. 7(a) and 7(b)) represents the failure loading, whereas the pressure pulse for panel C represents the threshold loading condition (fig 7(c)). Failure load is defined as the minimum load where the failure occurs, whereas, the threshold load is the maximum loading pressure which the panel can sustain before failure. For panel C, the threshold loading is discussed as at the next higher loading (failure load) the panel had a catastrophic failure and disintegrated into pieces. The failure load for panel C is 8 MPa. The threshold loading for Panel A is 3.65 MPa, for Panel B is 3 MPa, and for Panel C is 7.78 MPa.

The pressure profile for panel B shows a smooth exponential decay, whereas there are oscillations in the pressure profile of panel A (at t = 1 ms) and panel C (at t = 2 ms). The impulse imparted on the three panels has been calculated. The impulse in shock loading conditions is defined as the area under the pressure-time curve. The impulses for panel A, B, and C are 15 MPa-s, 7 MPa-s, and 28 MPa-s respectively. This shows that panel can sustain highest impulse whereas panel C has the lowest impulse sustainability.

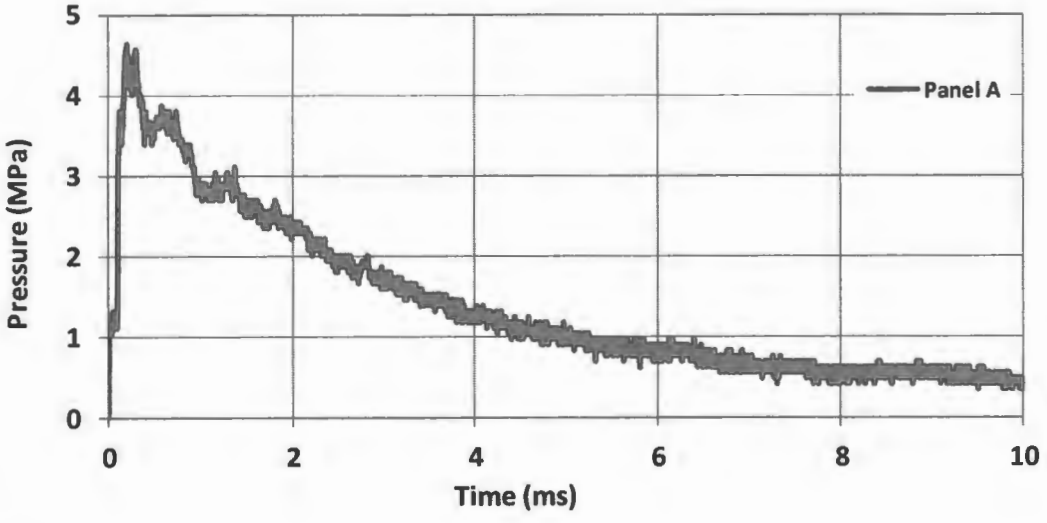

(a)

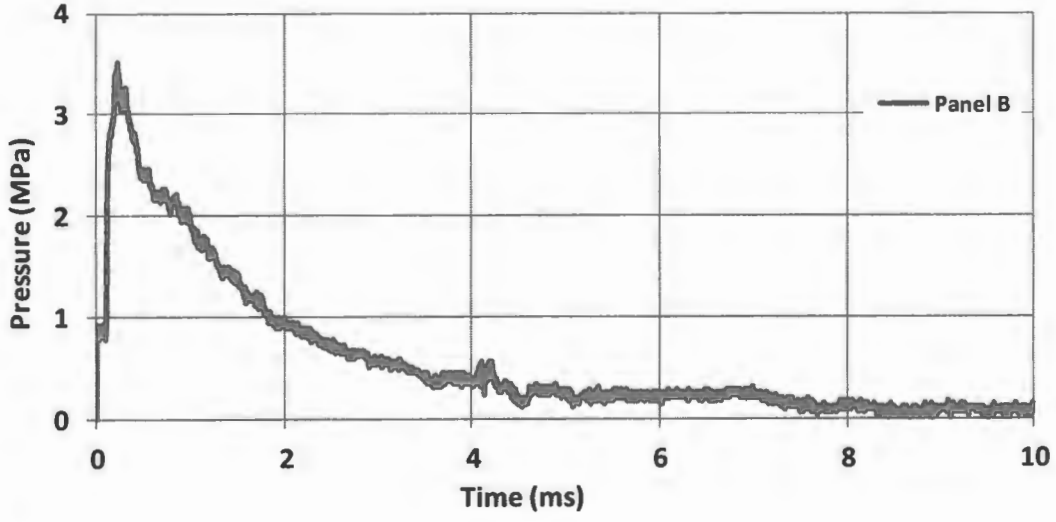

(b)

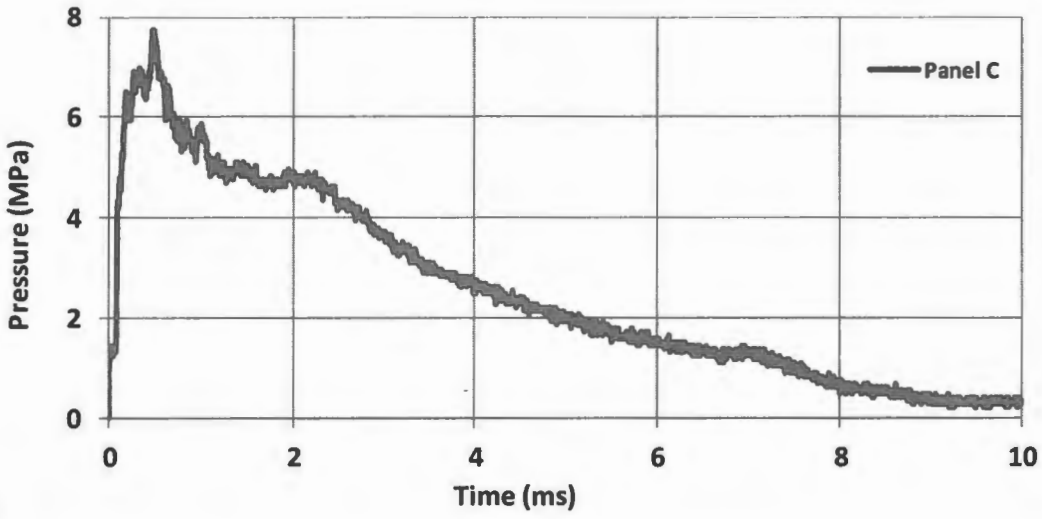

(c)

Figure 7: Pressure profile for (a) Panel A (failure load), (b) Panel B (failure load), (c) Panel C (threshold load).

4.2 DIC Analysis

The DIC technique is used to obtain the out-of-plane deflections and velocities as well as the in-plane strains on the back surface for all the three geometries. The shock tube used in this study provides a uniform pressure pulse over a circular area of 4562 mm^2 (muzzle area). This is verified by the DIC image of the out of plane displacement on flat plate during shock impingement as shown in fig. 8. The image taken at 50 μs shows a uniform displacement of 3 mm over a circular area equal to the muzzle area for panel A. As the radius of curvature decreases the circular loading area changes to elliptical loading area (fig. 8(a)). As the panels become curved, the shock loading starts acting on the projected area which causes it to change its shape from circular to elliptical.

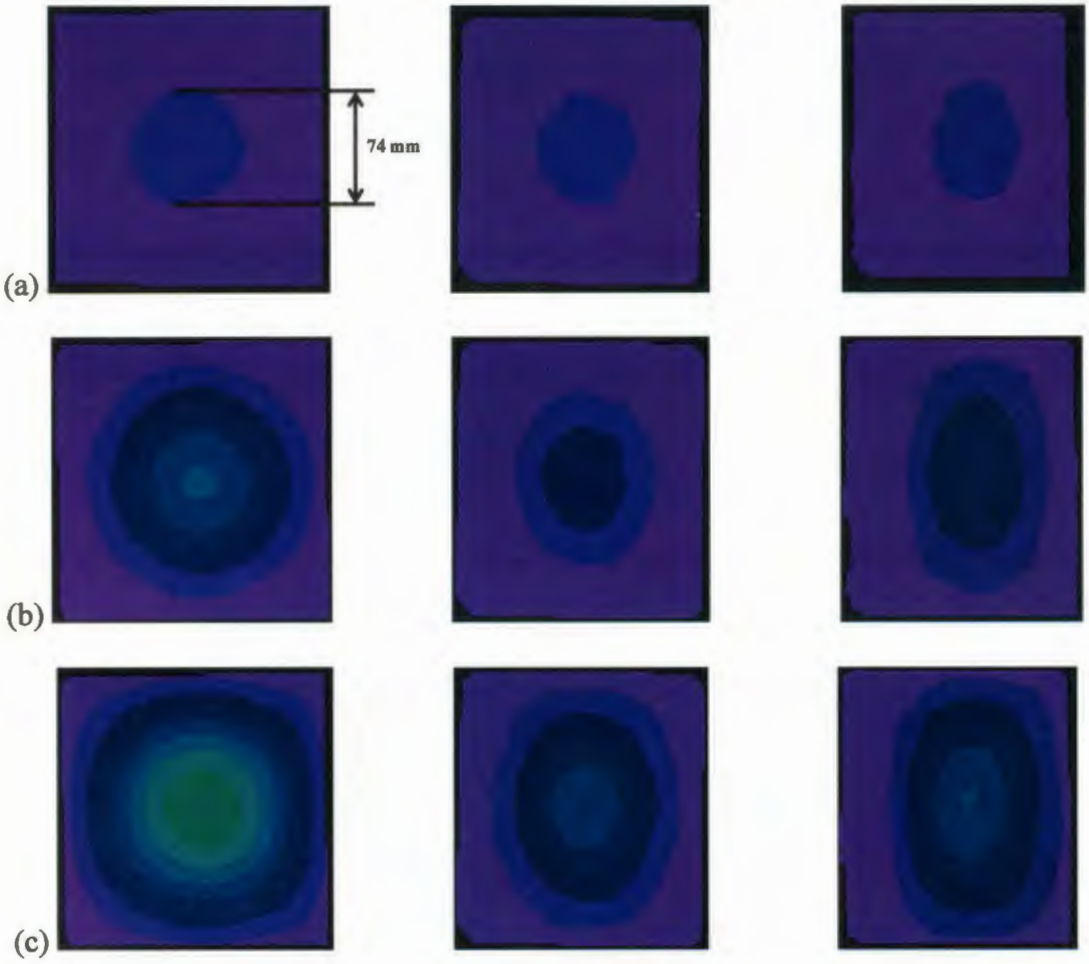

Figure 8: DIC analysis showing the loading area during shock impingement at (a) t = 50 μs, (b) t = 100 μs, (c) t = 150 μs.

The full-field deflection at 100 μs, 150 μs is shown in fig 8(b) and fig 8(c) respectively. During this early part of shock loading, when the fluid structure interaction takes place the contours of out of plane deflections are not influenced by the boundary conditions. The deflection in panel A starts as a circular region (fig. 8), which continues till 150 μs. This is a localized circular deflection contour, which has roughly the same diameter as that of the muzzle (at t = 50 μs). At t = 150 μs, the boundary conditions starts affecting the development of deflection contours in the

panel. The panel had fluid-structure interaction for first 150 μs at which time the boundary condition starts affecting the deflection development. As a result, the profile of deflection contour changes from circular to a rectangular regime. This fluid structure interaction time for panel A is around 150 μs at which times the boundary conditions start affecting the deflection development causing the circular shaped contour to change to rectangular. Panel B had fluid-structure interaction for first 200 μs (fig. 8 & 9) at which time the boundary condition starts affecting the deflection development. Around 200 μs, the elliptical deflection contour in panel B starts changing to rectangular shape because of the boundary conditions.

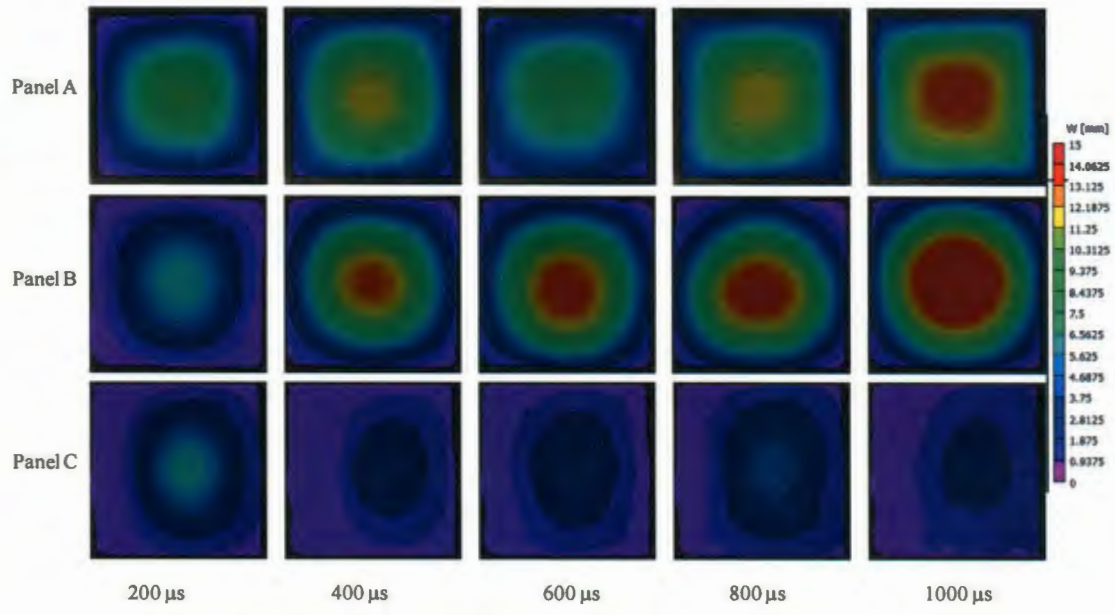

Figure 9: Full field deformation of panels from 3D-DIC analysis.

The full-field deflection for the panels is shown in fig. 9. The total deflection in these panels subjected to blast loading comprises of two distinct regions, namely, the indentation region followed by the flexural deflection. During indentation, localized deflection superpose onto the overall deflection. In case of flexure, the

overall deflection starts to overpass the localized deflection. The indentation deflection is localized around the loading area whereas a full field deflection over the area of the specimen being loaded is predominant in flexural mode. Also, the boundary conditions affect the deflection in case of flexural mode. Panels B and C had elliptical deflection contour at 200 μs (fig. 8 & 9). Since both these panels are curved, the shock wave impinges on the projected area and creates localized elliptical deflection contour (it is more clearly seen in fig. 8). Also, the deflection mode in panel B changes from indentation to flexural mode at this time. The deflection in panel C continues to develop further with elliptical contour. The deflection is primarily because of indentation and boundary conditions do not affect the deflection contours. As such, it retains its elliptical shape throughout the loading process (fig. 8 & 9). Panel A and C also shows oscillations (fig. 9) which correlates to the oscillations seen in the respective pressure profiles in fig. 7.

From the full-field DIC analysis, the out-of-plane deflection and velocities and the in-plane strain data were extracted at the center point of the three panels (fig. 10-12). From the time-deflection history (fig. 10) at the center point of the panels, it is seen that the deflection rate (35 m/sec) is almost same in all the three panels, but panels A & B attained a higher deflection as compared to panel C. This can be explained based on the fact that because of the curvature, the loading area decreases in Panel C. This also shows that the Panel C is stiffer than the other two panels as it can sustain higher pressures and have a lower deflection as compared to the other two panels. Panel A and B had a similar deflection trend till 1000 μs. At this time, panel B

failed catastrophically and this explains the change in deflection development in the panel.

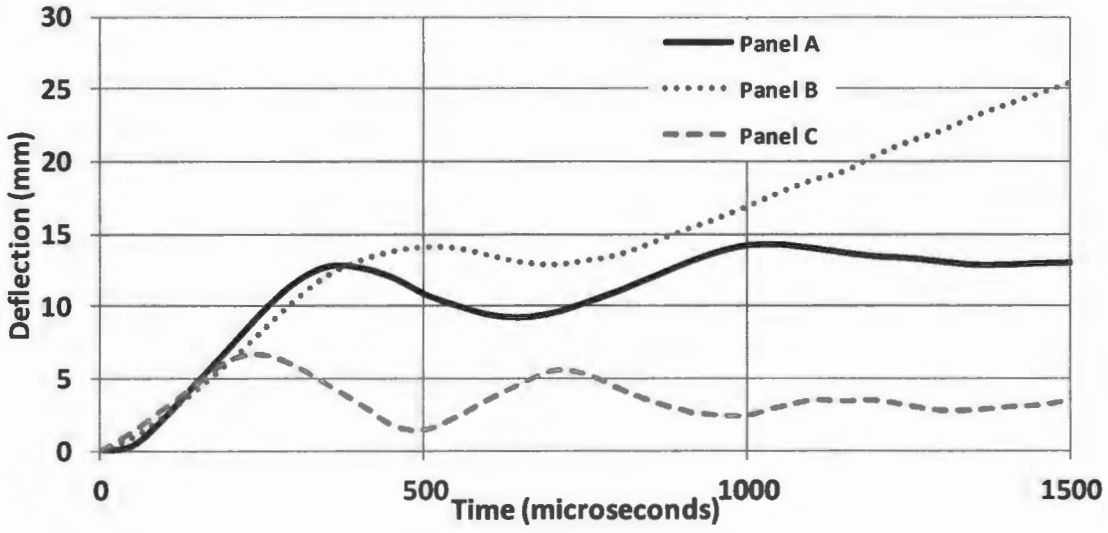

Figure 10: Time-deflection history at the center point on the back face for the three panels.

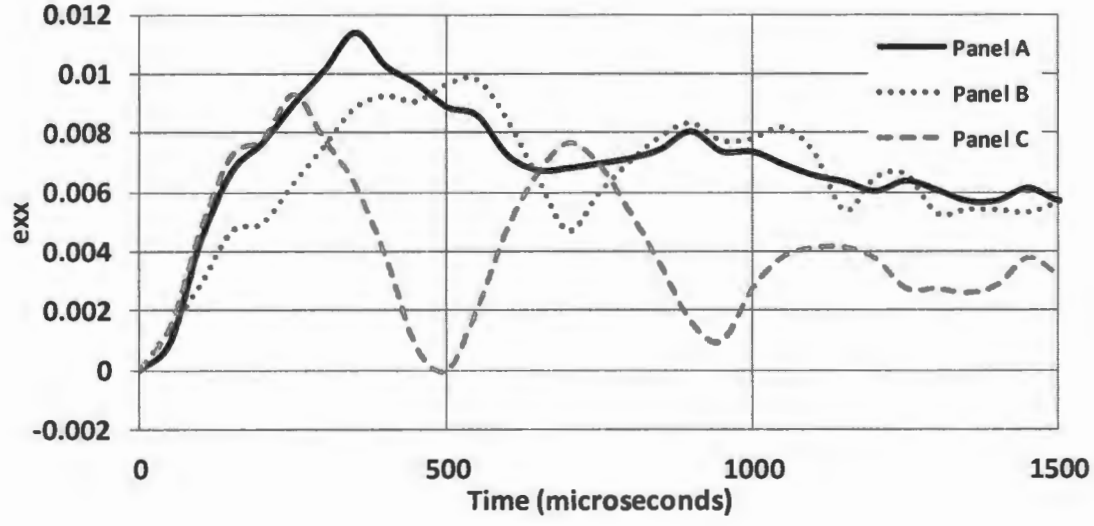

Figure 11: Time-in-plane strain history at the center point on the back face for the three panels.

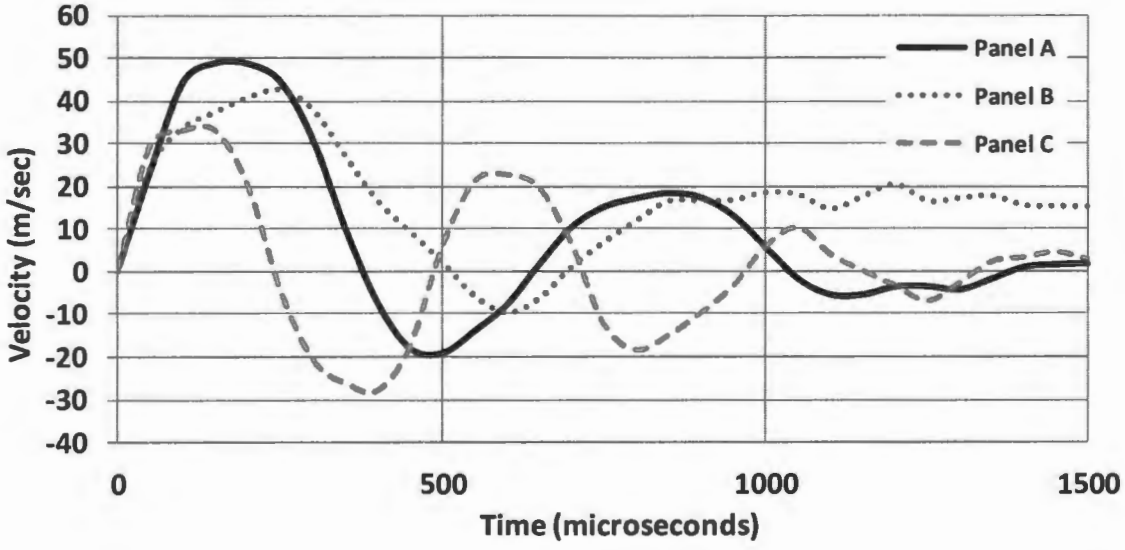

Figure 12: Time-Velocity history at the center point on the back face for the three panels.

The in-plane strain, e_{xx}, at the center-point of the three panels is shown in fig. 11. The in-plane strains, e_{xx}, are nearly same for all the three panels at the center point. The out-of plane velocity at the center point is shown in fig. 12. Panels A and C show an oscillation which explains the oscillation in deflection and pressure profile of these panels as discussed. Also the velocity in panel A and C becomes zero around 1000 μs but the panel B maintains a velocity of 20 m/s. This supports the fact that the failure initiates in Panel B at around 1000 μs.

4.3 Macroscopic post-mortem analysis

The post-mortem image of the shock loaded flat carbon composite panel (panel A) is shown in fig. 13. There is inter-layer delamination and fiber breakage evident in the post-mortem analysis. The fiber breakage initiated from the clamping edges. To better understand the failure, the panel was divided into three regions and a close postmortem analysis was done on each of the regions. The close-up postmortem

images of region 1 (fig. 13) shows that there is fiber breakage in multiple layers. The fiber breakage continues up to 7 layers from the side which was subjected to shock loading. Carbon composite panels are brittle. When they are subjected to shock loading, there is deflection in the panel, but the clamping tries to restrain this deflection. This restrain from the clamping causes the fiber breakage initiation. There is fiber breakage and delamination which extends to the third layer, is visible in region 2. As seen in the macroscopic postmortem image of region 2, there is transverse fiber breakage. The delamination and fiber breakage in region 2 also started from the clamping boundary as in the region 1. There is fiber breakage and delamintaion in region 3 around the clamping boundary. At the same time there is fiber breakage and delamination on the edge of the panel as seen in the macroscopic post-mortem image of region 3.

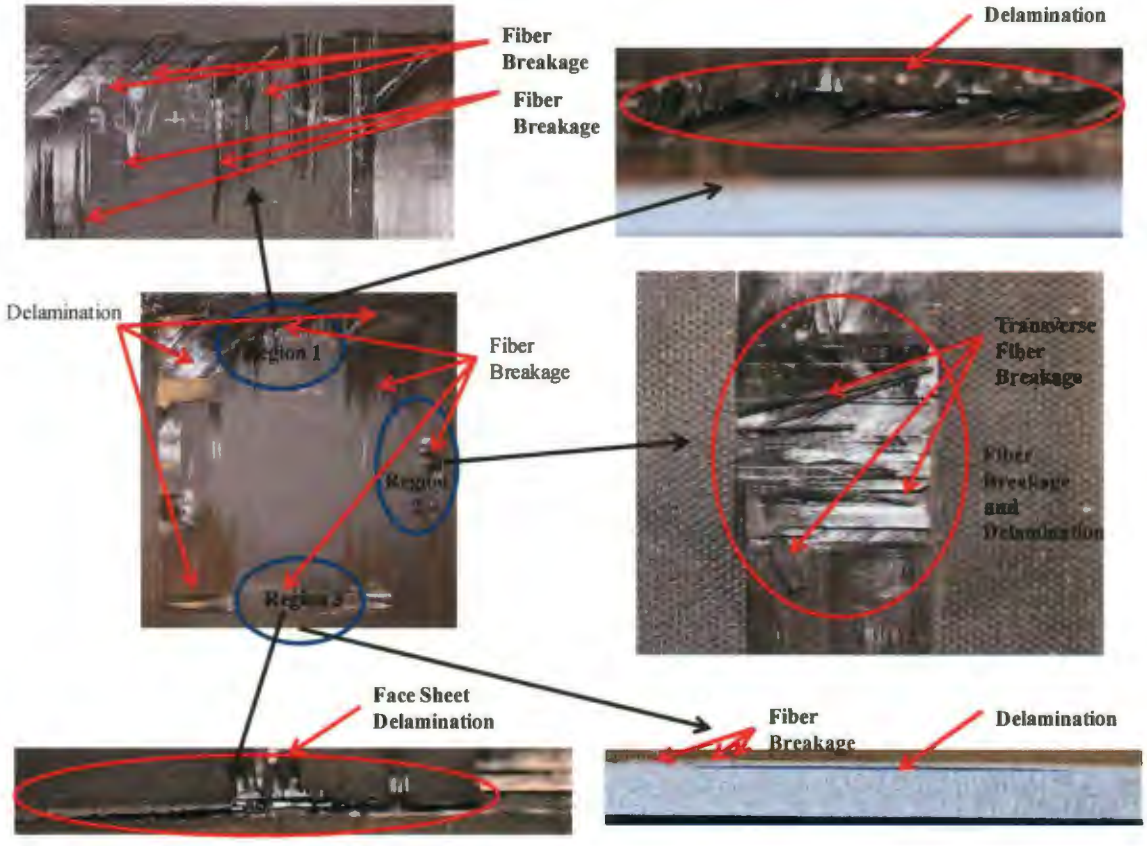

Figure 13: Post-mortem evaluation of Panel A.

The post-mortem image of panel B is shown in fig. 14. There is large scale inter-layer delamination and fiber breakage as evident in fig. 14. In particular, the inter-layer delamination extends through the thickness of the carbon composite panel as seen in the macroscopic image of region 1. Also in region 2, there is large scale fiber breakage as seen in region 2. Also the deflection in panel causes the fiber breakage along the clamping edges.

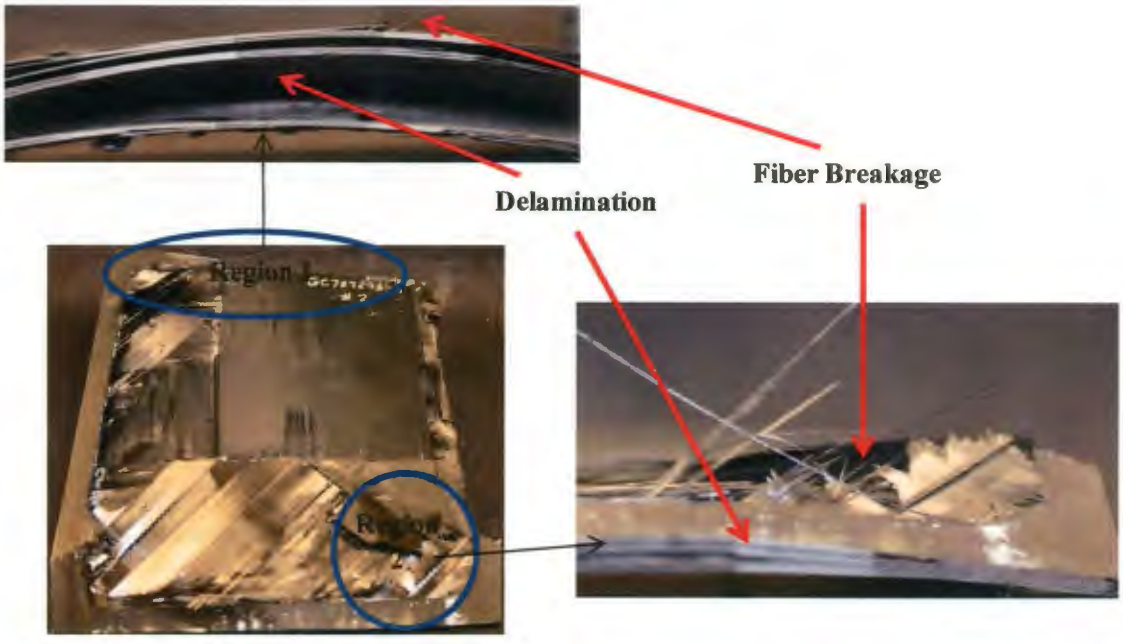

Figure 14: Post-mortem evaluation of Panel B.

The post-mortem image of panel C is shown in fig. 15. The panel had no fiber breakage or delamination as seen in other panels as this is just before failure. At the next higher pressure the panel had catastrophic failure and broke into pieces (see fig. 18). There is fiber burning on the face which was subjected to shock loading. As discussed previously, the impinging gas on the panel reaches the ionization temperature, which causes the charring of carbon fiber on the face. The deflection, and in-plane strain data at the center point of the panel C at the next higher pressure (8 MPa) is shown in fig. 16-17. The failure in panel occurred at around 1000 μs. The panel had a mid-point deflection of 12 mm (fig. 16) at the failure initiation as compared to 14 mm and 16 mm in Panel A and Panel B respectively at the failure initiation (fig. 10). The in-plane strain, e_{xx} (fig. 17) is considerably different as compared to the threshold loading (fig. 11). The maximum compressive in-plane strain reaches a value 0.018 at the center point.

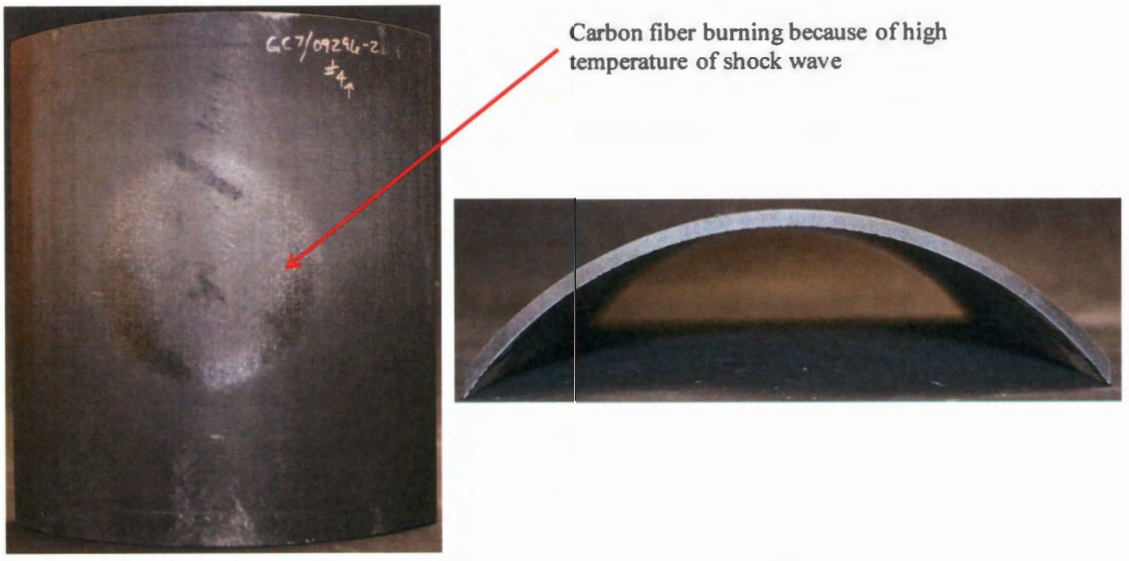

Figure 15: Post-mortem evaluation of Panel C

The NU interlaminar failure theory [26, 27] has been used to explain the failure in the panels. According to this NU criterion [27], failure occurs when the in-plane strain at any point on the panel exceeds the critical strain (ε_{crit}) which is defined by equation 4. This criteria is able to predict interlaminar/interfiber failure under transverse compressive loading.

$$\varepsilon_{crit} = F_{12}/E_2 \tag{4}$$

where, F_{12} = Compressive strength of the laminate in transverse direction

and E_2 = Transverse modulus

Using the material properties from table 1, we have

$$\varepsilon_{crit} = 0.018.$$

In case of panel A, the max in-plane strain over the full-field is 0.016, for panel B it 0.02, and for panel C it is 0.012 (fig. 19). The in-plane strain in panel B is greater than the critical strain, thus resulting in the catastrophic failure of the panel (fig. 14). In case of panel C, the maximum in-plane strain is 0.012. This is 33% less than the

critical strain, and as such no visible damage is seen in the post-mortem analysis (fig. 15). The maximum in-plane strain in panel A is near to the critical failure strain (lower by 12%). This results in partial failure of the panel and interlayer delamination which extends upto 7 layers from the shock loaded face (fig. 13). The maximum in-plane strain in one of the panels C, which was subjected to a pressure of 8 MPa is 0.022 (panel C_2 in fig. 19). Also, the overall in-plane strain in panel C_2 was closer to the critical strain (compressive strain of 0.018 at the center point, as seen in fig. 17). This explains the catastrophic failure and shattering as seen in fig. 18. Also, the damage initiation area in panel A, B, and C_2 corresponds to the maximum in-plane strain area from the full-field 3D-DIC results (fig. 20).

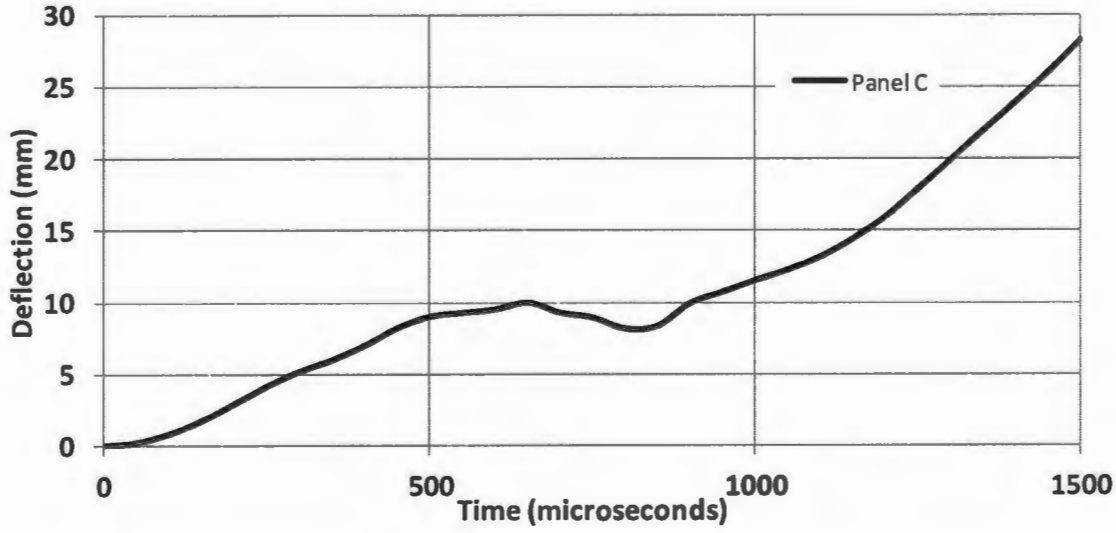

Figure 16: Time-Deflection history at the center point on the back face for Panel C at failure loading.

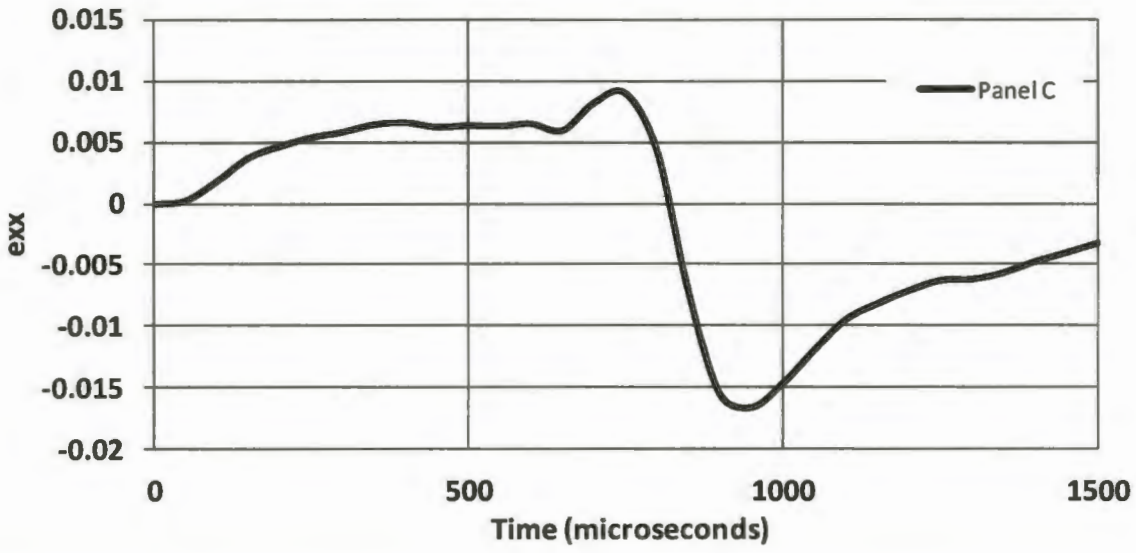

Figure 17: Time-In-plane history at the center point on the back face for Panel C at failure loading.

Figure 18: Post-mortem evaluation of Panel C.

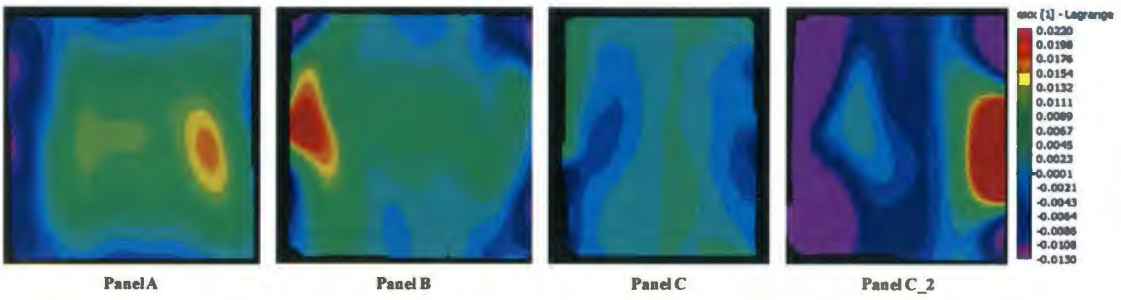

Figure 19: Full-field e_{xx} in-plane strain in the panels.

5. Conclusions

Three types of panels with varying curvature have been subjected to a controlled shock loading using a shock tube. 3D DIC technique coupled with high speed photography is used to obtain the out-of-plane deformation/velocity and in-plane strain on the back face of all the three panels.

1. The macroscopic post-mortem analysis and DIC deflection, velocity and in-plane strain analysis shows that panel C (112 mm radius of curvature) is capable of sustaining the highest threshold failure load.
2. The flexural deformation decreases and indentation deformation increases as the radius of curvature decreases. There is a limit to which the radius of curvature can be decreased. As the radius of curvature reduces to a limiting value, the shock wave will glide over the surface.

Overall, the threshold blast pressure, which is defined as the pressure just above which the panel fails and the damage observed (at threshold loading) in each of the panels are summarized in table 2.

Table 2: Threshold loading and damage observed in each panel.

	Threshold Blast Pressure	Damage Observed
Panel A	3.65 MPa	No Visible damage. At P = 4.68 MPa, there is fiber breakage, and surface delamination extending up to 7 layers.
Panel B	3 MPa	No Visible damage. At P = 3.58 MPa, there is catastrophic failure with fiber breakage and delamination.
Panel C	7.78 MPa	No visible failure except burning of carbon fiber on the surface exposed to blast loading. At P = 8 MPa, there is catastrophic failure with fiber breakage.

6. Acknowledgement

The authors acknowledge the financial support provided by the Department of Homeland Security (DHS) under Cooperative Agreement No. 2008-ST-061-ED0002.

7. References

[1] D.S. Stargel, Experimental and Numerical Investigation into the effects of Panel Curvature on the High Velocity Ballastic Impact Response of Aluminum and Composite Panels, Doctor of Philosophy Dissertation, University of Maryland, College Park, 2005.

[2] L. Chun, and K.Y. Lam, Dynamic analysis of clamped laminated curved panels, Compos. Struct., 30 (1995) 389-398.

[3] R. Rajendran, and J.M. Lee, Blast loaded plates, Mar. struct., 22 (2009) 99-127.

[4] J.M. Biggs, Introduction to structural Dynamics, McGraw-Hill, New York, 1964.

[5] R.W. Clough, and J. Penzien, Dynamics of structures, McGraw-Hill, New York, 1975.

[6] S.A. Tekalur, K. Shivakumar, and A. Shukla, Mechanical behavior and damage evolution in E-glass vinyl ester and carbon composites subjected to static and blast loads, Composites: Part B. 39 (2008) 57-65.

[7] H. Arora, P.A. Hooper, and J.P. Dear, Dynamic response of full-scale sandwich composite structure subject to air-blast loading, Composites: Part A, 42(2011) 1651-1662.

[8] M.V. Hosur, S.M.W. Islam, U.K. Vaidya, A. Kumar, P.K. Dutta and S. Jeelani, Dynamic punch shear characterization of plain weave graphite/epoxy composites at room and elevated temperature, Composite Structures, 70(2005) 295-307.

[9] M.V. Hosur, M. Adya, U.K. Vaidya, A. Mayer and S. Jeelani, Effect of stitching and weave architecture on the high strain rate compression response of affordable woven carbon/epoxy composites, Composite Structures, 59(2003) 507-523.

[10] M.V. Hosur, J. Alexander, U.K. Vaidya, S. Jeelani and A. Mayer, Studies on the off-axis high strain rate compression loading of satin weave carbon/epoxy composites, Composite Structures, 63(2004) 75-85.

[11] L.S. Kistler and A.M. Waas, On the response of curved laminated panels subjected to transverse impact loads, International Journal of Solids and Structures, 36(1999) 1311-1327.

[12] T. Franz, G.N. Nurick, M.J. Perry, Experimental investigation into the reponse of chopped strand mat glassfibre laminates to blast loading, International Journal of Impact Engineering, 27(2002) 639-667.

[13] S.M.R. Khalili, M. Soroush, A. Davar and O. Rahmani, Finite element modeling of low-velocity impact on laminated composite plates and cylindrical shells, Composite Structures, 93(2011) 1363-1375.

[14] R.O. Ochola, K. Marcus, G.N. Nurick and T. Franz, Mechanical behavior of glaa and carbon fiber reinforced composites at varying strain rates, Composites Structures, 63(2004) 455-467.

[15] M.V. Hosur, J. Alexander, U.K. Vaidya and S. Jeelani, High strain rate compression response of carbon/epoxy laminate composites, Composite Structures, 52(2001) 405-417.

[16] J. LeBlanc, and A. Shukla, Dynamic response of curved composite panels to underwater explosive loading: experimental and computational comparisions, Compos. Struct., 93 (2011) 3072-3081.

[17] M. Pankow, B. Justusson, A. Salvi, A.M. Waas, Chian-Fong Yen, and S. Ghiorse, Shock response of 3D woven composites: An experimental investigation, Composite Structures, 93(2011) 1337-1346.

[18] J. Shen, G. Lu, Z. Wang, L. Zhao, Experiments on curved sandwich panels under blast loading, International Journal of Impact Engineering, 37(2010) 960-970.

[19] D. Karagiozova, G.N. Nurick, G.S. Langdon, S. Chung Kim Yuen, Y. Chi, and S. Bartle, Response of flexible sandwich-type panels to blast loading, Composites Science and Technology, 69(2009) 754-763.

[20] T. Hause, and L. Librescu, Dynamic response of doubly-curved anisotropic sandwich panels impacted by blast loadings, International Journal of Solids and Structures, 44(2007) 6678-6700.

[21] M.M. Shokrieh and L.B. Lessard, Progressive Fatigue Damage Modeling of Composite Materials, Part II: Material Characterization and Model Verification, Journal of Composite Materials, 34(2000) 1081-1116.

[22] J. LeBlanc, A. Shukla, C. Rousseau, and A. Bogdanovich, Shock loading of three-dimensional woven composite materials, Compos. Struct., 79 (2007) 344–355.

[23] J. Wright, Shock Tubes, John Wiley and Sons Inc., New York, 1961.

[24] V. Tiwari, M.A. Sutton, S.R. McNeill, S. Xu, X. Deng, W.L. Fourney, and D. Bretall, Application of 3D image correlation for full-field transient plate deformation measurements during blast loading, Int. J. Impact Eng., 36 (2009) 862-874.

[25] N. Gardner, E. Wang, P. Kumar, and A. Shukla, Blast Mitigation in a Sandwich Composite Using Graded Core and Polyurea Interlayer, Exp. Mech., DOI 10.1007/s11340-011-9517-9 (2011).

[26] I.M. Daniel, B.T. Werner, and J.S. Fenner, Strain-rate-dependent failure criteria for composites, Composite Science and Technology, 71(2011) 357-364.

[27] I.M. Daniel, J.J. Luo, P.M. Schubel, and B.T. Werner, Interfiber/interlaminar failure of composites under multi-axial states of stress, Composite Science and Technology, 69(2009) 764-771.

CHAPTER 4

EFFECT OF PLATE THICKNESS ON BLAST RESPONSE OF E-GLASS/VINYL ESTER COMPOSITE PANELS

by

Puneet Kumar, James LeBlanc and Arun Shukla.

Under preparation for submission in Composite Structures.

Corresponding Author: Arun Shukla

Dynamic Photo Mechanics Laboratory

Department of Mechanical, Industrial and Systems Engineering

University of Rhode Island

206 Wales Hall, 92 Upper College Rd

Kingston, RI, 02881, USA

Phone: +1-401-874-2283

Email Address: shuklaa@egr.uri.edu

1. Abstract

Experimental studies were conducted to understand the effect of varying plate thickness on the blast response of doubly curved E-glass/vinyl Ester panels. A shock tube apparatus was utilized to impart controlled shock loading on glass fiber panels having three different thickness: 1.37 mm (panel A), 2.54 mm (panel B), and 4.40 mm (panel C). These panels with an 18.28 mm radius of curvature were held under clamped boundary conditions during the shock loading. A 3D Digital Image Correlation (DIC) technique coupled with high speed photography was used to obtain out-of-plane deflection and velocity, as well as in-plane strain on the back face of the panels. There were two types of failure mechanism observed in all the three panels: fiber breakage and inter-layer delamination. Macroscopic postmortem analysis and DIC results showed that panel C can mitigate higher intensity (pressure) shock waves without initiation of catastrophic damage in the panel. Panel A could sustain the least shock wave intensity and exhibited catastrophic failure.

Keywords

Glass fiber, Composite panels, 3D-digital image correlation, Shock tube, Curvature, Thickness, Blast mitigation.

2. Introduction

A controlled experimental study has been conducted to understand the effect of varying plate thickness on the blast response of glass fiber composite panels. Accidental explosions or bomb blasts cause extreme loading on structures, which have both flat and curved geometries with varying thicknesses (as in the USS Cole bombing and also the Oklahoma city bombing). Therefore curvature is an important parameter

and its effect on the blast response needs to be studied closely. At the same time, the thicknesses of the composite panels play an important role. The increase in thickness will improve the blast performance of the panel, but at the same time it will also increase the overall weight of the structure. Thus a balance between the mitigation property and overall weight of the structure is needed which will help in manufacturing new light weight structures with better blast resistant property. E-Glass fiber composite panels having three different thicknesses were subjected to shock loading using a shock tube in order to study their dynamic response. Real-time and post-mortem analysis was conducted on the panels to evaluate the effects of thickness on blast mitigation. In particular, the midpoint transient deflection, velocity, and macroscopic post-mortem analysis of the panels has been used to characterize the response of curved panels when subjected to a controlled blast loading.

There are two methods of imparting shock loading on structures: one is by using explosives and the other is by using shock tubes. The use of real explosives is dangerous and has added complications such as creation of spherical wave fronts and pressure signatures which are spatially complex and difficult to measure. On the contrary, shock tubes offer the advantage of planar wave fronts and wave parameters that can be easily controlled. Above all, these parameters are easy to replicate when using a shock tube as compared to using real explosives and therefore a shock tube was the preferred choice of applying blast loading in our experiments.

There is a large volume of literature dealing with the blast loading of structures [1-11]. For brevity of space, only a few studies are mentioned here. Franz *et al.* [12] analyzed the air pressure blast loading response of glassfiber chopped-strand mat

laminates. They found matrix cracking, delamination/debonding, and penetration as final damage in the experiments conducted on monolithic and layered laminates with varying areal density. Khalili *et al.* [13] studied the response of composite laminates and shell structures subjected to low-velocity impacts numerically. They studied the effect of element type, solution method, impactor modeling method, meshing pattern and contact modeling on the accurate numerical modeling in ABAQUS. Ochola *et al.* [14] concentrated on strain rate sensitivity of both carbon fiber reinforced polymer and glass fiber reinforced polymer by testing a single laminate configuration with strain rate varying from 10^{-3} and 450 s^{-1}. Results showed that the dynamic material strength for GFRP increases with increasing strain rate and the strain to failure for both CFRP and GFRP decreased with increasing strain rate. Chi *et al.* [15] investigated the behavior of circular sandwich panels with aluminum honeycomb care when subjected to air blast loading. They found that the panels exhibited permanent face plate deflection and tearing, and the honeycomb core exhibited crushing and densification. Increasing plate thickness was also found to decrease the back face deflection but at the same time increased the overall mass. LeBlanc and Shukla [16] studied the underwater shock loading response of E-glass/Vinyl ester curved composite panels. They used the 3D-DIC system for measuring the transient response during the experiments. They also compared the experimental results to simulation results obtained from the commercially available Ls-Dyna finite element code, which showed a high level of correlation using the Russell error measure. Pankow *et al.* [17] analyzed the effect of 3D weaving in composites to two different intensities of shock loading using the DIC technique. They found an optimal Z-fiber architecture (6%) out

of the three different architectures, which was responsible for largest panel stiffness and least amount of damage. They also observed matrix micro-cracking at the center of the panel which caused the failure initiation in the panels. Shen *et al.* [18] experimentally investigated the response of sandwich panels with aluminum face sheets and aluminum foam core. Panels with varying curvatures (two different curvatures), and different core/face sheet configurations were tested at three different blast intensities. They found that the initial curvature of the sandwich panel changes the deformation mode and improve the performance of the structure when compared to equivalent flat plate. Zhu *et al.* [19] studied the effect of foil thickness, cell size, mass of charge, relative density of the core, and the face sheet thickness and concluded that there is a compromise between strength and weight. They found that on increasing the thickness the mass of the panel increased but at the same time decreased the back face deflection. Hause and Librescu [20] developed a closed-form solution for comparison with numerical based solutions based on the extended Galerkin method for designing doubly-curved sandwich panels operating under dynamic loading.

The literature review shows lack in understanding the effect of plate thickness on blast response of composite panels. There are some studies on understanding the effect of thickness on blast response, but they concentrate on metallic face sheet panels. At the same time, these studies concentrated on using flat metallic face sheet and not curved panels. The present study aims to understand the effect of thickness in curved composite panels. The results from this study show that the plate thickness

affects the blast mitigation property. As the thickness of plate increases, the response of panels to sustain shock loading changes.

3. Experimental Procedure

3.1 Material Details

Panels with three different thicknesses were shock loaded: 1.37 mm (panel A), 2.54 mm (panel B), and 4.4 mm (panel C). The schematic of the specimen is shown in fig. 1. The specimens were fabricated using E-glass fiber and vinyl ester resin and manufactured by LBI Fiberglass, located in Groton, CT. The glass fabric is a balanced construction of 0^{o} and 90^{o} fibers with the two layers being stitched together in place of being woven. The areal weight of the dry fabric is 0.406 kg/m^2. The panels are manufactured using the vacuum infusion process. The mechanical properties for the material are provided in table 1 and that of vinyl ester resin are provided in table 2. The geometry of the plate consists of a curved mid-section with a flat boundary (fig. 1). The convex face of the plate represents the mold line in the manufacturing and has a radius of curvature of 18.28 cm, and the curved portion of the plate is 22.86 cm in diameter.

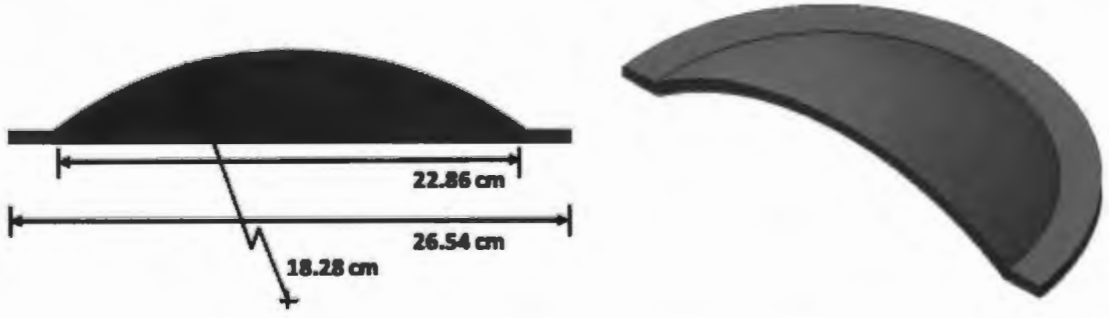

Figure 1: Schematics of the composite panel.

Table 1: E-glass/vinyl ester biaxial laminate - Material Properties

Tensile modulus (0^o)	15.8e3 MPa
Tensile modulus (90^o)	15.8e3 MPa
Tensile strength (0^o)	324 MPa
Tensile strength (90^o)	324 MPa

Table 2: Vinyl ester resin - Material Properties

Tensile modulus	3.44e3 MPa
Tensile strength	72.4 MPa

3.2 Shock loading apparatus and loading conditions

The shock tube apparatus used in this study to obtain the controlled dynamic loading is shown in fig. 2. A complete description of the shock tube and its calibration can be found in [22]. The shock tube consists of a long rigid cylinder, divided into a high-pressure driver section and a low pressure driven section, which are separated by a diaphragm. Helium gas is used to pressurize the high-pressure section which creates a pressure difference across the diaphragm. As this pressure differential reaches a critical value, the diaphragm ruptures. This causes a subsequent rapid release of gas which creates a shock wave traveling down the shock tube to impart shock loading on the specimen at the muzzle end.

Figure 2: The URI shock tube facility.

When the shock wave impacts the specimen located at the end of the muzzle, the wave is reflected at a higher pressure than that of the incident shock pressure. The theoretical detail on the equations for shock tubes has been previously established in the literature and is briefly discussed in the following section [23]. There are four basic theoretical assumptions which are used to describe the gas flow in shock tube:

1. The gas flow is one-dimensional.
2. The gas is ideal and has constant specific heats.
3. Heat transfer and viscosity effects are neglected.
4. Diaphragm rupture is instantaneous and does not disturb the subsequent gas flow.

Using conservation of energy, mass, and momentum as described by Wright [23], the following relationships for pressure, temperature and density across a shock front can be derived:

$$\frac{P_2}{P_1} = \frac{2\gamma M_1^2 - (\gamma - 1)}{\gamma + 1} \qquad (1)$$

$$\frac{T_2}{T_1} = \frac{\{2\gamma M_1^2 - (\gamma - 1)\}\{(\gamma - 1)M_1^2 + 2\}}{(\gamma + 1)^2 M_1^2} \tag{2}$$

$$\frac{\rho_2}{\rho_1} = \frac{M_1^2(\gamma + 1)}{(\gamma - 1)M_1^2 + 2} \tag{3}$$

where P_1, T_1, ρ_1 are pressure, temperature and density ahead of the shock front and P_2, T_2, ρ_2 are the pressure, temperature and density behind the shock front, γ is the adiabatic gas constant, and M_1 is the mach number of the shock wave relative to the driven gas. The pressure imparted on the specimen can be controlled by varying the above parameters in equations 1, 2, and 3. Different gases, such as nitrogen, and helium, have been used in the shock tube. Helium has been found to be most suitable gas as it replicates the actual blast loading (as in the case of real explosion) conditions and also offers the added advantage of repeatability.

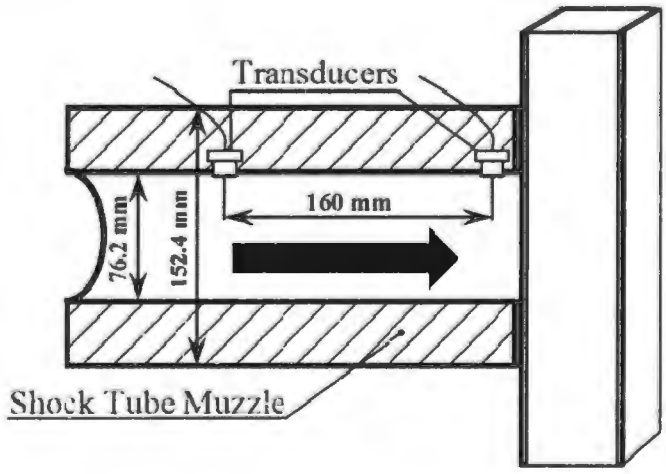

Figure 3: Schematic of the muzzle of the shock tube and fixture

The shock tube utilized in the present study has an overall length of 8 m, consisting of driver, driven, converging and muzzle sections. The diameter of the

driver and driven section is 0.15 m. The final muzzle diameter is 0.07 m. Two pressure transducers (fig. 3), mounted at the end of the muzzle section measure the incident shock pressure and the reflected shock pressure during the experiment. The incident shock wave pressure was kept constant for all of the experiments. A typical pressure profile obtained at the transducer location closest to the specimen is shown in fig. 4. The specimens were shock loaded at three different pressures varying from 1 MPa to 6 MPa. At all of the three pressures, experiments were repeated to validate the consistency. The specimens were held with clamped boundary conditions. Appropriate fixture for holding the plates is shown in fig. 5.

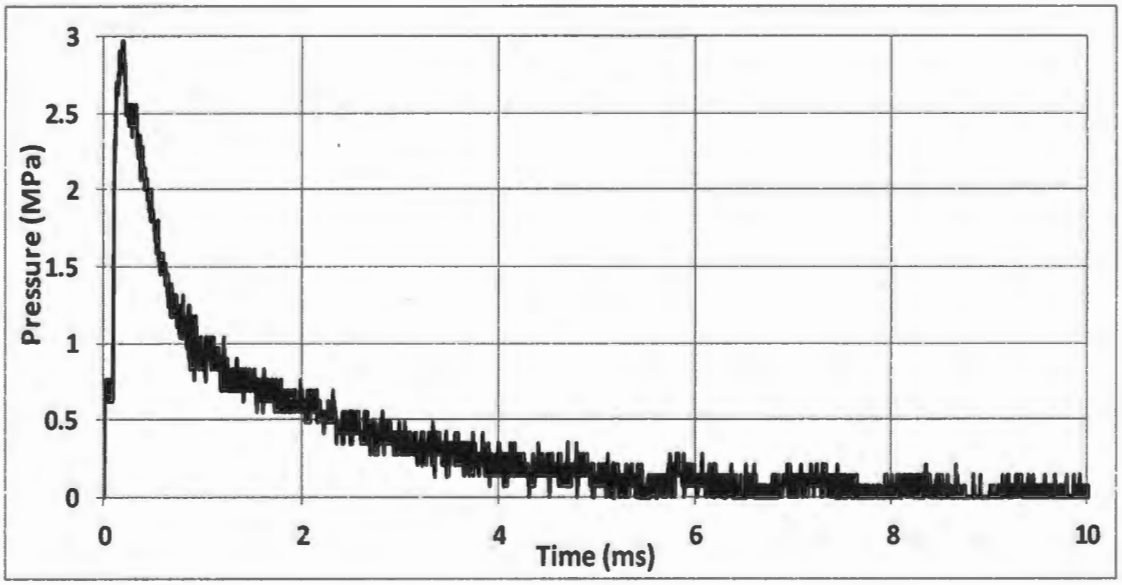

Figure 4: A typical pressure profile

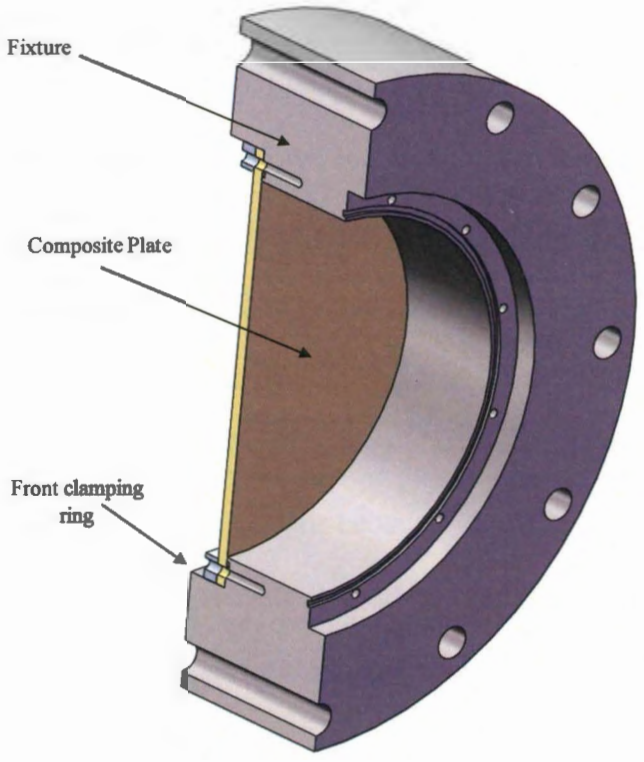

Figure 5: Loading fixtures

3.3 Digital Image Correlation (DIC) Technique

The digital image correlation technique is a recent non-contact optical method for analyzing full-field shape and deformation [24]. This process involves the recording of high speed digital real time images during the loading process and subsequent post-processing of these images using the commercially available software to get the full-field shape and deformation measurements. The post-processing software obtains the full-field shape and deformation measurement by mapping the predefined points on the specimen. Capturing the three dimensional response of the panels requires two cameras (fig. 6) which must be calibrated and have synchronized image recording throughout the event. The calibration of the cameras is performed by translating and rotating a predefined grid of pattern both in and out of the plane at the test space where the composite specimens is located during the experiment. As this

grid pattern has predetermined distances between the speckles, the coordinates of the center of each dot is extracted from each image. The coordinate locations of each dot extracted uniquely for each camera allows for a correspondence of the coordinate system of each camera. The DIC is then performed on the image pairs that are recorded during the shock event. Prior to testing, the back face of the sample is painted white and then coated with a randomized speckle pattern (fig. 7). The post processing is performed with the VIC-3D software package which matches common pixel subsets of the random speckle pattern between the deformed and un-deformed images. The matching of pixel subsets is used to calculate the three dimensional location of distinct points on the face of the panel throughout time. Dynamic experiments have been done in the past [25] to compare the back face deflection from the real time transient image and DIC to verify the accuracy of the DIC results. The error between the maximum deflection from DIC and real-time transient images is 5%.

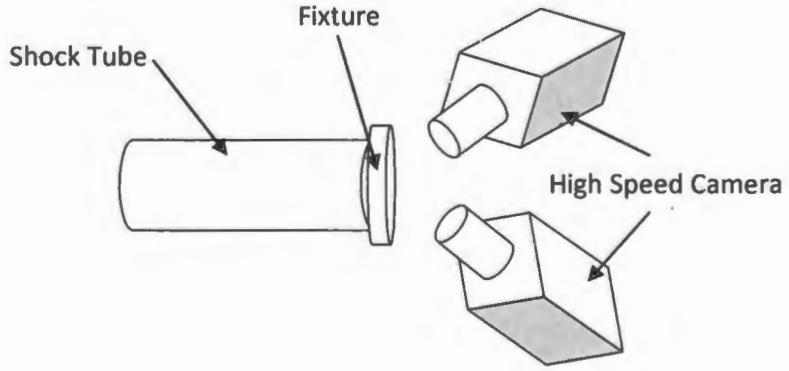

Figure 6: Schematic of DIC system

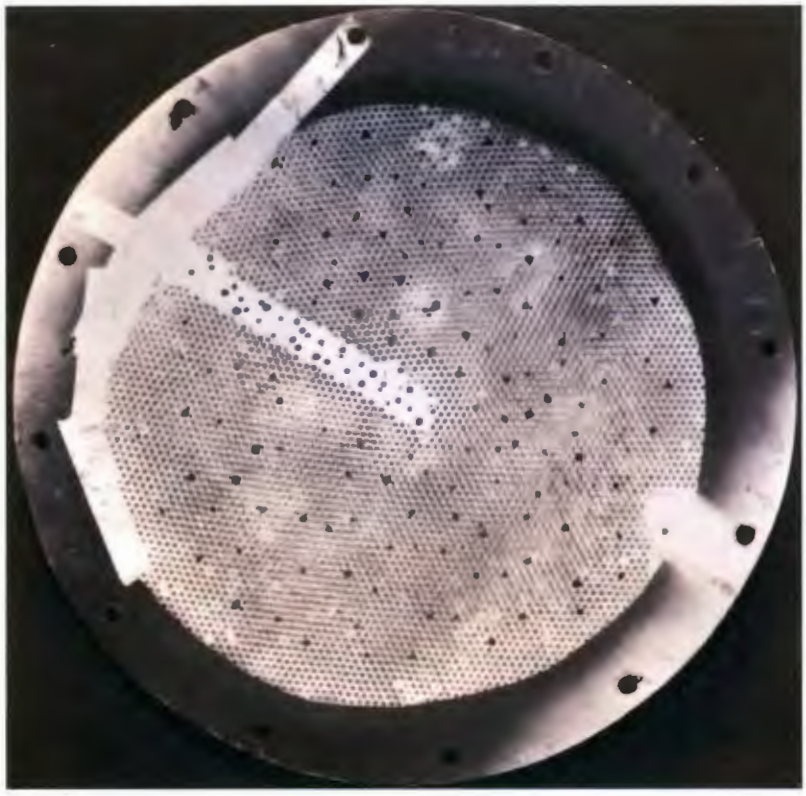

Figure 7: Speckle pattern on the back of the specimen

Two high speed digital cameras, Photron SA1s, were positioned behind the shock tube apparatus to capture the real time deformation and displacement of the panel. The high speed cameras were set to capture synchronized images at 20,000 frames per second (inter frame time of 50 μs). During the blast loading event, as the panel responds, the cameras record the speckles on the back face sheet. Once the event was over, the high speed images were analyzed using DIC software to correlate the images from the two cameras and generate real time in-plane strain and out-of-plane deflection/velocity histories. A schematic of the set-up is shown in fig. 6.

There are two key assumptions used in converting images to experimental measurements of objects shape, deflection and strain. First, it is assumed that there is a direct correspondence between the motion of the points in the image and that in the

object. This will ensure that the displacement of points on the image have a correlation with the displacement of points on the object. Second, it is assumed that each sub-region has adequate contrast so that accurate matching can be performed to define local image motion.

4. Experimental results and Discussion

4.1 Shock Loading

The URI shock tube apparatus (fig. 2) was used to obtain the controlled shock loading on the panels. Two pressure transducers were used to record the pressure profile of the shock wave. The pressure profile recorded by the sensor closest to the specimen (fig. 4) represents the loading profile which the specimen experiences. The pressure profile for the three panels (A to C) is shown in fig. 8. The first jump in the pressure pulse for all the three panels represents the intensity of the incoming shock wave. The second jump depends on the blast mitigation property of the panel and it represents the exact loading on the specimen. As such, we can control the intensity of the incoming shock pressure, but the second jump, which represents the exact loading on the specimen, depends on the shock behavior of the specimen.

The pressure profile for the three panels (fig. 8) represents the failure loading. Failure load is defined as the minimum load where the failure occurs. The failure loading for Panel A is 1.05 MPa, for Panel B is 2.96 MPa, and for Panel C is 6.20 MPa.

The pressure profile for panels A and B have a smooth exponentially decay, whereas there is oscillations in the pressure profile of panel C (at t = 2 ms) and panel C (at t = 5.5 ms). There is recovery (oscillations) in deflection in panel C around these

time which results in slight jump during the exponential decay as seen in fig. 8. The impulse imparted on the three panels has been calculated. The impulse in shock loading conditions is defined as the area under the pressure-time curve. The impulses for panel A, B, and C are 1320 Pa-s, 3515 Pa-s, and 10600 Pa-s respectively. This shows that panel C can sustain highest impulse whereas panel A has the lowest impulse sustainability.

(a)

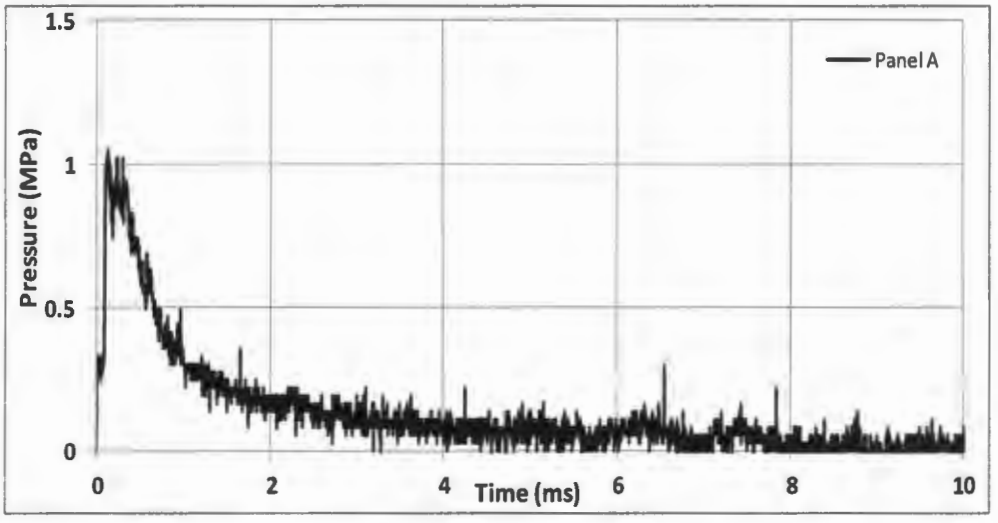

(b)

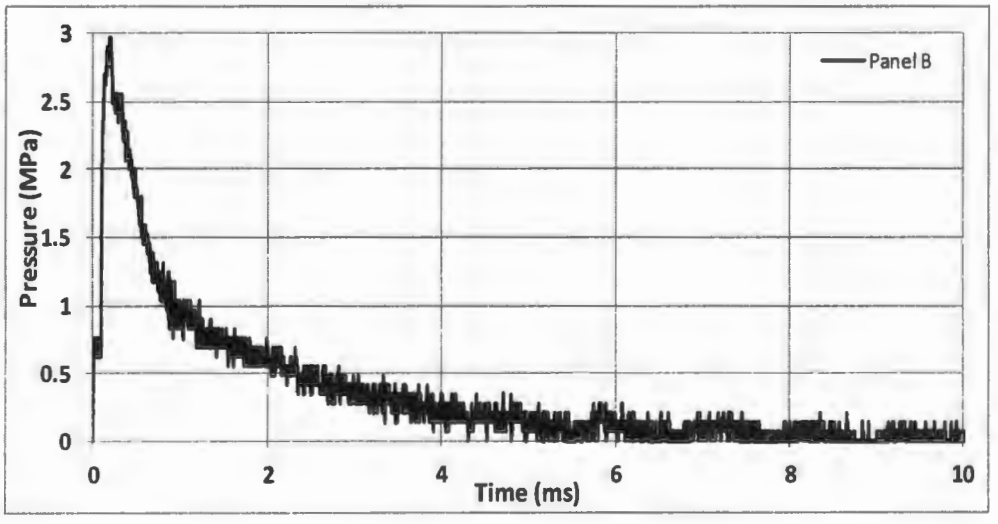

(c)

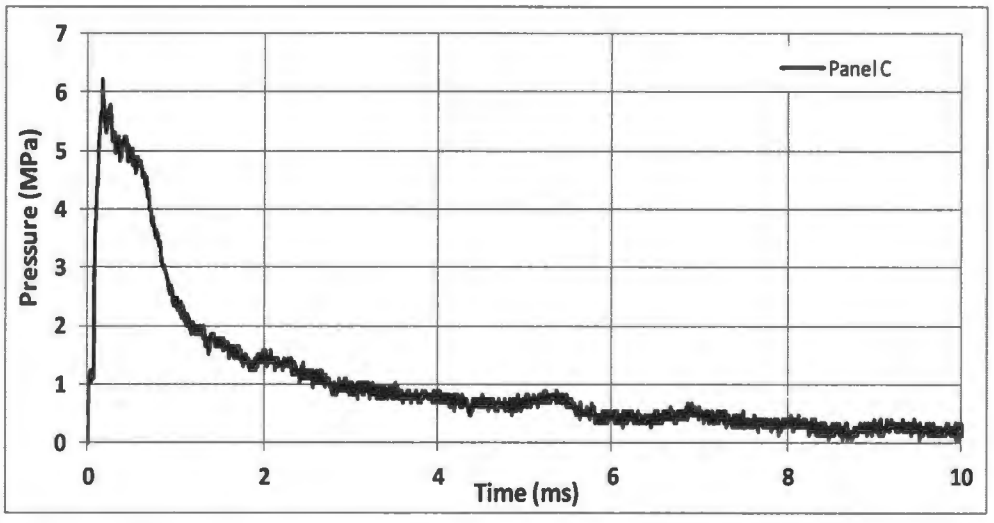

Figure 8: Failure Pressure profile for (a) Panel A, (b) Panel B, (c) Panel C.

4.2 DIC Analysis

The DIC technique is used to obtain the out-of-plane deflections and velocities as well as the in-plane strains on the back surface for all the three geometries. The full-field deflection for the three panels is shown in fig 9. The deflection contour for all the three panels is circular in shape. The total deflection in these panels subjected to blast loading can be separated in two distinct regions, namely, the indentation region followed by the flexural deflection. During indentation, localized deflection superpose onto the overall deflection. In case of flexure, the overall deflection starts to overpass the localized deflection. The indentation deflection is localized around the loading area whereas a full field deflection over the area of the specimen being loaded is predominant in flexural mode. Also, the boundary conditions affect the deflection in case of flexural mode.

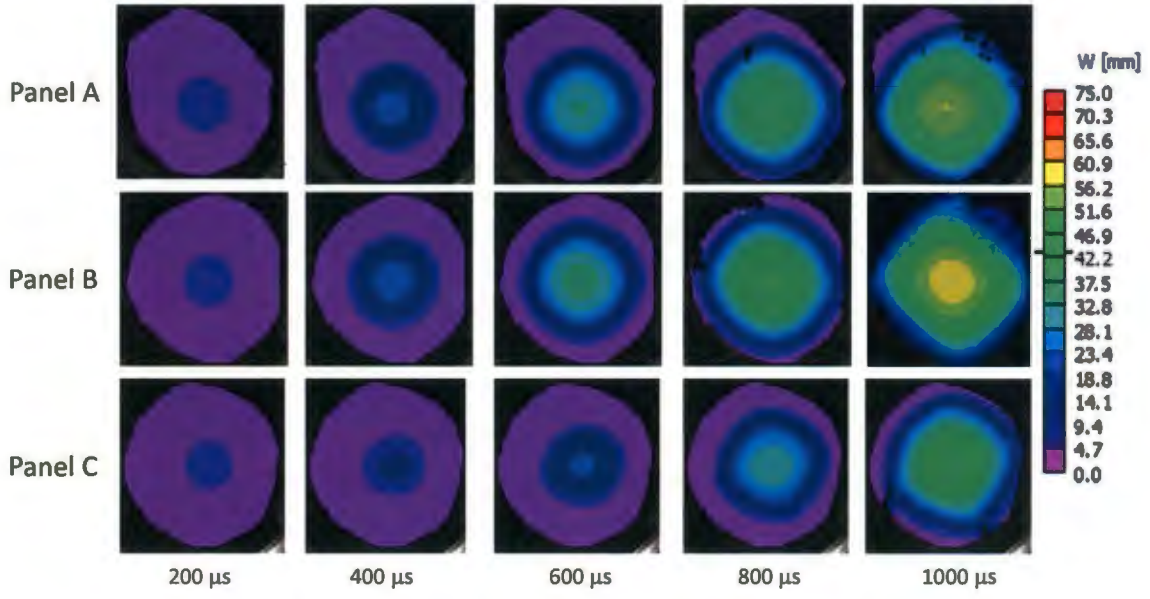

Figure 9: Full field deformation of panels from 3D-DIC analysis.

In panels A and B the deflection contours are affected by the boundary conditions at around 800 µs, whereas the boundary conditions does not affect the deflection contour development in panel C until 1000 µs. This delay in transition from indentation mode to flexural mode of deflection is because of the higher flexural rigidity. As seen in fig. 9, at t = 600 µs, the deflection development in panel C is at a slower rate than that in panels A and B. this results in smaller full-field deflection contour in panel C as compared to the other two panels even though it was subjected to higher pressure. Panel C has higher flexural rigidity which results in slower deflection rate and smaller full-field deflection area.

From the full-field DIC analysis, the out-of-plane deflection and velocities and the in-plane strain data were extracted at the center point of the three panels (fig. 10-12). From the time-deflection history (fig. 10) at the center point of the panels, it is seen that the deflection rate (65 m/sec) is almost same in all panels A & B, whereas it

is around 50 m/sec in panel C. This also shows that the Panel C is stiffer than the other two panels as it can sustain higher pressures and have a lower deflection rate (23% lower) as compared to the other two panels. The final deflection is almost same in all the three panels. Another important point to note here is that there was complete inversion in the curvature of all the three panels.

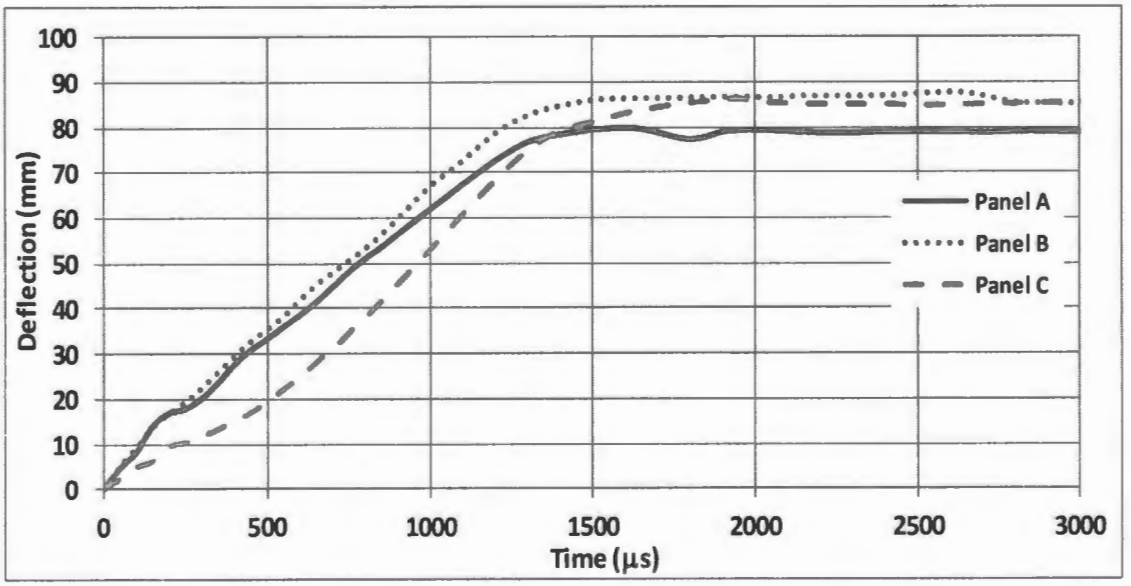

Figure 10: Time-deflection history at the center point on the back face for the three panels.

The in-plane strains, e_{xx}, e_{yy}, and e_{xy} at the center-point of the three panels is shown in fig. 11. The in-plane strains, e_{xx}, and e_{yy}, follow the same trend at the center point of the panel with almost the same magnitude expect in the case of panel C. It can be observed from fig. 11(a) and 11(b) that at t = 400 μs, the e_{yy} value in panel C is around 1.3% (compressive) as compared to 0.5% compressive e_{xx}. As regards to the in-plane shear strain, e_{xy}, panel C had the least among the three panels at failure load. It is important to remember here that the failure load is around 500% higher in panel C when compared with panel A.

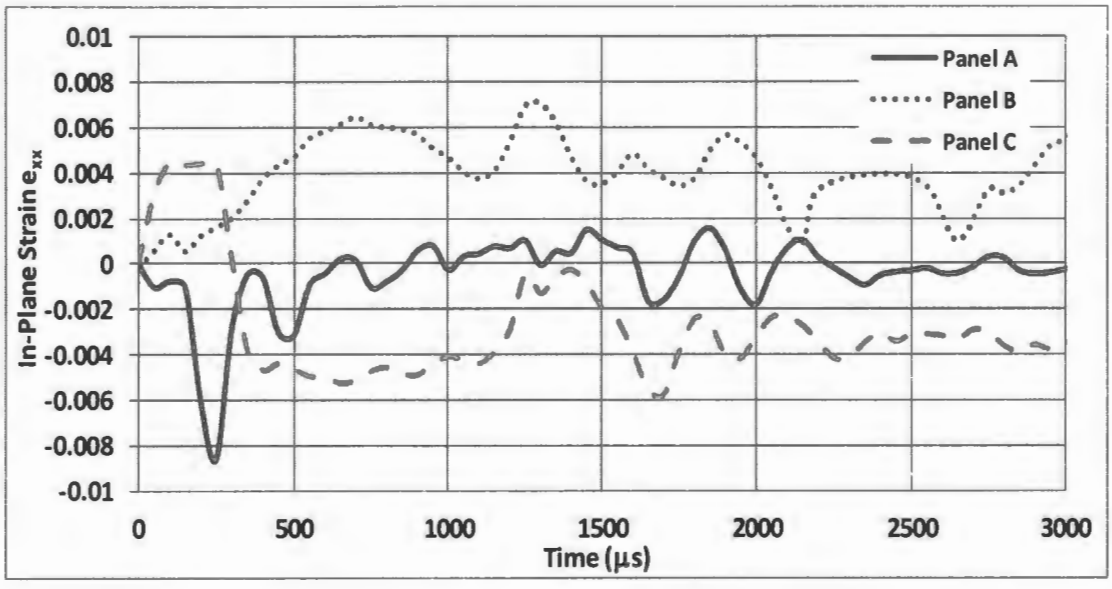
0.01
0.008
0.006
0.004
0.002
0
-0.002
-0.004
-0.006
-0.008
-0.01
In-Plane Strain e_{xx}
0
500
1000
1500
2000
2500
3000
Time (μs)
Panel A
Panel B
Panel C

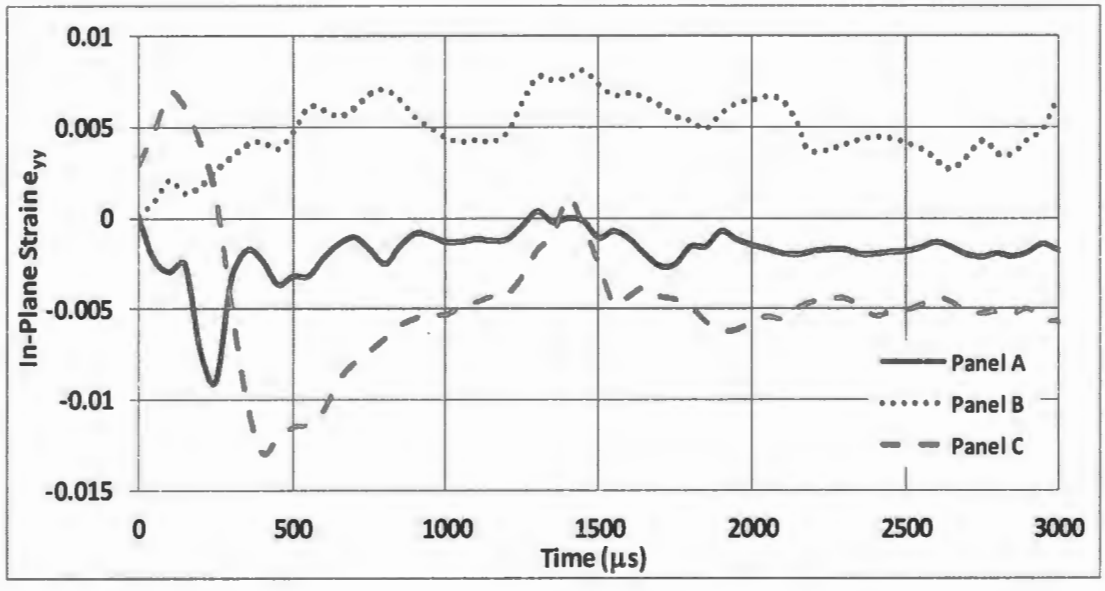
0.01
0.005
0
-0.005
-0.01
-0.015
In-Plane Strain e_{yy}
0
500
1000
1500
2000
2500
3000
Time (μs)
Panel A
Panel B
Panel C

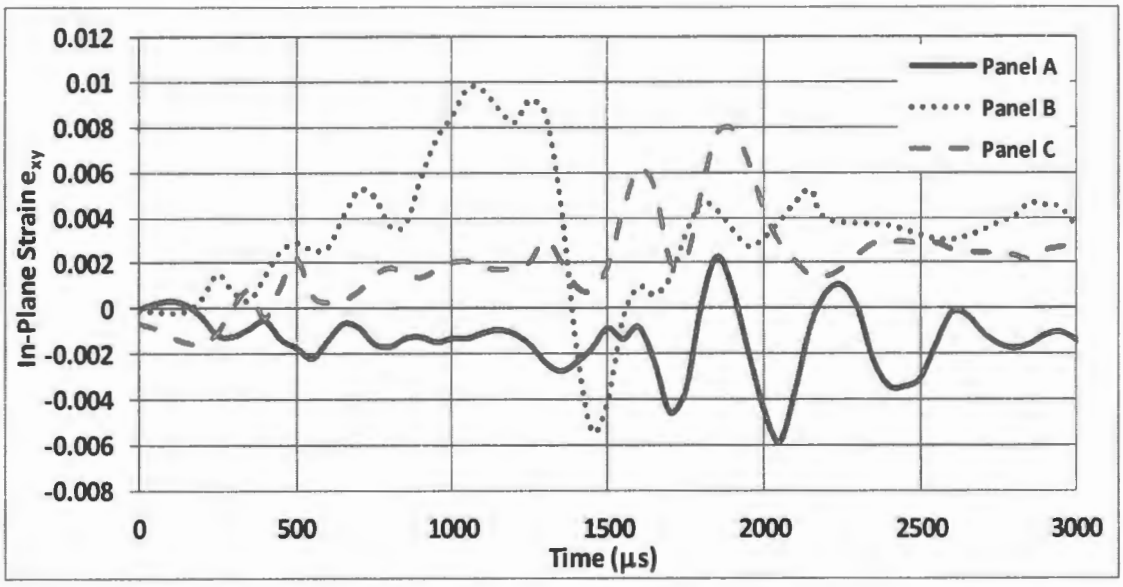

Figure 11: Time-in-plane strain history at the center point on the back face for the three panels.

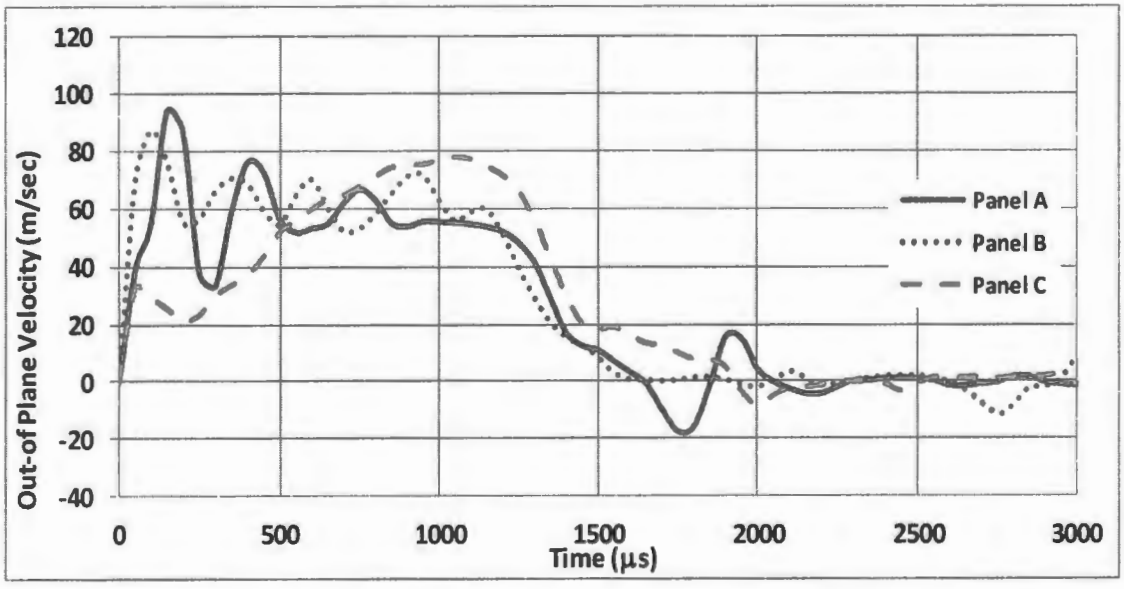

Figure 12: Time-Velocity history at the center point on the back face for the three panels.

The out-of plane velocity at the center point of the three panels is shown in fig. 12. Panels A and B had a kick-off velocity of around 95 m/sec, whereas panel C had a

kick-off velocity of 38 m/sec. this lower kick-off velocity in panel C (at a higher loading as compared to panels A and B) show that panel C has a higher flexural rigidity than the other two panels. Also, the panels A and B had almost same flexural response even though they are of different thicknesses.

4.3 Macroscopic post-mortem analysis

The post-mortem image of the shock loaded glass composite panel (panel A) is shown in fig. 13. This panel was subjected to a failure load of 1.05 MPa. First of all, there is complete inversion in the curvature of the panel at this loading. There is inter-layer delamination in the panel which can be easily seen by the color change in the post-mortem image of panel A around the periphery in fig. 13. There is also fiber breakage on both the faces of the panel. The fiber breakage initiated from the clamping edges. The panel was held under fully clamped boundary condition throughout the experiment as there was fiber breakage around four holes drilled in the panels to hold it.

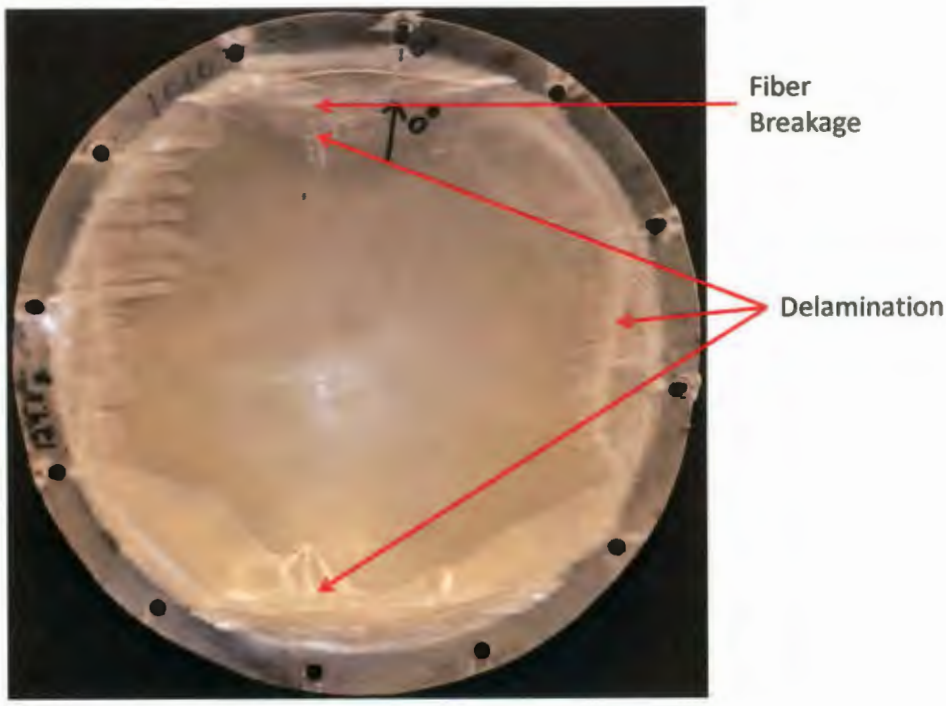

Figure 13: Post-mortem evaluation of Panel

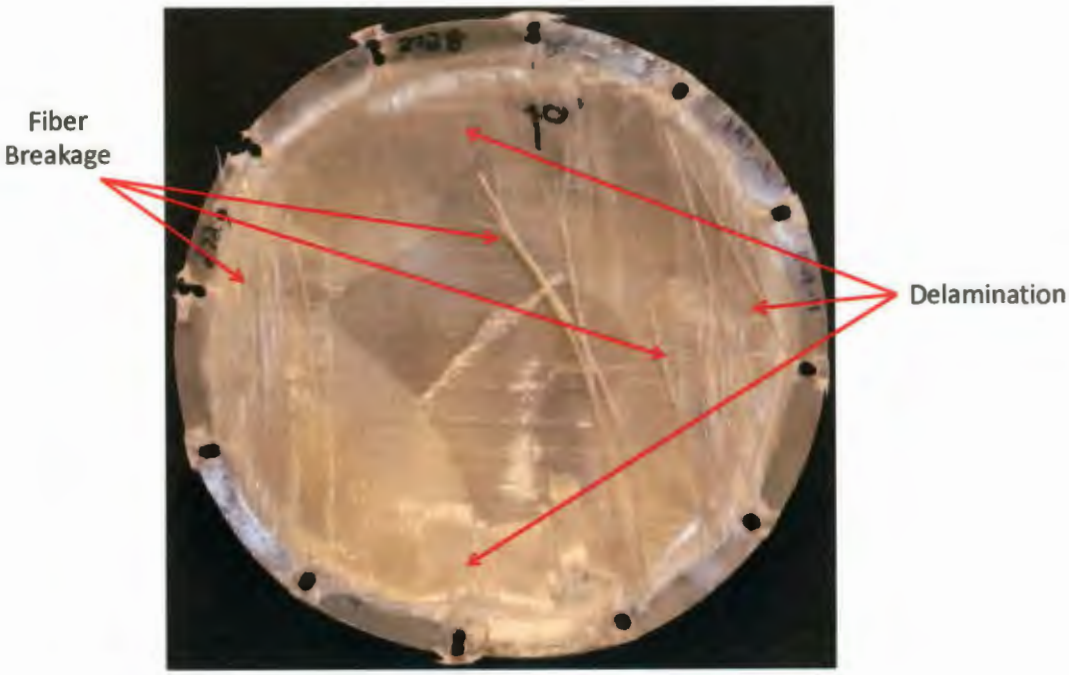

Figure 14: Post-mortem evaluation of Panel B.

The post-mortem image of panel B is shown in fig. 14. The panel was subjected to a loading of 2.96 MPa. As in the case of panel A, this panel also showed

complete inversion in curvature. There is large scale inter-layer delamination and fiber breakage as evident in fig. 14. The large scale discoloration on the front face (fig. 14) clearly shows the inter-layer delamination in panel B. also, there is lot of fiber breakage on both the right and left sides of the panel in fig. 14. This fiber breakage initiates from the clamping edges which shows that bending is the major cause of fiber breakage. There is also large scale delamination and fiber breakage on the back face of the panel.

The post-mortem image of panel C is shown in fig. 15. The panel was subjected to a failure load of 6.2 MPa. Similar to the other two panels, this panel also showed complete inversion in curvature. The discoloration on the front face of the panel shows large scale inter-layer delamination. There is fiber breakage which initiates from the edges caused because of the large scale bending in the panel. There is fiber breakage on the back face of the panel.

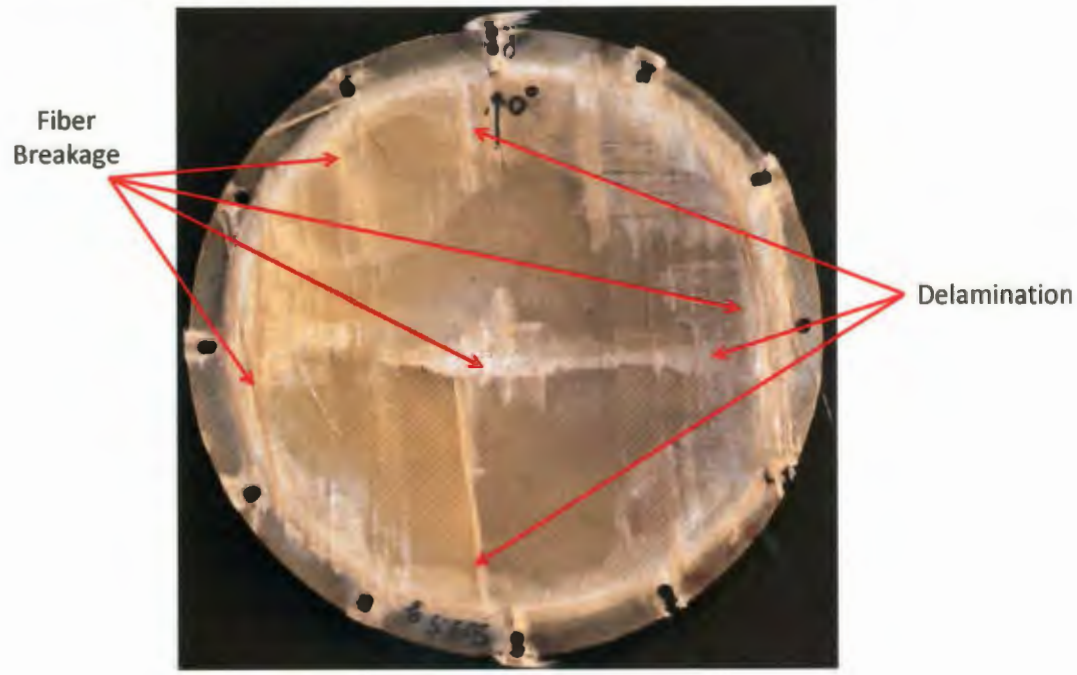

Figure 15: Post-mortem evaluation of Panel C

All the three panels were held under fully clamped boundary conditions. There is slight damage around the holes on the panels, which were drilled to fully clamp the panels. This shows that the panels had near perfect boundary conditions throughout the duration of the experiment.

4.4 Performance Analysis

Experiments were carried out at an incoming shock pressure of 0.52 MPa for all the three panels to compare the performance analysis. Panel A had catastrophic failure, whereas the results discussed above for panel B are at an incoming shock pressure of 0.52 MPa. There was no visible damage and inversion of curvature in panel C when it was subjected to the same incoming shock pressure. As discussed in section 3.2, DIC analysis was performed at this pressure. The center point out of plane deflection for all the three panels at incoming shock intensity (pressure) of 0.52 MPa is shown in fig. 16. The deflection is shown for first 700 μs only at which time there is catastrophic failure in panel A as shown in fig. 17.Panel A had fiber breakage and a complete interlayer delamination as seen in fig. 17.

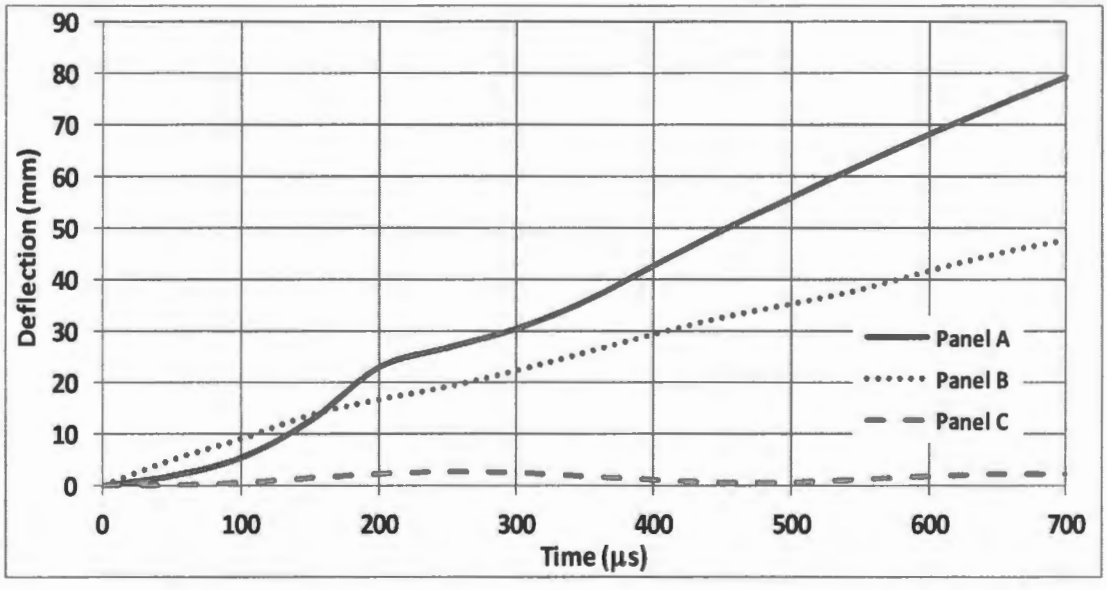

Figure 16: Time-deflection history at the center point on the back face for the three panels at 0.52 MPa.

The weight of individual panels tested at 0.52 MPa is 129 g for Panel A, 272 g for Panel B, 486.8 g for Panel C. the percentage change in weight from panel A to panel B is 110%, where as it is 280% change from Panel A to Panel C. for comparing the performance analysis, deflection per unit weight was calculated for each panels. The lower this value is the panel is expected to perform better. There is a 72% decrease in deflection per unit weight from panel A to panel B is where as it is 99% decrease from panel A to C. The percentage decrease in deflection per unit weight from panel A to panel C is 99% but panel C is 280% heavier than panel A. At the same time panel B had a decrease of 72% in deflection per unit weight from panel A to B, but the panel B was 110% heavier than panel A. Above facts need to be considered and analyzed when designing a material for better performance as there is an increase in weight as we go for thicker panels (for a better performance).

Figure 17: Post-mortem evaluation of Panel B at 0.52 MPa.

5. Conclusions

Three types of panels with varying thickness have been subjected to a controlled shock loading using a shock tube. 3D DIC technique coupled with high speed photography is used to obtain the out-of-plane deformation/velocity and in-plane strain on the back face of all the three panels.

1. The macroscopic post-mortem analysis and DIC deflection, velocity and in-plane strain analysis shows that panel C is capable of sustaining the highest threshold failure load.

2. There is a substantial increase of failure load from panel A to panel C but at the same time there is a limit to which the thickness can be increased. This is due to the fact that the increase in thickness also increases the weight of the panel. This will result in heavier and bulkier materials. Thus depending upon the requirements (performance vs. weight) an amicable material design needs to be chosen.

6. Acknowledgement

The authors acknowledge the financial support provided by the Department of Homeland Security (DHS) under Cooperative Agreement No. 2008-ST-061-ED0002. James LeBlanc acknowledges the financial support of the Naval Undersea Warfare Center, Division Newport through the NUWC Fellowship Program.

7. References

[1] G.S. Langdon, Y. Chi, G.N. Nurick, and P. Haupt, Response of GLARE panels to blast loading, Engineering Structures, 31 (2009) 3116-3120.

[2] J. LeBlanc, and A. Shukla, Dynamic response and damage evolution in composite materials subjected to underwater explosive loading: An experimental and computational study, Compos. Struct., 92 (2010) 2421-2430.

[3] L. Chun, and K.Y. Lam, Dynamic analysis of clamped laminated curved panels, Compos. Struct., 30 (1995) 389-398.

[4] R. Rajendran, and J.M. Lee, Blast loaded plates, Mar. struct., 22 (2009) 99-127.

[5] J.M. Biggs, Introduction to structural Dynamics, McGraw-Hill, New York, 1964.

[6] R.W. Clough, and J. Penzien, Dynamics of structures, McGraw-Hill, New York, 1975.

[7] S.A. Tekalur, K. Shivakumar, and A. Shukla, Mechanical behavior and damage evolution in E-glass vinyl ester and carbon composites subjected to static and blast loads, Composites: Part B. 39 (2008) 57-65.

[8] H. Arora, P.A. Hooper, and J.P. Dear, Dynamic response of full-scale sandwich composite structure subject to air-blast loading, Composites: Part A, 42(2011) 1651-1662.

[9] J. LeBlanc, and A. Shukla, Response of E-glass/vinyl ester composite panels to underwater explosive loading: Effect of laminate modification, Int. J. of Impact Engineering, 38 (2011) 796-803.

[10] T.J. Colete, G.N. Nurick, and R.N. Palmer, The deformation and shear failure of peripherally clamped centrally supported blast loaded circular plates, Int. Journal of Impact Engineering, 32 (2005) 92-117.

[11] L.S. Kistler and A.M. Waas, On the response of curved laminated panels subjected to transverse impact loads, International Journal of Solids and Structures, 36(1999) 1311-1327.

[12] T. Franz, G.N. Nurick, M.J. Perry, Experimental investigation into the reponse of chopped strand mat glassfibre laminates to blast loading, International Journal of Impact Engineering, 27(2002) 639-667.

[13] S.M.R. Khalili, M. Soroush, A. Davar and O. Rahmani, Finite element modeling of low-velocity impact on laminated composite plates and cylindrical shells, Composite Structures, 93(2011) 1363-1375.

[14] R.O. Ochola, K. Marcus, G.N. Nurick and T. Franz, Mechanical behavior of glaa and carbon fiber reinforced composites at varying strain rates, Composites Structures, 63(2004) 455-467.

[15] Y. Chi, G.S. Landon, and G.N. Nurick, The influence of core height and face plate thickness on the response of honeycomb sandwich panels subjected to blast loading, Materials and Design, 31 (2010) 1887-1899.

[16] J. LeBlanc, and A. Shukla, Dynamic response of curved composite panels to underwater explosive loading: experimental and computational comparisions, Compos. Struct., 93 (2011) 3072-3081.

[17] M. Pankow, B. Justusson, A. Salvi, A.M. Waas, Chian-Fong Yen, and S. Ghiorse, Shock response of 3D woven composites: An experimental investigation, Composite Structures, 93(2011) 1337-1346.

[18] J. Shen, G. Lu, Z. Wang, L. Zhao, Experiments on curved sandwich panels under blast loading, International Journal of Impact Engineering, 37(2010) 960-970.

[19] F. Zhu, L. Zhao, G. Lu, and Z. Wang, Deformation and failure of blast loaded metallic sandwich panels-experimental investigations, Int J Impact Eng, 35 (2008) 937-951.

[20] T. Hause, and L. Librescu, Dynamic response of doubly-curved anisotropic sandwich panels impacted by blast loadings, International Journal of Solids and Structures, 44(2007) 6678-6700.

[21] M.M. Shokrieh and L.B. Lessard, Progressive Fatigue Damage Modeling of Composite Materials, Part II: Material Characterization and Model Verification, Journal of Composite Materials, 34(2000) 1081-1116.

[22] J. LeBlanc, A. Shukla, C. Rousseau, and A. Bogdanovich, Shock loading of three-dimensional woven composite materials, Compos. Struct., 79 (2007) 344–355.

[23] J. Wright, Shock Tubes, John Wiley and Sons Inc., New York, 1961.

[24] V. Tiwari, M.A. Sutton, S.R. McNeill, S. Xu, X. Deng, W.L. Fourney, and D. Bretall, Application of 3D image correlation for full-field transient plate deformation measurements during blast loading, Int. J. Impact Eng., 36 (2009) 862-874.

[25] N. Gardner, E. Wang, P. Kumar, and A. Shukla, Blast Mitigation in a Sandwich Composite Using Graded Core and Polyurea Interlayer, Exp. Mech., DOI 10.1007/s11340-011-9517-9 (2011).

CHAPTER 5

CONCLUSIONS AND FUTURE WORKS

1. Conclusions

The main objective of this project has been to investigate the blast resistance and mitigation behaviors of structural materials. Different structural materials varying from glass to metals and composites have been studied. An equivalent loading experienced during an actual explosion was created using the shock tube facility. The fluid/structure interaction behavior during a blast loading was visualized for different materials. 3D- Digital Image Correlation technique coupled with high speed imaging was used to obtain the back face out-of-plane deflections and velocities and in-plane strains during the experiments. Failure mechanisms were investigated for different structural materials with the intent of designing an designing light weight structures with a better blast mitigating property. The findings from the present study are summarized below.

1. Five different glass panels were subjected to a controlled air blast loading using a shock tube. The high speed photography and DIC analysis is applied to obtain the out-of-plane deflection and in-plane strain on the back face of all the five panels. The macroscopic post-mortem analysis and DIC deflection analysis shows that the sandwich glass panel has less damage due to blast loading as compared to the wired, tempered and clear glass panels. The PVB interlayer increases the flexural rigidity of the panels, and results in less damage when subjected to the shock loading. The area of the through hole

formed in the case of the sandwich glass panel was smaller as compared to that in the case of the other three glass panels. This will minimize the blast overpressure entering in the buildings and thus lower the damage inflicted as compared to the wired, tempered and plain glass panels. The application of the protective film (XO-ARMOR®) on the front and back face of the sandwich panel further improves the blast mitigation property of the sandwich glass panel. The laminated sandwich glass panel has fragmentation and cracking in the glass panel but the protective film is able to withhold the shattered glass pieces from flying off. Also, there is no through hole formation in the case of the laminated sandwich glass panel. This prevents the blast overpressure from entering the building and thus restricting the damage because of the overpressure. Overall, the laminated sandwiched glass panels with PVB interlayer and protective film on both the faces has a better blast mitigation properties as compared to the other four panels.

2. Aluminum panels having three different curvatures have been subjected to a controlled shock loading using a shock tube. 3D DIC technique coupled with high speed photography was used to obtain the out-of-plane deformation/velocity and in-plane strain on the back face of all the three panels. Computational simulations using DYSMAS are performed. The macroscopic post-mortem analysis and DIC deflection, velocity and in-plane strain analysis shows that panel C (111.76 mm radius of curvature) has the least plastically deformed area out of the three panels. Also it has practically no yield line (hinge) formation as compared to the other two panels. This

shows that panel C has better blast mitigation property as compared to the other two panels. As the radii of curvature becomes sharper the plastic deformation decreases. Also the flexural deformation decreases as the radius of curvature decreases. There is a limit to which the radius of curvature can be decreased. As the radius of curvature reduces to a limiting value, the shock wave will glide over the surface. The displacement and velocity data from the DIC analysis from the experiments are correlated to the computational model by utilizing the Russell error. The Russell error analysis showed that all the comparisons fall within the acceptable regime, including four in the excellent regime.

3. Three types of carbon composite panels with varying curvature have been subjected to a controlled shock loading using a shock tube. 3D DIC technique coupled with high speed photography is used to obtain the out-of-plane deformation/velocity and in-plane strain on the back face of all the three panels. The macroscopic post-mortem analysis and DIC deflection, velocity and in-plane strain analysis shows that panel C (112 mm radius of curvature) is capable of sustaining the highest threshold failure load. The flexural deformation decreases and indentation deformation increases as the radius of curvature decreases. There is a limit to which the radius of curvature can be decreased. As the radius of curvature reduces to a limiting value, the shock wave will glide over the surface.

4. Three types of glass/vinyl ester composite panels with varying thickness have been subjected to a controlled shock loading using a shock tube. 3D DIC

technique coupled with high speed photography is used to obtain the out-of-plane deformation/velocity and in-plane strain on the back face of all the three panels. The macroscopic post-mortem analysis and DIC deflection, velocity and in-plane strain analysis shows that panel C is capable of sustaining the highest threshold failure load. There is a substantial increase of failure load from panel A to panel C but at the same time there is a limit to which the thickness can be increased. This is due to the fact that the increase in thickness also increases the weight of the panel. This will result in heavier and bulkier materials. Thus depending upon the requirements (performance vs. weight) an amicable material design needs to be chosen.

2. Future Works

The current research is a step forward in understanding the dynamic response of structural materials during an air blast loading. It brings forth a better understanding on the dynamic failure mechanism of different materials varying from glass to metals and composites under different loading conditions. The proposed future projects are summarized as follows:

1. Conduct a comprehensive study to understand the effect of temperature on the dynamic behavior of the laminated sandwich glass panel. A suitable fixture for heating the laminated panels should be designed and implemented to understand the dynamic behavior of the panels.
2. Conduct a series of experiments to understand the effect of using different face-sheets on the dynamic behavior of composite panels when subjected to blast loading. The face-sheet material can be varied from glass fiber composite

panels to metallic face-sheets, such as aluminum. Either the overall thickness or the weight of the two panels should be kept same to correlate the difference in behavior to air shock loading.

3. An in-depth cost effective analysis is needed between the weight and performance of the composite material.

BIBLIOGRAPHY

Arora, H., Hooper, P.A., and Dear, J.P., "Dynamic response of full-scale sandwich composite structure subject to air-blast loading", *Composites: Part A*, 42 (2011) 1651-1662.

Biggs, J.M., "Introduction to structural Dynamics", *McGraw-Hill*, New York, 1964.

Bouzid, S., Nyoungue, A., Azari, Z., Bouaouadja, N., and Pluvinage, G., "Fracture criterion for glass under impact loading", *International Journal of Impact Engineering*, 25 (2001) 831-845.

Carson, S.W., and Papanu, V.D., "", *Journal of Non-Crystalline Solids*, 218 (1997) 169-173.

Chi, Y., Langdon, G.S., and Nurick, G.N., "The influence of core height and face plate thickness on the response of honeycomb sandwich panels subjected to blast loading", *Materials and Design*, 31 (2010) 1887-1899.

Chun, L., and Lam, K.Y., "Dynamic analysis of clamped laminated curved panels", *Composite Structures*, 30 (1995) 389-398.

Clough, R.W., and Penzien, J., "Dynamics of structures", *McGraw-Hill*, New York, 1975.

Colete, T.J., Nurick, G.N., and Palmer, R.N., "The deformation and shear failure of peripherally clamped centrally supported blast loaded circular plates", *International Journal of Impact Engineering*, 32 (2005) 92-117.

Daniel, I.M., Werner, B.T., and fenner, J.S., "Strain-rate-dependent failure criteria for composites", *Composite Science and Technology*, 71 (2011) 357-364.

Daniel, I.M., Luo, J.J., Schubel, P.M., and Werner, B.T., "Interfiber/interlaminar failure of composites under multi-axial states of stress", *Composite Science and Technology*, 69 (2009) 764-771.

Franz, T., Nurick, G.N., and Perry, M.J., "Experimental investigation into the reponse of chopped strand mat glassfibre laminates to blast loading", *International Journal of Impact Engineering*, 27 (2002) 639-667.

Gardner, N., Wang, E., Kumar, P., and Shukla, A., "Blast Mitigation in a Sandwich Composite Using Graded Core and Polyurea Interlayer", *Experimental Mechamics*, DOI 10.1007/s11340-011-9517-9 (2011).

Gogtsi, G.A., and Mudrik, S.P., "Glasses: New approach to fracture behavior analysis", Journal of Non-Crystalline Solids, 356 (2010) 1021-1026.

Hause, T., and Librescu, L., "Dynamic response of doubly-curved anisotropic sandwich panels impacted by blast loadings", *International Journal of Solids and Structures*, 44 (2007) 6678-6700.

Hooper, P., Arora, H., and Dear, J.P., "Blast and impact resistance of laminated glass structures", *Proceedings of the IMPLAST 2010 Conference*, October 12-14 2010, Providence, RI, USA.

Hosur, M.V., Islam, S.M.W., Vaidya, U.K., Kumar, A., Dutta, P.K. and Jeelani, S., "Dynamic punch shear characterization of plain weave graphite/epoxy composites at room and elevated temperature", *Composite Structures*, 70 (2005) 295-307.

Hosur, M.V., Adya, M., Vaidya, U.K., Mayer, A., and Jeelani, S., "Effect of stitching and weave architecture on the high strain rate compression response of

affordable woven carbon/epoxy composites", *Composite Structures*, 59 (2003) 507-523.

Hosur, M.V., Alexander, J., Vaidya, U.K., Jeelani, S., and Mayer, A., "Studies on the off-axis high strain rate compression loading of satin weave carbon/epoxy composites", *Composite Structures*, 63 (2004) 75-85.

Hosur, M.V., Alexander, J., Vaidya, U.K., Jeelani, S., and Mayer, A., "High strain rate compression response of carbon/epoxy laminate composites", *Composite Structures*, 52 (2001) 405-417.

Jacinto, A.C., Ambrosini, R.D., and Danesi, R.F., "Experimental and computational analysis of plates under air blast loading", *International Journal of Impact Engineering*, 25 (2001) 927-47.

Karagiozova, D., Nurick, G.N., Langdon, G.S., Yuen, S.C.K., Chi, Y., and Bartle, S., "Response of flexible sandwich-type panels to blast loading", *Composites Science and Technology*, 69 (2009) 754-763.

Khalili, S.M.R., Soroush, M., Davar, A. and Rahmania, O., "Finite element modeling of low-velocity impact on laminated composite plates and cylindrical shells", *Composite Structures*, 93 (2011) 1363-1375.

Kistler, L.S., and Waas, A.M., "On the response of curved laminated panels subjected to transverse impact loads", *International Journal of Solids and Structures*, 36 (1999) 1311-1327.

Krauthammer, T., and Altenberg, A., "Negative phase blast effects on glass panels", *International Journal of Impact Engineering*, 24 (2000) 1-17.

Langdon, G.S., Chi, Y., Nurick, G.N., and Haupt, P., "Response of GLARE panels to blast loading", *Engineering Structures*, 31 (2009) 3116-3120.

Langdon, G.S., and Schleyer, G.K., "Inelastic deformation and failure of profiled Stainless steel blast wall panels. Part I: experimental investigation", *International Journal of Impact Engineering*, 31 (2005) 341-369.

Langdon, G.S., and Schleyer, G.K., "Inelastic deformation and failure of profiled Stainless steel blast wall panels. Part II: analytical modeling consideration", *International Journal of Impact Engineering*, 31 (2005) 371-399.

LeBlanc, J., and Shukla, A., "Dynamic response and damage evolution in composite materials subjected to underwater explosive loading: An experimental and computational study", *Composite Structures*, 92 (2010) 2421-2430.

Leblanc, J., and Shukla, A., "Dynamic response of curved composite panels to underwater explosive loading: experimental and computational comparisons", *Composite Structures*, 93 (2011) 3072-3081.

LeBlanc, J., Shukla, A., Rousseau, C., and Bogdanovich, A., "Shock loading of three-dimensional woven composite materials", *Composite Structures*, 79 (2007) 344–355.

LeBlanc, J., and Shukla, A., "Response of E-glass/vinyl ester composite panels to underwater explosive loading: Effect of laminate modification", *International Journal of Impact Engineering*, 38 (2011) 796-803.

Mencik, J., "Strength and fracture of glass and ceramics", *Elsevier*, New York, 1992.

Nurick, G., Olson, M.D., Fagnan, J.R., and Levi, A., "Deformation and tearing of blast loaded stiffened square plates", *Interantional Journal of Impact Engineering*, 16 (1995) 273-291.

Nurick, G., and Shave, G.C., "The deformation and tearing of thin square plates subjected to impulsive loads - an experimental study", *International Journal of Impact Engineering*, 18 (1996) 99-116.

Ochola, R.O., Marcus, K., Nurick, G.N. and Franz, T., "Mechanical behavior of glass and carbon fiber reinforced composites at varying strain rates", *Composites Structures*, 63(2004) 455-467.

Pankow, M., Justusson, B., Salvi, A., Waas, A.M., Yen, Chian-Fong, and Ghiorse, S., "Shock response of 3D woven composites: An experimental investigation", *Composite Structures*, 93(2011) 1337-1346.

Rajendran, R., and Lee, J.M., "Blast loaded plates", *Marine Structures*, 22 (2009) 99-127.

Redekop, D., "Dynamic response of short curved pipes to impulsive loading", *International Journal of Pressure Vessels and Piping*, 61 (1995) 41-47.

Russell, D.M., "Error measure for comparing transient data, Part I: development of a comprehensive error measure, Part II: error measure case study", *In Proceedings of the 68th shock & Vibration symposium*, 3-6th November 1997.

Russell, D.M., "DDG53 Shock trial simulation acceptance criteria", *In 69th shock and vibration symposium*, 12-19th October 1998.

Saito, H., and Masuda, M., "Modeling of blast process using indenting method", *Precision Engineering*, 28 (2004) 369-377.

Shen, J., Lu, G., Wang, Z., Zhao, L., "Experiments on curved sandwich panels under blast loading", *International Journal of Impact Engineering*, 37 (2010) 960-970.

Shokrieh, M.M., and Lessard, L.B., "Progressive Fatigue Damage Modeling of Composite Materials, Part II: Material Characterization and Model Verification", *Journal of Composite Materials*, 34 (2000) 1081-1116.

Stargel, D.S., "Experimental and Numerical Investigation into the effects of Panel Curvature on the High Velocity Ballastic Impact Response of Aluminum and Composite Panels", Doctor of Philosophy Dissertation, University of Maryland, College Park, 2005.

Stoffel, M., Schmidt, R., and Weichert, D., "Shock wave loaded plates", *International Journal of Solids and Structures*, 38 (2001) 7659-80, 2001.

Sutton, M.A., Orteu, J., and Schreier, H.W., "Image Correlation for Shape, Motion and Deformation Measurements: Basic Concepts, Theory and Applications:, *Springer*, 2009.

Tekalur, S.A., Shivakumar, K., and Shukla, A., "Mechanical behavior and damage evolution in E-glass vinyl ester and carbon composites subjected to static and blast loads", *Composites: Part B,* 39 (2008) 57-65.

Tiwari, V., Sutton, M.A., McNeill, S.R., Xu, S., Deng, X., Fourney, W.L., and Bretall, D., "Application of 3D image correlation for full-field transient plate deformation measurements during blast loading", *International Journal of Impact Engineering*, 36 (2009) 862-874.

Wei, J., and Dharani, L.R., "Fracture mechanics of laminated glass subjected to blast loading", *Theoretical and Applied Fracture Mechanics*, 44 92005) 157-167.

Wei, J., Shetty, M.S., and Dharani, L.R., "Stress characteristics of a laminated architectural glazing subjected to blast loading", *Computers & Structures*, 84 (2006). 699-707.

Wei, J., and Dharani, L.R., "Response of laminated architectural glazing subjected to blast loading", *International Journal of Impact Engineering*, 32 (2006) 2032-2047.

Wright, J., "Shock Tubes", *John Wiley and Sons Inc.*, New York, 1961.

Wierzbicki, T., and Nurick, G., "Large deformation of thin plates under localized impulsive loading", *International Journal of Impact Engineering*, 18 (1996) 899-918.

Zhu, F., Zhao, L., Lu, G., and Wang, Z., "Deformation and failure of blast loaded metallic sandwich panels-experimental investigations", *International Journal of Impact Engineering*, 35 (2008) 937-951.